SEISMIC FRAGILITY ANALYSIS AND LOSS ESTIMATION FOR CONCRETE STRUCTURES

A Dissertation

by

JONG WHA BAI

Submitted to the Office of Graduate Studies of
Texas A&M University
in partial fulfillment of the requirements for the degree of

DOCTOR OF PHILOSOPHY

December 2011

Major Subject: Civil Engineering

SEISMIC FRAGILITY ANALYSIS AND LOSS ESTIMATION FOR CONCRETE STRUCTURES

Dissertation

by

JONG WHA BAI

Submitted to the Office of Graduate Studies of
Texas A&M University
in partial fulfillment of the requirements for the degree of

DOCTOR OF PHILOSOPHY

Approved by:

Co-Chairs of Committee,	Mary Beth D. Hueste
	Paolo Gardoni
Committee Members,	Joseph M. Bracci
	J.N. Reddy
Head of Department,	John Niedzwecki

December 2011

Major Subject: Civil Engineering

ABSTRACT

Seismic Fragility Analysis and Loss Estimation for Concrete Structures.

(December 2011)

Jong Wha Bai, B.S., Yonsei University; M.S., Texas A&M University

Co-Chairs of Advisory Committee: Dr. Mary Beth D. Hueste
Dr. Paolo Gardoni

The main objective of this study is to develop a methodology to assess seismic vulnerability of concrete structures and to estimate direct losses related to structural damage due to future seismic events. This dissertation contains several important components including development of more detailed demand models to enhance accuracy of fragility relationships and development of a damage assessment framework to account for uncertainties.

This study focuses on concrete structures in the Mid-America region where a substantial seismic risk exists with potential high intensity earthquakes in this geographic region. The most common types of concrete structures in this area are identified based on the building inventory data and reinforced concrete (RC) frame buildings and tilt-up concrete buildings are selected as case study buildings for further analysis. Using synthetic ground motion records, the structural behavior of the representative case study buildings is analyzed through nonlinear time history analyses. The seismic performance of the case study buildings is evaluated to describe the structural behavior under ground motions. Using more detailed demand models and the

corresponding capacity limits, analytical fragility curves are developed based on appropriate failure mechanisms for different structural parameters including different RC frame building heights and different aspect ratios for tilt-up concrete structures. A probabilistic methodology is used to estimate the seismic vulnerability of the case study buildings reflecting the uncertainties in the structural demand and capacity, analytical modeling, and the information used for structural loss estimation. To estimate structural losses, a set of damage states and the corresponding probabilistic framework to map the fragility and the damage state are proposed. Finally, scenario-based assessments are conducted to demonstrate the proposed methodology. Results show that the proposed methodology is successful to evaluate seismic vulnerability of concrete structures and effective in quantifying the uncertainties in the loss estimation process.

ACKNOWLEDGMENTS

I would like to gratefully acknowledge my advisors, Dr. Mary Beth D. Hueste and Dr. Gardoni for their guidance and inspiration throughout my graduate studies. They have been always supportive even when I made a decision to leave College Station in 2007 before I finished my PhD. I really appreciate their continuous support and encouragement to make this finally happen. I also wish to sincerely acknowledge the contribution of Dr. Joseph M. Bracci and Dr. J.N. Reddy as committee members and for their guidance and helpful review of this document.

I wish to acknowledge the National Science Foundation (NSF), who sponsored this research through the Mid-America Earthquake Center under "CM-4 Structure Retrofit Strategies" and "EE-1 Vulnerability Functions" projects (NSF Grant Number EEC-9701785). I also wish to acknowledge the financial support provided by the Zachry Department of Civil Engineering at Texas A&M University. Additionally, I am grateful for the dissertation fellowship (PERIShip) which is sponsored by a partnership between the Natural Hazards Center and PERI (Public Entity Risk Institute) with funding from Swiss Re and NSF. It has provided me an opportunity to do more comprehensive study in seismic vulnerability assessment.

It has been a while but I spent a lot of time working on my research since 2001 with an excellent group of people including faculty and other graduate students at Texas A&M University. I really appreciate their support and friendship throughout my graduate studies. I also wish to thank all of my other friends in Texas (College Station,

Austin, and Dallas), California and Korea for their prayer, support and encouragement to complete this work.

Finally, special thanks to my wife, Namhee, and my two boys Juhan (Michael) and Kyuhan (Daniel) for their love, sacrifice and encouragement all the time. Without their love and continuous support, I would not be able to do this. I would like to thank my mom, parents-in-law, and other family members in Korea for their support and prayer. I also would like to dedicate this dissertation to my dearest dad who is in heaven. Last but not least, I thank God for everything He has done for me!

TABLE OF CONTENTS

Page

Page

Page

Page

LIST OF FIGURES

Page

Page

Page

LIST OF TABLES

Page

Page

Page

1. INTRODUCTION

Seismic hazards can cause lots of casualties and economic losses. There have been significant consequences in our society due to earthquake events in the past. However, it is not possible to forecast the exact time when a damaging earthquake of a specific magnitude will occur in a particular region. Only limited predictions can be done for well-understood faults on a statistical basis. While structures located near a seismically active geologic setting are at risk of being damaged during a potential seismic event, it is possible to mitigate future structural damage by identifying vulnerable structures and applying appropriate retrofit or replacement strategies. As such, seismic loss estimation is an important tool for developing a plan for seismic hazard mitigation.

Earthquakes are of concern to cities in the Mid-America Region because of the history of seismic activity around the New Madrid Seismic Zone (NMSZ). The New Madrid earthquakes are among the largest ones that have occurred in North America. Three major earthquakes took place in 1811-1812 with moment magnitude (M_w) estimates of 8.1, 7.8, and 8.0 and with hundreds of aftershocks that followed over a period of several years (Johnston 1996). Beside this series of events, damaging earthquakes have not occurred in the Mid-America Region. However, a substantial risk still exists with potential future high intensity seismic events.

This dissertation follows the style of *Journal of Structural Engineering, ASCE.*

According to the investigation of damage due to past earthquakes, concrete structures in the Mid-America Region built before the 1990s may be vulnerable to moderate or severe seismic events. Many existing concrete structures in this region were not designed on the basis of the seismic provisions of design codes until the early 1990s following the 1989 Loma Prieta earthquake in San Francisco, California (Moehle 2000). In general, concrete structures designed without seismic considerations are known to have significant deficiencies, such as discontinuity of positive moment reinforcement in beams and slabs, wide spacing of transverse shear reinforcement and inadequate force transfer between the horizontal and vertical components of the lateral system. Therefore, it is important to evaluate the seismic performance of typical structures in Mid-America and estimate their seismic fragility to predict structural losses in future seismic events.

Research studies related to the development of fragility curves have been conducted for a number of building types. By developing fragility curves that link measures of earthquake intensity to the conditional probability of attaining or exceeding a particular performance level, the seismic vulnerability of a structure can be estimated. In addition, a number of research projects have tried to estimate the potential losses due to future seismic events. For estimating the losses of a system, structural damage data and the resulting social and economic impacts are needed. Structural damage data based on fragility curves are provided by the engineering community, while the social and economic impacts are estimated based on direct and indirect losses by social scientists. To link the research of engineers and social scientists, a consistent framework and a set

of damage state definitions are fundamental to integrate the accomplishments from both groups. A methodology to estimate the economic losses resulting from structural damage that can be used in both fields is needed.

In the proposed study, seismic fragility curves are developed based on nonlinear dynamic analysis considering appropriate failure mechanisms. In addition, a probabilistic framework to estimate direct losses related to the structural damage is developed. Finally, loss estimations for concrete buildings using scenario earthquakes are conducted to demonstrate the proposed methodology.

1.1. Research Objectives

The main goals of this study are to estimate seismic vulnerability of concrete structures through seismic fragility analysis and to assess the structural losses by calculating structural damage factors. The following objectives are addressed:

1. *Identification of case study structures*

   Identify representative building structures in the Mid-America Region. The building inventory data for Shelby County, Tennessee, are used to find the most common types of structures. The focus of this research is concrete building structures.

2. *Evaluation of seismic performance*

   Evaluate the seismic performance of existing concrete structures in the Mid-America Region. To estimate the seismic performance, structural analyses are conducted using nonlinear time-history analyses with synthetic ground motions.

3. *Estimation of seismic fragility*

   Develop fragility curves based on appropriate failure mechanisms for drift-controlled and force-controlled components. Probabilistic models are developed to account for the uncertainties in the demand and capacity of the selected systems.

4. *Development of a Probabilistic Framework to Assess Structural Losses*

   Develop a loss estimation framework to estimate direct structural losses due to seismic events. To reflect the uncertainties in the data collection process and the information used in the loss estimation framework, probabilistic models are used.

5. *Assessment of Seismic Losses using Scenario Earthquakes*

   Illustrate the proposed framework for seismic vulnerability assessment of concrete building structures using scenario earthquakes for the Mid-America Region. Structural losses are estimated for the case study structures using these scenario earthquakes.

1.2. Background

1.2.1. Typical Damage of Concrete Structures from Past Earthquakes

During the past earthquakes, many concrete structures including tilt-up and flat slab buildings were damaged and had extensive losses. The common types of damage for these buildings are described to understand the dynamic behavior of the structures during the excitations. Because construction detailing and workmanship can be different depending on the region, it is limited to the cases only for the earthquakes that occurred in the United States. The following earthquakes are considered to investigate the types of damage for tilt-up and RC flat slab structures: the 1971 San Fernando earthquake, the 1987 Whittier earthquake, the 1989 Loma Prieta earthquake, the 1994 Northridge earthquake, and the 2001 Seattle earthquake,

1.2.1.1. Reinforced Concrete (RC) Flat Slab Moment Resisting Frame (MRF) Structures

Concrete moment resisting frame (MRF) buildings are structural systems of beams and columns resisting lateral loads. Reinforced Concrete (RC) flat slab structures often are designed to provide lateral resistance only along the perimeter of structure using perimeter MRFs so the interior frames are designed primarily for gravity loads without beams. Buildings designed based on the previous building codes had severe damage during earthquakes of moderate to high intensity. Typical damage included failure of column lap splices, strong beam/weak column failures, captive column failures,

punching shear failures in flat slabs, and shear and axial load failure of columns with wide transverse reinforcement spacing.

Many concrete flat slab MRF structures suffered due to inadequate strength and ductility from the past earthquakes (Shepherd et al. 1990, Osteraas et al. 1996, and EQE International Inc. 1989, 1994, 2001). For example, the Holiday Inn, a seven-story concrete flat slab building with perimeter frames built in 1966, had severe structural damage during the 1994 Northridge earthquake. Damage included shear failure and buckling failure of concrete columns. Minor concrete spalling and flexural cracks was observed in several spandrel beams. In addition, many shear cracks were observed at the lower stories.

Many cases of damage due to a punching shear failure were also observed during the past earthquakes. There were hundreds of wood-frame apartment and condominium buildings in the San Fernando Valley and the City of Santa Monica constructed on concrete flat slabs over parking garages. The deficiencies at roof and floor slabs included insufficient detailing at diaphragm openings and slabs doweled into frames without hooks. Punching shear failure occurred at column-slab joints with 45 degree cracks propagating at openings and re-entrant corners during the 1994 Northridge earthquake.

1.2.1.2. Damage to Tilt-Up Concrete Structures

Many tilt-up structures were damaged during previous earthquakes including the 1964 Alaska earthquake, the 1971 San Fernando earthquake, the 1987 Whittier Narrows

earthquake, the 1989 Loma Prieta earthquake, and the 1994 Northridge earthquake (Hamburger et al. 1988, Adham et al. 1990, Carter et al. 1993, Shepherd 1990, EQE International Inc. 1994). Typical damage includes tearing and collapse of roof diaphragms, collapse of wall panels due to connection failures, and concrete panel separation. Based on previous research (Wallace et al. 1999, Johnson and Fonseca 1998, SEAONC 2001), the horizontal response of the diaphragm can be fairly large compared to that of the in-plane concrete wall panels. Due to the large horizontal response of the diaphragm, damage can include large out-of-plane deflections of wall panels and separation of the panels and diaphragms. Therefore, the shear capacity of the diaphragm against the horizontal response and the capacity of connections between the diaphragm and out-of-plane walls are critical for acceptable seismic performance under severe lateral loads. In addition, typical damage observations have included splitting cracks in the pilasters at the glulam beam seats, out-of-plane bending cracks in the wall panels and pilasters, leakage from separation of joints in the sprinkler pipes, failure of ties between the subdiaphragms and the wall panels, and failure of suspended ceilings.

Thurston (1990) summarized the major factors affecting the structural performance, as well as the potential failure mechanisms for tilt-up concrete buildings. According to Thurston (1990), because there is little or no structural redundancy for typical tilt-up buildings, the ultimate strength and ductility of the connections between rigid walls and a flexible diaphragm are critical. It is noted that the design capacity of diaphragm-to-wall connections was improved by the Uniform Building Code (ICBA 1991) after the damage to tilt-up concrete structures in the Western U.S. However, there

are still many existing buildings designed according to the previous specifications such that the seismic design forces are lower than the current requirement.

1.2.2. Identification of Case Study Structures

The concrete building inventory data for Shelby County, Tennessee, is evaluated to identify parameters that describe the most typical concrete building structures in this region. Figure 1.1 shows the distribution of concrete structures based on the inventory data developed by French (2004). According to this data, tilt-up concrete is the most common type of concrete structure in this area. The total number of tilt-up concrete structures is 1060 out of 1776 concrete structures (59.7 percent) in Shelby County, Tennessee, with many more throughout Mid-America and other regions of the U.S. The second most common type of structure in this region is the concrete moment resisting frame (MRF) with 461 structures out of 1776 (26.0 percent).

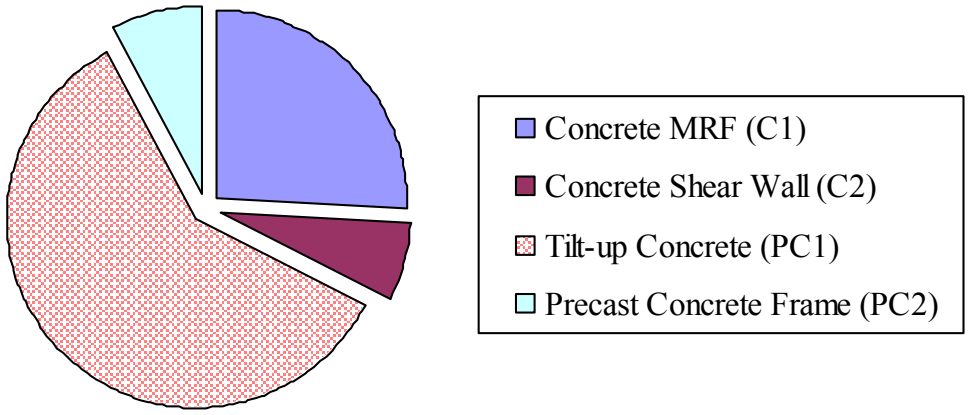

Fig. 1.1. Distribution of concrete building structures in Shelby County, Tennessee

Based on this database, tilt-up concrete buildings are generally one-story and used as industrial buildings. On the other hand, the customary story distribution of concrete MRF structures ranges from one story to five stories, and these structures are used most commonly as multi-residential and office buildings.

1.2.3. Evaluation of Seismic Performance

ASCE/SEI 41-06 (ASCE 2007), formerly FEMA 356 (ASCE 2000), is a standard covering general information and a methodology for the seismic rehabilitation of existing building structures. This document can be used to evaluate the expected seismic performance of existing structures using performance levels that are defined qualitatively. ASCE/SEI 41-06 provides analytical procedures and criteria for the performance-based evaluation of existing buildings and the design of seismic rehabilitation alternatives. Structural performance levels in ASCE/SEI 41-06 include Immediate Occupancy (IO), Life Safety (LS), and Collapse Prevention (CP). Structures at IO should have only minor damage, while structures at LS may have sustained significant damage but still provide an appreciable margin against collapse. Structures at CP are expected to remain standing but with little margin against collapse.

Many research studies have been conducted on the seismic performance evaluation of concrete structures. For a RC flat slab MRF structure, Hueste and Bai (2007a,b) evaluated the seismic performance based on the ASCE/SEI 41-06 global-level and member-level criteria. Punching shear drift limits were considered to establish an upper bound drift limit for CP due to damage to the interior slab-column frame system.

Several seismic retrofit techniques were applied to the original structure to improve the seismic performance.

A limited number of studies have focused on seismic evaluation of tilt-up concrete structures (Carter et al. 1993, Wood and Hawkins 1994, Fonseca 1997, Johnson and Fonseca 1998, Wallace et al. 1999). However, few studies have evaluated the expected seismic performance and fragility of typical tilt-up structures in the Central U.S. In addition, only general component-level recommendations for tilt-up buildings are included in ASCE/SEI 41-06 (ASCE 2007).

1.2.4. Estimation of Seismic Fragility

The fragility of a structure is defined as the conditional probability of attaining or exceeding a particular performance level for a specified seismic demand, such as the spectral acceleration (S_a). Therefore, the evaluation of the seismic fragility of a structure requires knowledge of the structural capacity and the response under a certain seismic demand.

Research related to seismic vulnerability and the methodology of developing fragility curves has been actively conducted in the past several years. Cornell et al. (2002) developed a probabilistic framework for seismic design and assessment of structures and applied this framework to steel moment-resisting frame buildings. Demand and capacity were expressed in terms of the maximum interstory drift ratio with a nonlinear dynamic relationship. In addition, probabilistic models for structural demand and capacity were used to include uncertainties.

Gardoni et al. (2002, 2003) developed multivariate probabilistic capacity and demand models for RC bridges that account for the prevailing aleatory and epistemic uncertainties. A Bayesian approach was used to account for different types and sources of information including lower and upper bound data. The fragility of structural components and systems were estimated. Point and predictive fragilities were revealed as well as confidence intervals that reflect the influence of the epistemic uncertainties.

Rossetto and Elnashai (2003) categorized recent research into four methodologies: empirical, judgmental, analytical, and hybrid fragility estimation. Empirical fragility estimation is a method to develop fragility curves based on real observation data such as post-earthquake surveys. This source is the most realistic; therefore, the empirical fragility curves reflect many effects including soil-structure interaction, site, source and path characteristics. For example, Shinozuka et al. (2000) developed empirical fragility curves for the Hanshin Expressway Public Corporation's (HEPC's) bridges following the 1995 Kobe earthquake. However, this procedure can be applied only to regions and structures for which earthquake data are available.

Judgmental fragility estimation is a method based on experts' opinions and their predictions to generate fragility relationships. The damage probability matrices and vulnerability curves in ATC-13 (ATC 1985) and ATC-40 (ATC 1996) are based on judgment. This approach has large uncertainties and does not use the available objective information like laboratory experiment or field measurements.

Analytical fragility curves are developed using structural responses from simulations of analytical models with seismic loads. For example, Dumova-Jovanoska

(2000) developed analytical fragility curves for two RC structures (6-story and 16-story frame structures) in Skopje, Macedonia, using 240 synthetic ground motion data for this region. The fragility curves were developed using discrete damage states from the damage index defined by Park et al. (1985). Analytical fragility estimation can reduce bias and limitations in the seismic vulnerability assessment. However, this method still has modeling uncertainties due to assumptions in the analytical models, ground motion characteristics, structural analysis programs, and damage models.

1.2.5. Development of a Probabilistic Framework to Assess Structural Losses

Several research studies have been conducted to assess the direct losses due to structural damage during a seismic event. The HAZUS (FEMA 2010) program can be used to estimate potential losses at a regional scale due to various hazards including floods, earthquakes, and hurricanes. The HAZUS methodology provides estimates of losses due to structural and nonstructural damage in terms of repair costs, expressed as a percentage of building replacement costs. The repair costs are provided by building occupancy class and model building type.

The Applied Technology Council (ATC) conducted surveys on building structures after the Northridge, California, earthquake of January 17, 1994. The outcomes of this survey were documented in the ATC-38 report (ATC 2000). Four categories of qualitative damage states were used for the overall damage inspection: “None,” “Insignificant,” “Moderate,” and “Heavy.” In addition to the overall damage

rating, the same group of engineers categorized the building damage using the damage states provided in ATC-13 (ATC 1985).

The National Center for Earthquake Engineering Research (NCEER) conducted the Loss Assessment of Memphis Buildings (LAMB) project to estimate economic losses due to structural damage in the Memphis Region (Abrams and Shinozuka 1997). In the LAMB study, average loss factors were developed based on the ATC-13 (ATC 1985) methodology and preliminary ATC-38 damage data. According to the LAMB study, average loss factors for repair cost increase as the overall damage state increases. However, for higher damage, loss factor values were quite low for the expected repair costs. In addition, the central damage factors for higher damage from the LAMB study were also relatively small numbers for structures that may have heavy damage.

1.2.6. Assessment of Seismic Losses Using Scenario Earthquakes

Bartoletti and Pierepiekarz (2006) documented a research project on simulating a scenario with a magnitude 6.7 earthquake on the Seattle Fault conducted by the Structural Engineers Association of Washington through the Earthquake Engineering Committee. In this project, total losses due to the scenario earthquake were estimated using HAZUS. Essential facilities including hospitals, fire stations, police stations, and schools were also considered. According to Bartoletti and Pierepiekarz (2006), unreinforced masonry (URM) buildings and older tilt-up concrete buildings were shown to be the most vulnerable structures. Low-rise and mid-rise concrete frame structures also sustained severe damage under the scenario earthquake.

1.3. Proposed Methodology

The objectives of this study are to evaluate seismic performance and estimate the seismic vulnerability of concrete structures in the Mid-America Region through seismic fragility analysis and to assess the structural losses due to potential future seismic events. Five tasks are proposed to accomplish the above objectives. Details of the five tasks are summarized below.

1.3.1. Task 1: Identification of Case Study Structures

The two most representative types of concrete buildings in the Mid-America Region based on the building inventory data developed by French (2004) are considered: tilt-up concrete structures and RC flat slab MRF structures. Based on this building inventory data, the tilt-up concrete structure is selected as an industrial one-story building, while the RC flat slab MRF structure is selected as a low to moderate rise office building. Details of each case study structure are described below.

In the proposed study, one-story tilt-up concrete structures with a metal deck roof diaphragm system are selected. Two different aspect ratios of diaphragm dimension are selected based on the previous studies (Carter et al. 1993, Fonseca et al. 1996, Wallace et al. 1999): 1.4:1 and 4:1. When the aspect ratio is large, the relative flexibility of the diaphragm action causes structural behavior to fluctuate. The structures are designed according to the load requirements of the 1990s building code used in this region. The seismic design provisions that were adopted in the previous code have since been

updated; therefore, the seismic design forces are significantly lower than what is now required by the IBC 2009 for the Mid-America Region.

The second type of case study structure is a RC flat slab MRF structure not specially detailed for ductile behavior. Low to mid-rise flat-slab buildings were found to be of particular interest because of their prevalence in the Mid-America Region and the concern for potential damage to this type of structure during an earthquake of moderate intensity. The structure is designed according to the load requirements of the 1980s building code used in this region. The seismic fragility analysis for a five-story RC flat slab structure was already evaluated in previous studies (Hueste and Bai 2007a,b). In the proposed study, a two-story RC flat slab structure is selected as representative of low-rise buildings. The analysis of the five-story structure is updated to include a bilinear demand model to obtain a better fit with the response data and to incorporate lower bounds data for response data that are outside the calibration range of the model (Ramamoorthy et al. 2006).

1.3.2. Task 2: Evaluation of Seismic Performance

The push-over and nonlinear dynamic analyses are performed using finite element analysis software to evaluate the seismic performance of the case study buildings. To predict the response of the selected structures during an earthquake, representative earthquake data for that location should be used. However, there is not adequate recorded ground motion data to characterize the high seismicity of specific locations in the Mid-America Region. Therefore, synthetic ground motions for Memphis,

Tennessee, developed by Rix and Fernandez (2010) are used in this study. A total of 40 ground motions are provided for each of two earthquake hazard levels, one with 2% and one with 10% probability of exceedance in 50 years. Each hazard level has 20 ground motions for each of two types of soil conditions (lowlands and uplands) for Memphis, Tennessee.

Because the failure mechanisms for the two types of case study structures are not the same, different parameters representing the structural behavior are considered. According to ASCE/SEI 41-06 (ASCE 2007), potential failures in flexure and shear should be considered to estimate the maximum interstory drift as well as the maximum shear force. In addition, punching shear failures are evaluated for the flat slab buildings. The behavior of tilt-up concrete structures is governed by force-controlled mechanisms and the major concerns are the connection between the concrete wall panels and the roof diaphragm, and the in-plane strength of the diaphragm. Therefore, those components are considered as critical elements for assessing damage. The diaphragm drift ratio (DDR) is also assessed to check for unseating of open-web joists.

1.3.3. Task 3: Estimation of Seismic Fragility

The goal of this task is to construct fragility curves for the selected structures by developing probabilistic demand and capacity models. Fragility curves are developed using performance levels from ASCE/SEI 41-06 as well as performance levels based on additional quantitative limits.

To develop fragility curves, several parameters are needed, including structural response characteristics, earthquake intensities, and uncertainties for capacity and demand. More detailed seismic demand models are developed using the synthetic ground motion data developed by Rix and Fernandez (2010). Different factors are used to develop the demand models for the two case study structures. For RC flat slab structures, the maximum drift value is used to develop probabilistic demand models. However, the maximum forces are likely be the critical parameter for constructing the demand models for tilt-up concrete structures. The bilinear demand model and the proper accounting of lower bound data developed by Ramamoorthy et al. (2006) can be used to reduce errors and represent data better if it is needed.

Relationships to describe the seismic fragility curves for each structure type are investigated. The number of stories is considered as a main parameter for the RC flat slab structure, while aspect ratio is the main parameter for the tilt-up concrete structures.

1.3.4. Task 4: Development of a Probabilistic Framework to Assess Structural Losses

The goal of this task is to propose a more suitable set of structural damage state descriptions and develop a probabilistic methodology for estimating structural losses. The ATC-38 damage state classification is modified to provide more refinement for higher levels of damage where the damage factors have a larger range.

A probabilistic framework for assessing structural losses due to seismic events is proposed. The framework includes damage state classifications based on the ATC-13

and ATC-38 damage states and the ATC-38 database of building damage. Damage factors are given for each damage state to quantify structural damage as a percentage of building replacement cost. To account for the inherent uncertainties, these factors are described using a Beta distribution.

A set of fragility curves quantifying the seismic vulnerability of a building can then be mapped onto the proposed damage framework to determine the expected structural damage in monetary terms. The total damage factor for a given seismic intensity is then calculated using a probabilistic approach. Confidence and prediction bands are also be constructed to account for the prevailing uncertainties. The prediction and confidence bands can be constructed using different percentiles to reflect different levels of confidence.

1.3.5. Task 5: Assessment of Seismic Losses Using Scenario Earthquakes

The goal of this task is to develop a scenario-based assessment for moderate to high intensity earthquakes in the Mid-America Region. The scenario earthquakes have magnitude 5.5, 6.5, and 7.5 and they are assumed to occur near Shelby County, Tennessee. The buildings considered are limited to the same types considered in this study. Seismic vulnerability of the structures is estimated and structural losses due to these events are assessed. Through this scenario-based application, decision makers in the Mid-America Region including government officials, business owners, emergency managers and engineers, can predict structural damage due to possible seismic events,

estimate expected losses more accurately, and determine whether seismic retrofitting is beneficial for high risk structures.

1.4. Dissertation Outline

This dissertation is organized into the following sections. Section 2 provides sets of seismic fragility curves for reinforced concrete (RC) frame buildings. This section proposes a methodology describing how to develop seismic fragility curves using story-specific demand models for multi-story building structures. In Section 3, the seismic vulnerability of tilt-up concrete buildings are assessed and the impact of different aspect ratio on fragility estimates is determined. Section 4 provides a probabilistic framework to assess structural damage for structural systems. In Section 5, seismic losses are estimated based on three scenario earthquakes in Mid-America. All the fragility curves and the framework for assessing structural damage developed in earlier sections are implemented into open-source loss estimation software and the corresponding seismic losses are estimated for scenario earthquakes. Finally, Section 6 summarizes the research and draws conclusions, as well as discusses the suggestions for future research. Additional information is provided in the Appendices.

2. SEISMIC VULNERABILITY ASSESSMENT FOR REINFORCED CONCRETE FRAME BUILDING STRUCTURES*

2.1. Introduction

Seismic fragility analysis can be used to evaluate the performance and vulnerability of structures under earthquake events. It plays an important role in estimating seismic losses and in the decision making process based on building performance during seismic events. To develop seismic fragility curves, structural capacity limits and demand models are needed.

Traditionally, seismic demand models have been developed based on the overall maximum interstory drift over the height of a building. The overall maximum interstory drift is a convenient measure to describe the structural response of a building to lateral loads. However, for multi-story buildings, fragility estimates developed using only the overall maximum interstory drift may not reflect the actual vulnerability of a building. This is because there is only one limit state function defined based on the overall maximum interstory drift. To assess the probability that any interstory drift exceeds a specified limit for a given structural performance level, it is important to evaluate the specific drift demand for each story within the structure. This section develops story-specific demand models that consider the maximum interstory drift of each story. A Bayesian approach is used to estimate the unknown parameters in the proposed demand

*Reprinted with permission from "Story-specific demand models and seismic fragility estimates for multi-story buildings" by Bai, J.-W., Gardoni, P., and Hueste, M.B.D., 2011, *Structural Safety*, 33, 96-107, Copyright © 2011, Elsevier.

models. The computation of the posterior statistics is carried out using an adaptive Markov Chain Monte Carlo (MCMC) simulation technique (Laine 2008).

Finally, the fragility estimates for two example buildings are developed based on the proposed story-specific demand models and compared with the traditional fragility estimates computed based on a demand model for the overall maximum interstory drift. The results show that traditional fragility estimates may underestimate the actual vulnerability of a building, especially when the interstory drifts for one or more stories are close to the maximum value.

2.2. Seismic Fragility Analysis

Seismic fragility is defined as the conditional probability of attaining or exceeding a specific performance level for a given earthquake intensity, such as spectral acceleration S_a. In general, the fragility can be written as

$$F\left(S_a;\boldsymbol{\Theta}\right)=P\left[g\left(S_a;\boldsymbol{\Theta}\right)\le 0\middle|S_a\right] \tag{2.1}$$

where $g(S_a;\boldsymbol{\Theta})=C-D(S_a;\boldsymbol{\Theta})$ is a limit state function used to define the failure event, C and D represent the drift capacity and demand of the building, respectively, and $\boldsymbol{\Theta}$ is a vector of unknown parameters in the demand model.

Wen et al. (2004) developed the following approximate equation to estimate $F(S_a;\boldsymbol{\Theta})$:

$$F\left(S_a;\boldsymbol{\Theta}\right)\cong 1-\Phi\left(\frac{\lambda_C-\lambda_D}{\sqrt{\sigma_D^2+\sigma_C^2+\sigma_M^2}}\right) \tag{2.2}$$

where λ_C is the median capacity limit for a given performance level in the logarithmic space; λ_D is the median drift demand given S_a in the logarithmic space; σ_D and σ_C represent the uncertainties associated with the demand and capacity, respectively; and σ_M is the modeling uncertainty.

As shown in Equation (2.1), probabilistic capacity and demand models are needed to develop seismic fragility curves. Traditionally, the overall maximum interstory drift experienced over the different stories has been used as a measure of the building response (Wen et al. 2004, Cornell et al. 2002, Ramamoorthy et al. 2006, Ramamoorthy et al. 2008, Ellingwood et al. 2007, Hueste and Bai 2007b, Ay and Erberik 2008). However, the structural behavior of a multi-story building tends to be more complex. Based on traditional approaches, the seismic fragility may be underestimated, particularly if the interstory drifts for one or more stories are close to the overall maximum interstory drift of the building. Therefore, to assess the conditional probability that any interstory drift exceeds a specified capacity limit, the drift demand for each story within the structure should be evaluated. In this section, story-specific demand models are developed as the maximum interstory drift for each story for a given S_a.

2.3. Probabilistic Demand Models

2.3.1. Overall Maximum Demand Models

Probabilistic demand models have been developed to describe the relationship between earthquake intensity, the spectral acceleration (S_a), and the overall maximum interstory drift over the height of a building (e.g., Ramamoorthy et al. 2006, Ramamoorthy et al. 2008). Equation (2.3) shows the model form of a probabilistic linear model.

$$D(S_a;\boldsymbol{\Theta}) = \theta_0 + \theta_1 \ln(S_a) + \sigma\varepsilon \tag{2.3}$$

where $D(S_a;\boldsymbol{\Theta}) = \ln[\delta(S_a;\boldsymbol{\Theta})] =$ natural logarithm of the drift demand, $\boldsymbol{\Theta} = (\theta_0, \theta_1, \sigma)$ is a vector of unknown parameters; ε is a random variable representing the error in the model with zero mean and unit standard deviation; and σ is the standard deviation of the model error. The logarithmic transformation is used to approximately satisfy the normality assumption (i.e., ε has the Normal distribution) and the homoskedasticity assumption (i.e., σ is constant). Based on Equation (2.3), $\lambda_D = \theta_0 + \theta_1 \ln(S_a)$.

Ramamoorthy et al. (2006 and 2008) found that the formulation in Eq. (2.3) tends to underestimate the drift demand for small and large values of S_a, and to overestimate the drift demand for intermediate values of S_a. In response to this observation, Ramamoorthy et al. (2006 and 2008) developed bilinear probabilistic models that provide a better fit over the entire range of S_a. The bilinear model can be written as

$$D_1(S_a;\boldsymbol{\Theta}_1)=\theta_{10}+\theta_{11}\ln(S_a)+\sigma_1\varepsilon_1 \qquad S_a \le \theta_{S_a}$$
$$D_2(S_a;\boldsymbol{\Theta}_2)=\left(\theta_{10}+\theta_{11}\times\theta_{S_a}\right)+\theta_{21}\left[\ln(S_a)-\theta_{S_a}\right]+\sigma_2\varepsilon_2 \qquad S_a > \theta_{S_a} \tag{2.4}$$

where the terms in Equation (2.4) have definitions analogous to those in Equation (2.3). In particular, Figure 2.1 illustrates the definition of each model parameter in the bilinear model.

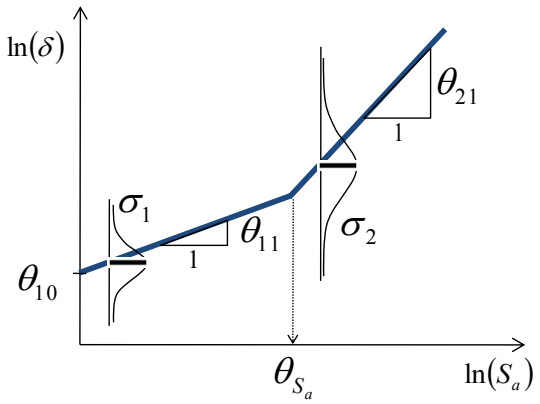

Fig. 2.1. Illustration of the parameters in the bilinear model

2.3.2. Story-Specific Demand Models

The general formulation for bilinear probabilistic models to develop story-specific demand models is adopted to estimate the drift demand for each story within the structure for a given S_a. In addition, the correlations among individual model errors are considered to properly capture their potential dependence. The story-specific demand models are written as

$$D_{1,j}(S_a;\boldsymbol{\Theta}_{1,j})=\theta_{10,j}+\theta_{11,j}\ln(S_a)+\sigma_{1,j}\varepsilon_{1,j} \qquad S_a \le \theta_{S_a}$$
$$D_{2,j}(S_a;\boldsymbol{\Theta}_{2,j})=\left(\theta_{10,j}+\theta_{11,j}\times\theta_{S_a}\right)+\theta_{21,j}\left[\ln(S_a)-\theta_{S_a}\right]+\sigma_{2,j}\varepsilon_{2,j} \qquad S_a > \theta_{S_a} \tag{2.5}$$

where $\varepsilon_{1,j}$ and $\varepsilon_{1,k}$ have correlation $\rho_{1,j,k}$, $\varepsilon_{2,j}$ and $\varepsilon_{2,k}$ have correlation $\rho_{2,j,k}$, and j and k indicate the specific story. It is assumed that θ_{S_a} is the same for each story-specific demand model because story responses are correlated with each other for a given S_a.

2.4. Assessment of Demand Models

2.4.1. Bayesian Parameter Estimation

The unknown parameters $\boldsymbol{\Theta}$ are estimated using the Bayesian updating rule (Box and Tiao 1992).

$$f(\boldsymbol{\Theta}) = \gamma L(\boldsymbol{\Theta}) p(\boldsymbol{\Theta}) \tag{2.6}$$

where $p(\boldsymbol{\Theta})$ is the prior distribution of $\boldsymbol{\Theta}$, which is based on previous knowledge before obtaining the observation; $L(\boldsymbol{\Theta})$ is the likelihood function representing the objective information on $\boldsymbol{\Theta}$, which is proportional to the conditional probability for given values of $\boldsymbol{\Theta}$; γ is a normalizing factor; and $f(\boldsymbol{\Theta})$ is the posterior distribution of $\boldsymbol{\Theta}$ that incorporates the prior information in $p(\boldsymbol{\Theta})$ and the information from the observation. The mean vector, $\mathbf{M}_{\boldsymbol{\Theta}}$, and the covariance matrix, $\boldsymbol{\Sigma}_{\boldsymbol{\Theta}\boldsymbol{\Theta}}$, can be obtained once $f(\boldsymbol{\Theta})$ is known. In the analysis presented in this section, a non-informative prior distribution is assumed to reflect that there is little or no information available about $\boldsymbol{\Theta}$ before collecting the observation.

The posterior statistics of the unknown model parameters are obtained using an adaptive MCMC simulation method, the DRAM method, which combines the Delayed Rejection (DR) method and the Adaptive Metropolis (AM) (Laine 2008). Markov chains are generated with the likelihood formulation of the demand models based on the initial points and non-informative prior distribution until a convergence criterion is met. To check the convergence of the simulated Markov chains, the Geweke convergence criterion is used (Geweke 1992). It is based on the comparison between the mean values of the first 10% and last 50% of the samples. If the difference of the mean values is less than 5%, the MCMC simulation is terminated.

2.4.2. Virtual Experimental Data

Two representative structures are selected to assess the proposed demand models: a two-story and a five-story reinforced concrete (RC) flat slab office building typical of those in the Central United States (U.S.). These buildings represent a significant number of low- to mid-rise structures in this region constructed during the early 1980s. Design load requirements are based on the ninth edition of the Building Officials and Code Administrators (BOCA) Basic/National Code (BOCA 1987), in which St. Louis, Missouri, and Memphis, Tennessee are considered to be in Seismic Zone 1. The structural member design follows the provisions of the American Concrete Institute (ACI) Building Code Requirements for Reinforced Concrete, ACI 318-83 (ACI Committee 318 1983). The first story is 4.58 m high, and the height of the remaining stories is 3.97 m. The buildings are rectangular in plan with a length of 42.7 m and a

width of 34.2 m. The bay size is 8.54 × 8.54 m. The slab thickness is 254 mm, and the columns are 406 × 406 mm and 508 × 508 mm for the two-story and five-story buildings, respectively. The buildings have a moment frame system, not specially detailed for moderate to severe earthquakes. The floor system is composed of an interior flat slab with shear capitals and perimeter moment resisting frames with spandrel beams. Figure 2.2 shows a plan view of the selected buildings.

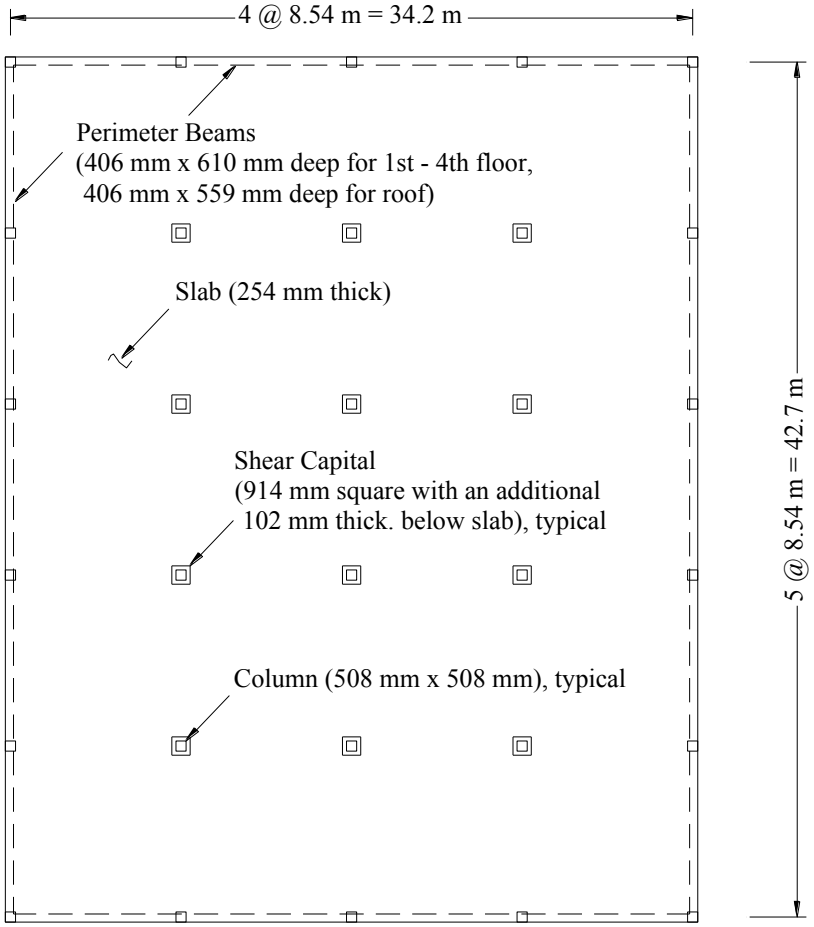

Fig. 2.2. Plan view of selected buildings (five-story building)

The selected structures are analyzed using ZEUS-NL, a finite element structural analysis program developed for nonlinear dynamic, conventional and adaptive push-over, and eigenvalue analyses (Elnashai et al. 2002). The program uses a fiber element approach where the cross-sections are divided into fibers monitoring the confined concrete section, the unconfined concrete cover, and the steel reinforcement. A two-dimensional analytical model is used, which is adequate for the regular floor plan of the selected buildings. The model takes advantage of the building's symmetry, and only half of the structure is analyzed. One exterior frame and two interior frames oriented along the short direction of the building are linked with rigid truss elements such that only lateral forces and displacements are transmitted between frames. Rigid zones are used to define the joint regions, and the inelastic behavior is monitored outside the joint.

Fundamental periods are important parameters to quantify the seismic demand of the structure. In this study, the fundamental periods of the selected structures are computed based on the cracked section properties and the values are 0.914 *s* and 1.62 *s* for the two-story and five-story buildings, respectively. More details about the design requirements and analytical modeling are found in Hueste and Bai (2007a).

2.4.3. Ground Motion Records

Because strong ground motion records for the Central U.S. are not available, synthetic ground motions developed specifically for this region are used for the dynamic analyses and seismic performance evaluation of the selected structures. Two sets of ground motions for Memphis, Tennessee, are used. The first ground motion set consists of a

suite of synthetic records based on stochastic ground motion models for different scenarios, developed by Rix and Fernandez (2004). The second ground motion set consists of a suite of synthetic records for two earthquake hazard levels, developed by Rix and Fernandez (2010).

For the first set, two source models were considered, one according to Atkinson and Boore (1995) and one according to Frankel et al. (1996). The two sources were used to capture the impact of modeling uncertainty. This study uses the synthetic ground motions for a body wave magnitude equal to 5.5, 6.5 and 7.5, and a hypocentral distance equal to 20 km. Twenty ground motions are available for each body wave magnitude and source model combination, giving a total of 120 ground motions.

For the second set, a total of 40 ground motions are provided for each of two earthquake hazard levels, one with 2% and one with 10% probability of exceedance in 50 years. Each hazard level has 20 ground motions for each of two types of soil conditions (lowlands and uplands) for Memphis, Tennessee. These motions reflect more recent attenuation relationships for the soil condition and the effect of soil nonlinearity in the site response parameters than the first set of motions. Therefore, a total of 160 records, from the two sets of ground motions, are used in this study.

2.4.4. Story-Specific Responses

To account for the story-specific responses, the maximum interstory drift values for each story are considered. Figures 2.3 and 2.4 show the maximum interstory drift values in a logarithmic space for the two-story and five-story buildings, respectively.

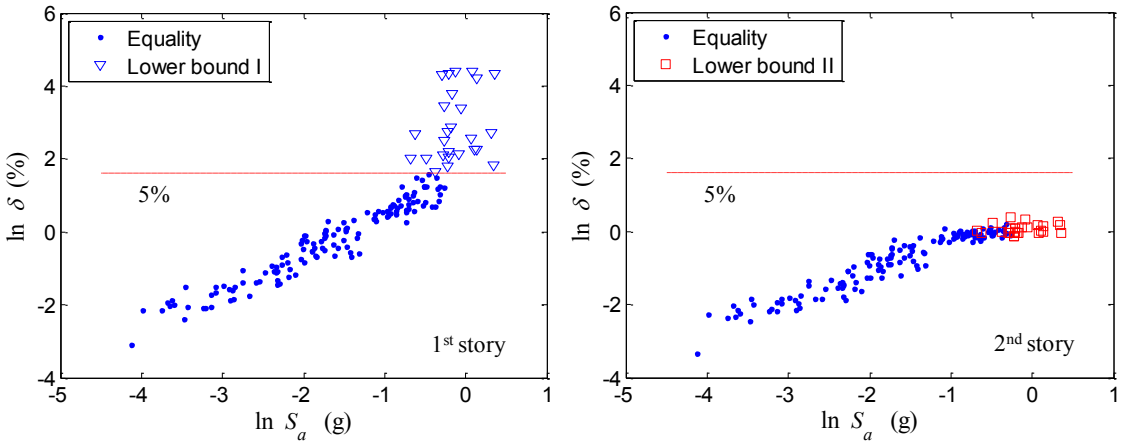

Fig. 2.3. Story-specific responses for two-story building

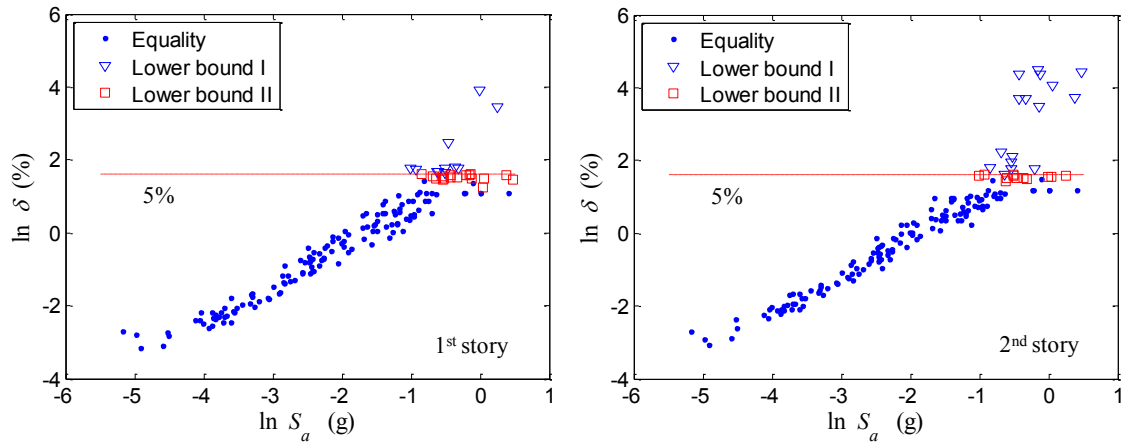

Fig. 2.4. Story-specific responses for five-story building

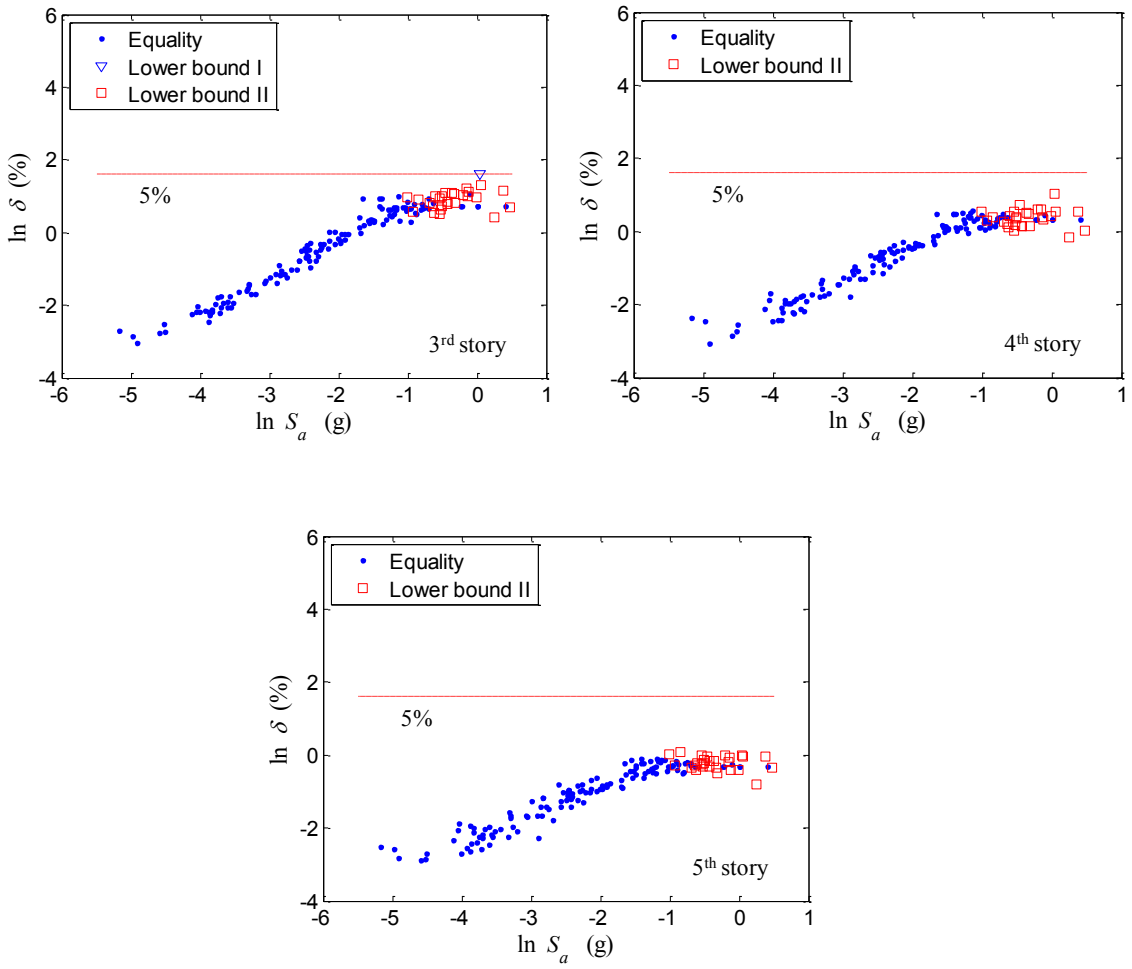

Fig. 2.4. Continued

Some maximum interstory drift values determined by the dynamic analysis are relatively large, corresponding to earthquake intensities that are also quite large. Based on experimental data for punching shear failures at the slab-column joints (Hueste et al. 2007), a 5% maximum interstory drift is selected as the threshold for valid data points. Once the maximum interstory drift for one of the stories exceeds this threshold, the responses from the dynamic analysis are deemed no longer reliable because this mode of

failure is not included in the nonlinear model. For those cases, the time when at least one of the interstory drifts exceeds 5% is determined based on the time histories of each interstory drift. The threshold drift is then taken as a lower bound data for the drift of the story that exceeded the threshold. Similarly, the maximum interstory drift values up to that time for the other stories are considered as lower bound data. In Figures 3 and 4, the dots (●) represent the equality data, while the triangles (▽) and the squares (□) represent the lower bound data. The triangles indicate the data exceeding 5% drift, and the squares indicate the corresponding lower bound data for the other stories. As shown in Figures 2.3 and 2.4, the maximum interstory drift values at the first story dominate the building responses for the two-story building. However, for the five-story building, the maximum interstory drift values at the first and second stories are close for most ground motions.

2.5. Results of Model Assessment

Three probabilistic demand models are developed for the selected buildings: (1) overall maximum linear model (OLM), (2) overall maximum bilinear model (OBM), and (3) story-specific demand models (SSM) using the bilinear formulation.

2.5.1. Overall Maximum Linear Models

Initially, a linear model based on the overall maximum interstory drift for the entire building is used to predict the seismic demand relationship. Equation (2.3) is used to predict the seismic demands. More details on the likelihood formulation and the

treatment of the lower bound data can be found in Gardoni et al. (2002). Table 2.1 shows the posterior statistics of the unknown parameters. The data for the five-story building is less dispersed than that for the two-story building, so the corresponding σ value is smaller.

Figure 2.5 shows the predicted demand (solid line) along with the one standard deviation confidence interval (dashed line) for the two-story structure (on the left) and the five-story structure (on the right). While the overall maximum linear model provides a good fit of the data, due to the lower bound data, the standard deviation tends to be overestimated for $\ln(S_a) \le -0.5$.

Table 2.1. Posterior statistics of unknown parameters for the overall maximum linear models

Building	Parameters	Mean	St. dev.	Correlation coefficient		
				θ_0	θ_1	σ
2-story	θ_0	1.74	0.0649	1.0		
	θ_1	1.14	0.0320	0.87	1.0	
	σ	0.326	0.0253	−0.31	−0.27	1.0
5-story	θ_0	1.71	0.0493	1.0		
	θ_1	0.946	0.0192	0.86	1.0	
	σ	0.261	0.0200	−0.31	−0.24	1.0

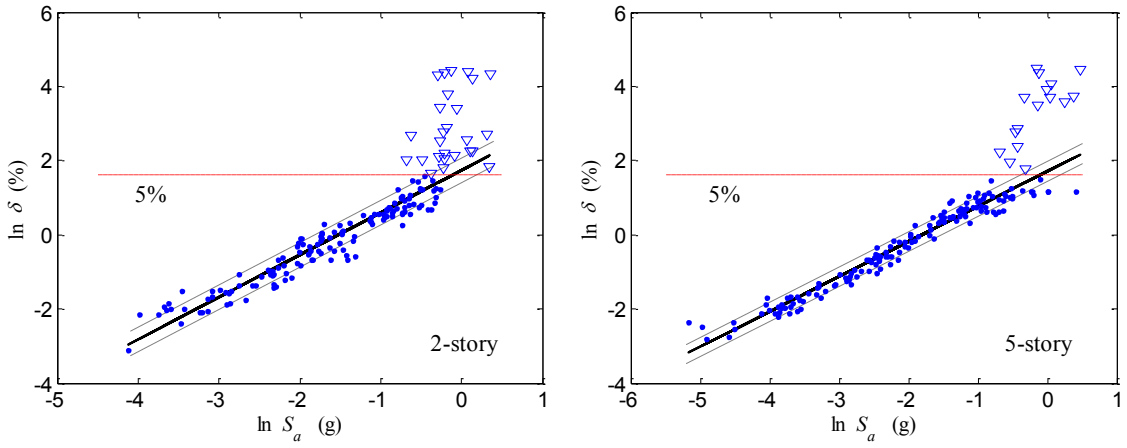

Fig. 2.5. Overall maximum linear models for the selected structures

2.5.2. Overall Maximum Bilinear Models

A probabilistic bilinear demand model is developed to more accurately predict the interstory drift demands. The bilinear models are assessed using the same overall maximum interstory drifts used to assess the linear models. The posterior statistics of the parameters, $\boldsymbol{\Theta}_1 = (\theta_{10}, \theta_{11}, \sigma_1)$ and $\boldsymbol{\Theta}_2 = (\theta_{20}, \theta_{21}, \sigma_2)$, are estimated using the adaptive MCMC method described earlier. Table 2.2 shows the posterior statistics of the unknown parameters. Figure 2.6 shows the predicted demand model for the two-story structure (on the left) and the five-story structure (on the right). The top horizontal dashed lines indicate 5% drift and the bottom dashed lines provide the location of the transition point between the first and second branches.

Table 2.2. Posterior statistics of unknown parameters for the overall maximum bilinear models

Building	Parameters	Mean	St. dev.	Correlation coefficient					
				θ_{10}	θ_{11}	σ_1	θ_{20}	θ_{21}	σ_2
2-story	θ_{10}	1.50	0.0555	1.0					
	θ_{11}	1.04	0.0254	0.91	1.0				
	σ_1	0.285	0.0202	−0.0067	0.031	1.0			
	θ_{20}	0.757	0.0691	0.74	0.69	−0.031	1.0		
	θ_{21}	2.44	0.413	−0.043	0.072	0.057	0.35	1.0	
	σ_2	0.490	0.0886	−0.0096	0.042	−0.017	0.33	0.63	1.0
5-story	θ_{10}	1.78	0.0476	1.0					
	θ_{11}	0.969	0.0179	0.91	1.0				
	σ_1	0.214	0.0143	−0.013	−0.0077	1.0			
	θ_{20}	0.980	0.0958	0.28	0.23	0.21	1.0		
	θ_{21}	0.924	0.184	−0.26	−0.22	0.0039	−0.071	1.0	
	σ_2	0.481	0.0961	−0.037	−0.030	0.012	0.26	0.40	1.0

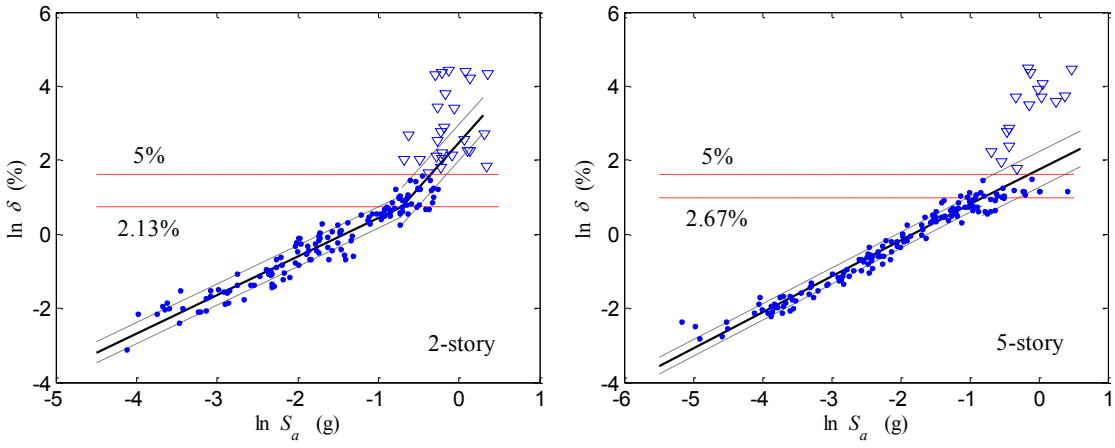

Fig. 2.6. Overall maximum bilinear models for the selected structures

For the two-story building, the overall maximum bilinear demand models provide a better fit to the drift demand over the entire range of S_a. The slope for the second branch is steeper than that for the first branch to capture the highly nonlinear behavior of the building at larger values of S_a. It is also noted that not only does the bilinear model provide a better fit to the data, but also it provides a more accurate account of the model uncertainties. For the five-story building, the slopes for both branches are similar and the predicted drift values are close to each other. However, the two standard deviation values in the bilinear formulation also better reflect the change in the variability of the data as a function of S_a. In the linear model, σ tends to overestimate the uncertainties in the structural responses for $S_a \le 0.49\,g$ for the two-story building and $S_a \le 0.44\,g$ for the five-story building, and to underestimate the uncertainties for higher values of S_a, providing an average account of the uncertainty

over the entire range of S_a. When using the bilinear formulation, the values of σ_1 for both buildings are smaller than σ and the values for σ_2 are larger because of the onset of nonlinearities in the structural responses. A proper account of the uncertainties inherent in the demand models is important because of their effect on the shape of the fragility curves.

2.5.3. Story-Specific Models

Story-specific demand models for each story level are developed using the bilinear formulation in Equation (2.5). Table 2.3 provides the posterior means and standard deviations of the unknown parameters for the two-story building. The posterior mean of the correlations between model errors ($\rho_{1,2,1}$ and $\rho_{2,2,1}$) are 0.922 and 0.108 for the first and second branch, respectively. The model errors for the first branch where $S_a \le 0.353g$ ($\ln(S_a) \le \theta_{S_a}$) are highly correlated. Furthermore, the slope of the second branch ($S_a > 0.353g$) is steeper than the slope of the first branch for the 1st story but less steep for the 2nd story. This is because when the 1st story behaves nonlinearly, it attenuates the demand on the 2nd story based on a mechanism similar to the one of a base-isolated structure.

Table 2.3. Posterior statistics of parameters for two-story building using story-specific models

Parameters		θ_{S_a}	$\theta_{10,j}$	$\theta_{11,j}$	$\sigma_{1,j}$	$\theta_{21,j}$	$\sigma_{2,j}$
1st story	Mean	−1.04	1.45	1.03	0.300	1.64	0.348
	St. dev.	0.00212	0.0271	0.0153	0.0109	0.0634	0.0193
2nd story	Mean		0.725	0.873	0.270	0.420	0.119
	St. dev.		0.0157	0.0112	0.0108	0.0240	0.00334

Figure 2.7 shows the probabilistic story-specific demand models for the two-story building. For the two-story building, the corresponding drift values at the transition point are 1.46% and 0.829%, respectively. By comparing Figures 2.6 and 2.7, it can be noted that the 1st story response dominates the overall behavior.

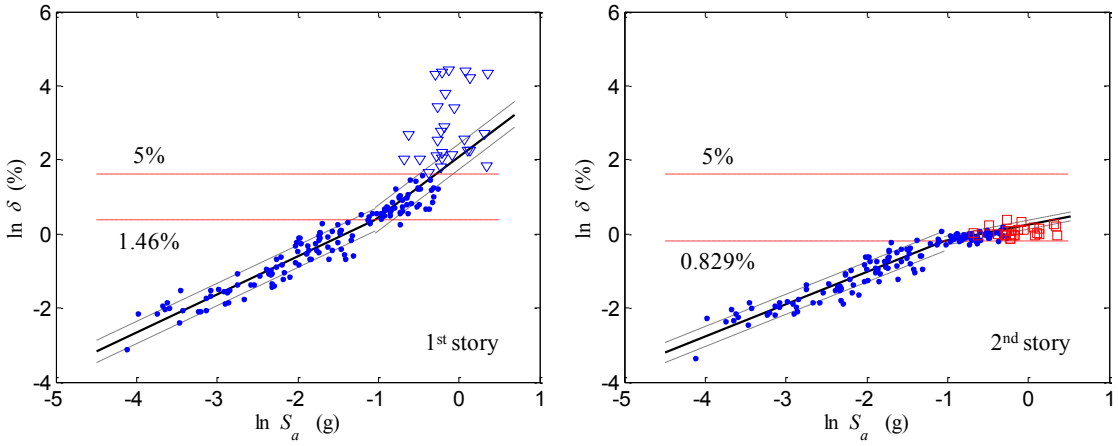

Fig. 2.7. Story-specific models for two-story building

Table 2.4 provides the posterior statistics of the unknown parameters for the five-story building using the story-specific demand models. Table 2.5 shows the posterior mean of the correlations among the individual model errors; they represent the potential

dependence between the maximum interstory drifts. The highest correlation between model errors is observed along the first branch between the 1st and 3rd story levels.

Table 2.4. Posterior statistics of parameters for five-story building using story-specific models

Parameters		θ_{S_a}	$\theta_{10,j}$	$\theta_{11,j}$	$\sigma_{1,j}$	$\theta_{21,j}$	$\sigma_{2,j}$
1st story	Mean	−1.01	1.66	1.02	0.261	1.62	0.82
	St. dev.	0.0012	0.0027	0.0018	0.0050	0.0045	0.0044
2nd story	Mean		2.02	1.04	0.211	1.13	0.595
	St. dev.		0.0020	0.0034	0.0041	0.0041	0.0026
3rd story	Mean		1.80	0.997	0.190	0.543	0.398
	St. dev.		0.0064	0.0026	0.0033	0.0025	0.0027
4th story	Mean		1.20	0.823	0.224	0.281	0.253
	St. dev.		0.0046	0.0017	0.0041	0.0026	0.0019
5th story	Mean		0.399	0.659	0.232	0.251	0.229
	St. dev.		0.0070	0.0065	0.0056	0.0045	0.0031

Table 2.5. Posterior mean of correlations for five-story building using story-specific models

Parameters	$\rho_{i,2,1}$	$\rho_{i,3,1}$	$\rho_{i,4,1}$	$\rho_{i,5,1}$	$\rho_{i,3,2}$	$\rho_{i,4,2}$	$\rho_{i,5,2}$	$\rho_{i,4,3}$	$\rho_{i,5,3}$	$\rho_{i,5,4}$
1st branch	0.106	0.679	0.628	0.189	0.408	0.490	−0.275	0.400	0.400	0.398
2nd branch	0.416	−0.282	0.299	0.395	−0.294	0.0683	−0.0854	−0.394	0.0236	−0.299

Figure 2.8 shows the probabilistic story-specific demand models for the five-story building. For the five-story building, the corresponding drift values at the transition points are 1.89%, 2.62%, 2.21%, 1.44%, and 0.764% for the 1st to 5th story,

respectively. The value for S_a is 0.364 g. The slope of the first branch is slightly increased from the 1st story to the 2nd story, and then it is decreased for the remaining story levels. For most ground motions, the maximum interstory drift values at the 1st and 2nd stories are largest, and the values for these two stories are close to each other.

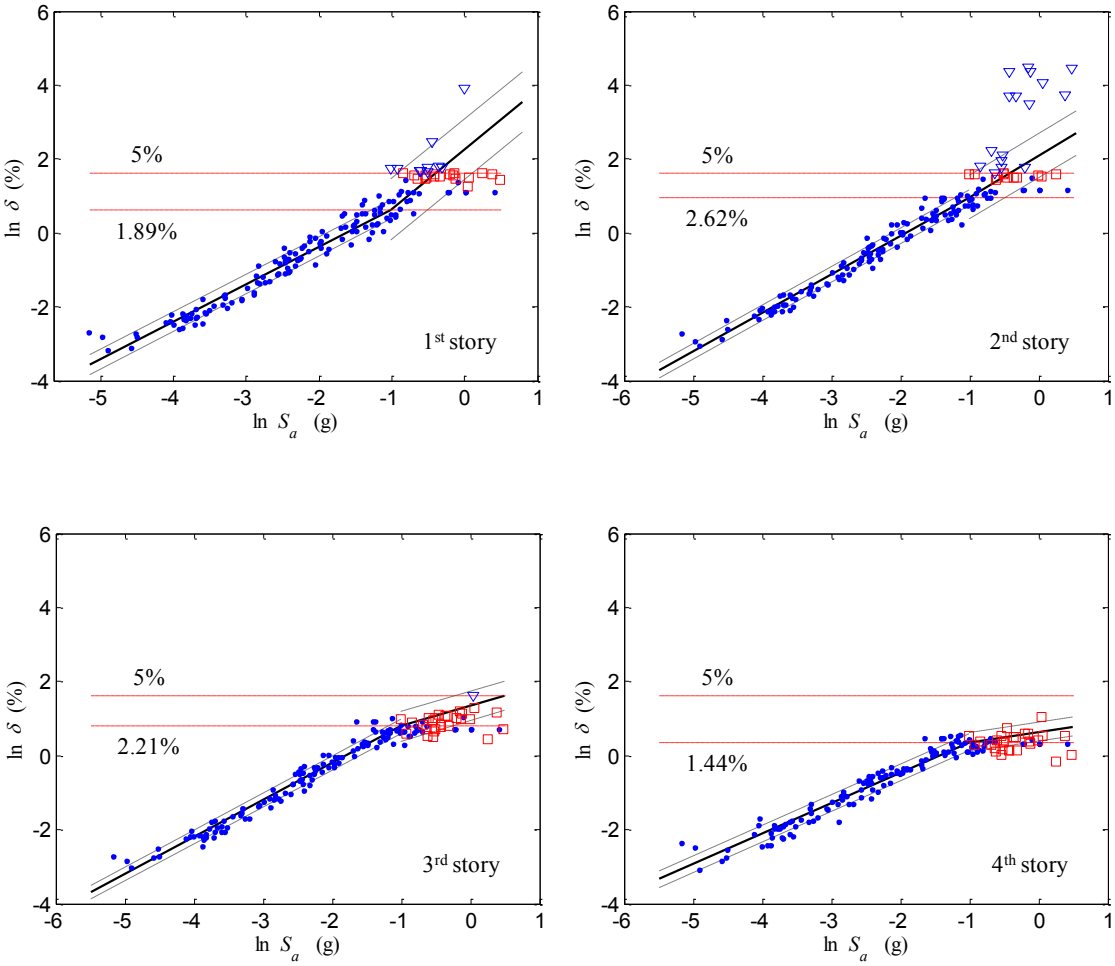

Fig. 2.8. Story-specific models for five-story building

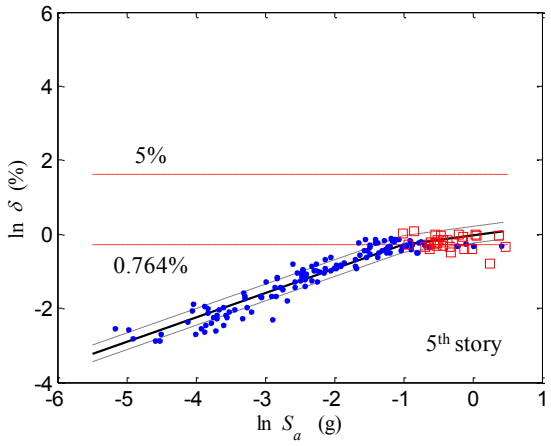

Fig. 2.8. Continued

Based on the further study on the transition point of the demand model, there is a correlation between transition points from incremental dynamic analysis (IDA) and seismic demand models. Therefore, IDA is conducted for the case study buildings and the results and figures are included in Appendix A.

2.6. Probabilistic Capacity Models

To develop fragility curves based on story-specific responses, capacity limits for each story level are needed. Several types of drift-based capacity limits related to performance levels can be considered, including limits provided in ASCE/SEI 41-06 (ASCE 2007).

ASCE/SEI 41-06 (ASCE 2007) provides guidance for the seismic evaluation and rehabilitation of existing building structures and is based on FEMA 356 (ASCE 2000). ASCE/SEI 41-06 provides approximate interstory drift limits as a function of the general

structure type and performance level. However, these limits do not account for specific member detailing. ASCE/SEI 41-06 also provides "member-level" plastic rotation limits based on specific member details. The corresponding interstory drift limits are estimates based on the plastic rotation limits provided by the ASCE/SEI 41-06. Additional quantitative limits are described by Wen et al. (2004), including first yield and plastic mechanism initiation. First yield corresponds to the interstory drift at which a structural member initiates yielding under an imposed lateral load. Plastic mechanism initiation corresponds to the interstory drift at which a story mechanism begins. To determine the interstory drift corresponding to the member-level or quantitative limits, a story-by-story push-over analysis is used (Dooley and Bracci 2001). It is noted that this loading approach may increase the potential for column yielding under a first-mode response (Elwood and Moehle 2002) and, as such, tends to provide a lower limit when used to estimate interstory drift capacity values.

Capacity limits for the entire structure are needed for the fragility curves based on the overall maximum interstory drifts, and capacity limits for each individual story level are needed for the fragility curves based on the story-specific demand models. Drift limits are determined to correspond to the three drift-based capacity limits described previously. In addition, the potential for punching shear failure is considered because RC flat slab buildings are vulnerable to punching shear under lateral movement. A set of three performance levels, and their corresponding capacity limits, are selected: first yield (FY), life safety (LS) based on the ASCE/SEI 41-06 member-level limits, and collapse prevention (CP) based on the occurrence of punching shear failure. The

corresponding median capacity limits for the selected structures are summarized in Table 2.6. Table 2.7 shows the corresponding plastic rotation limits for the LS performance level based on the ASCE/SEI 41-06 criteria. For the CP limit state, the drift limits are derived from the punching shear prediction model suggested by Hueste et al. (2007), which is based on the relationship between interstory drift limits and the gravity shear ratio (ratio of the gravity shear to the nominal two-way shear strength) at a slab-column connection. The corresponding gravity shear ratios are 0.33 and 0.39 for the two-story and five-story buildings, respectively. More details for selecting the capacity limits are found in a previous study (Hueste and Bai 2007b). Furthermore, σ_C needed in Equation (2.2) is assumed to be equal to 0.3 based on Wen et al. (2004).

Table 2.6. Selected performance levels and median capacity limits for two-story and five-story buildings

Performance level	Drift limits (%)						
	2-story		5-story				
	1st story	2nd story	1st story	2nd story	3rd story	4th story	5th story
FY	0.68*	0.87	0.36*	0.51	0.52	0.50	0.79
LS	0.99*	1.20	0.66*	0.86	0.89	0.83	0.82
CP	2.66*	2.97	2.97	2.97	2.97	2.97	2.24*

* Indicates the median capacity limits also used for the maximum interstory drift for the entire building.

Table 2.7. Plastic rotation limits for LS performance level

Structural member	Plastic rotation (rad)						
	2-story		5-story				
	1st story	2nd story	1st story	2nd story	3rd story	4th story	5th story
Beams	0.01	0.01	0.01	0.01	0.01	0.01	0.01
Columns	0.00481	0.005	0.00418	0.00453	0.00481	0.005	0.005
Slabs	0.005	0.0085	0.00825	0.00825	0.00825	0.00825	0.00075

2.7. Seismic Fragility Curves

In this section fragility estimates are developed based on the overall maximum linear and bilinear demand models, and based on the proposed story-specific demand models for the selected buildings. When using the overall maximum demand models, the fragility is estimated using the approximate form in Equation (2.2). When using the story-specific demand models, the approximate form cannot be used because there are as many limit state functions as the number of stories; therefore, Monte Carlo simulations are used to estimate the fragilities (Ditlevsen and Madsen 1996). It is noted that no modeling uncertainty (σ_M) is included either in the approximate form in Equation (2.2) or the Monte-Carlo simulation for consistency.

2.7.1. Fragility Estimates Based on Overall Maximum Linear and Bilinear Models

Fragility curves are first estimated using the overall maximum linear models for the two-story and five-story buildings. Figure 2.9 shows the seismic fragility curves for the selected buildings using the overall maximum linear demand models. The fragility

curves indicated as OLM are shown using dashed lines of varying thickness to represent each capacity limit. In addition, the fragility estimates in a logarithmic space are shown in the zoom-in window for each structure. Because the capacity limits for the five-story building are smaller than those for the two-story building, the corresponding fragility estimates for a given S_a are higher.

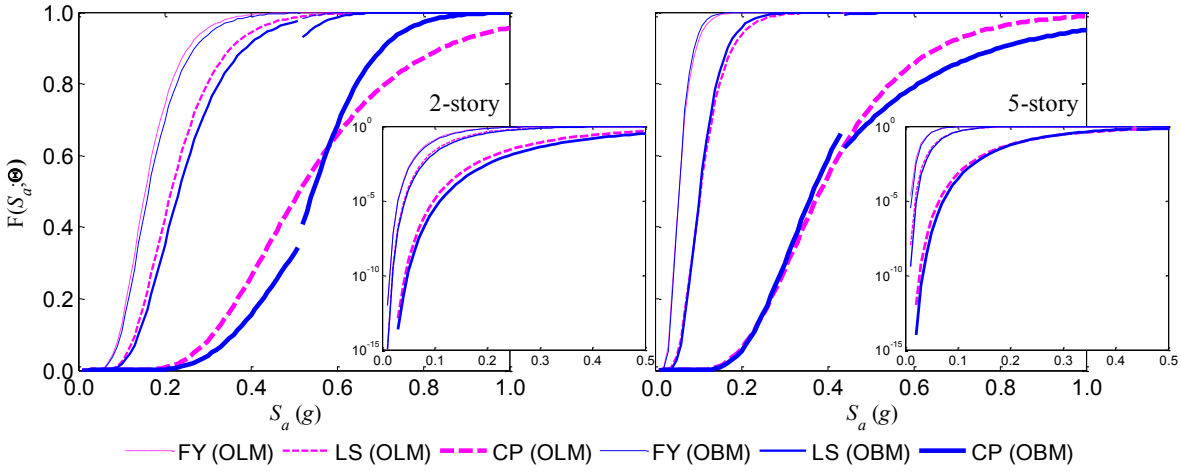

Fig. 2.9. Comparison of seismic fragility curves using OLM and OBM

Figure 2.9 also shows the seismic fragility curves assessed using the overall maximum bilinear demand models. The fragility curves indicated as OBM are shown using solid lines of varying thickness to represent each capacity limit. These fragility estimates have a jump at the transition point between the two linear branches. This is due to the different values of σ_i for the two branches.

By comparing the seismic fragility curves for the two-story building, it can be observed that the overall maximum linear model provides a marginally overestimated fragility compared to the overall maximum bilinear model for the FY and LS limit states

for the entire range of S_a. Furthermore, for the CP limit state, the overall maximum linear model overestimates the fragility for $S_a \le 0.58g$ and underestimates the fragility for $S_a > 0.58g$. For the five-story building, the fragility estimates from both demand models for the FY and LS limit states are similar. This is because the model parameters for the bilinear demand model are close to those for the linear demand model. However, because $\sigma_2 > \sigma$, the slope of the fragility curve based on the bilinear model is less steep after the transition point. Furthermore, for the CP limit state, the linear model marginally underestimates the fragility for $0.24g < S_a \le 0.44g$ and overestimates the fragility for $S_a > 0.44g$.

2.7.2. Fragility Estimates Based on Story-Specific Models

To develop the fragility curves using the story-specific demand models, a Monte Carlo simulation technique is used. Because different demand models are developed for each story, there is a limit state function g_j corresponding to each story j. Therefore, Equation (2.2) is not applicable for developing the fragility curves.

Consistent with the assumptions made in the approximate solution in Equation (2.2), during the Monte Carlo simulation, the capacity limit for each story is defined as a random variable having a Normal distribution in the logarithmic space with the median capacity given in Table 2.6 and a standard deviation of 0.3. A standard deviation of 0.3 corresponds to a coefficient of variation, c.o.v., of 0.31 in the original space based on the equation $\text{c.o.v.} = \sqrt{\exp\left(\sigma^2\right) - 1}$. In addition, no modeling uncertainty is added in the

Monte Carlo simulation. Figures 2.10 and 2.11 show the seismic fragility curves for the selected buildings using the story-specific demand models (SSM). The fragility curves indicated as SSM are shown using solid lines of varying thickness to represent each capacity limit. The traditional fragility curves developed based on the overall maximum linear and bilinear models are also shown for comparison purposes.

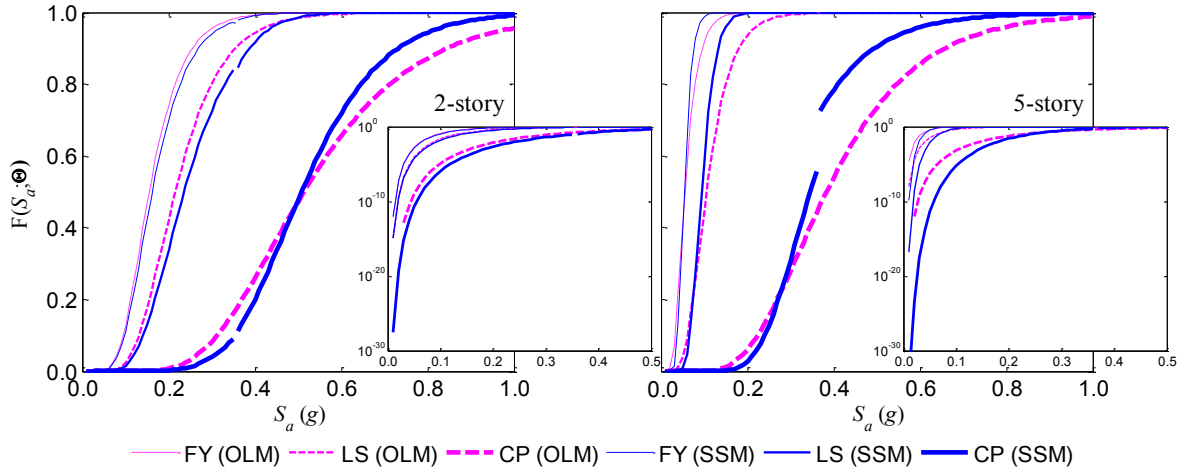

Fig. 2.10. Seismic fragility curves using OLM and SSM

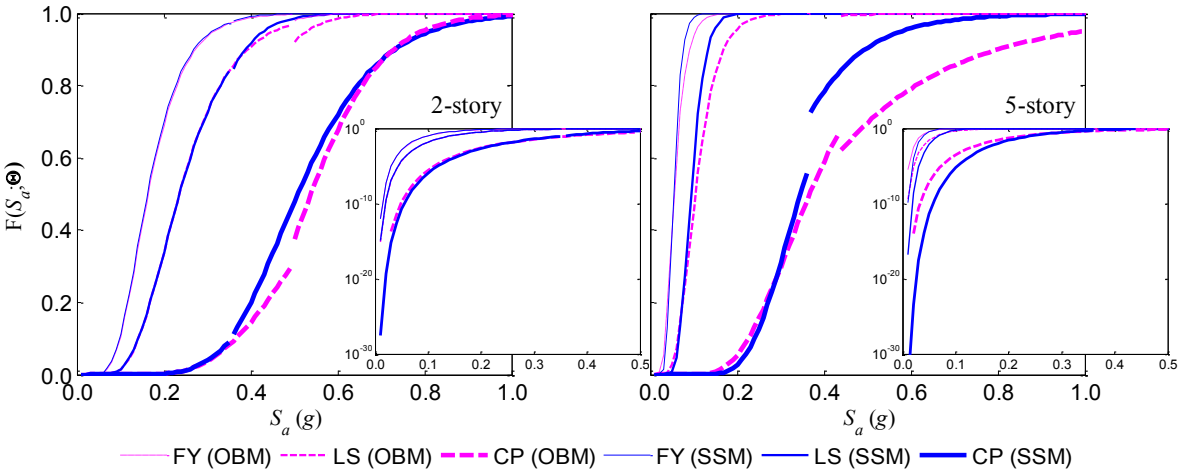

Fig. 2.11. Seismic fragility curves using OBM and SSM

Two observations can be made: one in relation to the effects on modeling uncertainties, and one with respect to the effects of considering the possibility of failure of multiple stories using story-specific demand models. There are two major sources of modeling uncertainty: uncertainties in the structural analysis model and in the reliability model. Because all the data points for this study came from the same finite element model, there is no effect on modeling uncertainty from the structural analysis model. Therefore, the difference in the slopes is the modeling uncertainty from different reliability formulations. As already observed in Figure 2.9, using a bilinear model affects the slopes of the fragility curves (see Figure 2.10). The slopes of the fragility curves developed using the story-specific demand models are steeper than those developed using the overall maximum linear models for both structures. This means that the uncertainty associated with the story-specific demand models is less than the uncertainty based on the linear model. In addition, the fragility curves using the story-specific demand models have steeper slopes than those using the overall maximum bilinear models for both structures. This is because the story-specific demand models and the corresponding fragility estimates provide better predictions based on the reduced uncertainty.

Furthermore, considering the possibility of failure of multiple stories increases the overall fragility for the five-story building where the 1st and 2nd story have drift demands of comparable magnitude (see Figure 2.11). The seismic fragility estimates from OBM and SSM for the two-story building are closer to each other than those for the five-story building. This is because the 1st story behavior dominates the failure for

the two-story building, while the drift response is more complex for the five-story building. The formulation of the story-specific demand models captures the possibility of failure of multiple stories and reduces uncertainty in fragility estimates. Therefore, the story-specific demand models better reflect seismic fragility of multi-story buildings when the interstory drifts for one or more stories are close to the overall maximum interstory drift of the building.

Tables 2.8 and 2.9 show a comparison among three fragility estimates (OLM, OBM and SSM), for the selected buildings for the median S_a computed over the synthetic ground motions for the 10% and 2% in 50 years motions. As defined earlier, seismic fragility estimates are the conditional probability of attaining or exceeding a specific performance level for a given S_a. It is also noted that these estimates are based on the fragility curves developed by three demand models without modeling uncertainty for consistency.

Table 2.8. Seismic fragility estimates for two-story building

Ground motion	$S_a(g)$	Performance level	OLM	OBM	SSM
10% in 50 years	0.154	FY	0.499	0.442	0.454
		LS	0.198	0.147	0.148
		CP	0.001	0.0003	0.0002
2% in 50 years	0.616	FY	0.999	0.998	1.00
		LS	0.997	0.989	0.998
		CP	0.679	0.714	0.749

Table 2.9. Seismic fragility estimates for five-story building

Ground motion	$S_a(g)$	Performance level	OLM	OBM	SSM
10% in 50 years	0.104	FY	0.934	0.951	0.992
		LS	0.495	0.509	0.657
		CP	0.001	0.0005	0
2% in 50 years	0.535	FY	1.00	1.00	1.00
		LS	0.999	0.997	1.00
		CP	0.786	0.735	0.929

As shown in Tables 2.8 and 2.9, for both structures, the overall maximum linear model underestimates the CP seismic fragility for 2% in 50 years when compared to the story-specific models. In addition, for the 2-story building, the linear model provides higher fragility estimates for the 10% in 50 years motions when compared to the story-specific models.

For the motions with a 10% probability of exceedance, the fragility estimates using the FY and LS limit states for the five-story building are significantly higher than those for the two-story building. For the 2% in 50 years motions, both structures are estimated to have a high probability of exceeding the FY, LS and CP limit states. This indicates significant damage for these structures during a high intensity, but less frequent, earthquake event in the Central U.S.

2.8. Summary

The focus of this section is on the development of probabilistic demand models for multi-story reinforced concrete (RC) buildings to account for the response of each story during an earthquake excitation. This is because fragility estimates developed using only the overall maximum interstory drift may not reflect the actual vulnerability of multi-story buildings. Story-specific demand models that consider the maximum interstory drift of each story are developed. Correlations among individual story demand models are also assessed to properly capture the potential dependence between maximum interstory drifts over the height of a building. Both linear and bilinear formulations in logarithmic space are considered to represent the relationships between drift demand and earthquake intensity. A Bayesian approach is used to estimate the unknown parameters in the proposed demand models. The computation of the posterior statistics is carried out using an adaptive Markov Chain Monte Carlo (MCMC) simulation technique. Then the fragility estimates are developed based on the proposed story-specific demand models and compared with traditional fragility estimates computed based on a demand model for the overall maximum interstory drift. It is shown that when only the maximum interstory drift of a building is considered, the fragility might be underestimated; particularly if the interstory drifts for one or more stories are close to the maximum value. The proposed methodology provides a refined approach that includes more building response information than typical demand models, allowing for more accurate estimates of the seismic fragility of multi-story buildings.

3. SEISMIC VULNERABILITY ASSESSMENT FOR TILT-UP CONCRETE BUILDING STRUCTURES

3.1. Introduction

Tilt-up concrete buildings are widely constructed because of their advantages in construction costs and schedule. They are commonly used for low-rise structures that require a large open space including distribution centers, warehouses, retail centers, and other commercial and industrial facilities. According to the Tilt-Up Concrete Association (TCA), over 15% of all industrial buildings in the United States (U.S.) are tilt-up concrete buildings. Particularly, tilt-up concrete is the most common type of concrete structure in Shelby County, Tennessee, based on the inventory data developed by French (2008) that covers all of Shelby County, Tennessee including the City of Memphis. The reported total number of tilt-up concrete structures is 1110 out of 2139 concrete structures (or 51.9 percent) in Shelby County, Tennessee, with many more throughout Mid-America and other regions of the U.S. A tilt-up concrete structure consists of perimeter concrete wall panels, the roof diaphragm, diaphragm-to-wall connections, and the foundation. The roof diaphragm system includes structural members to support a metal deck or plywood overlay. Connections include panel-to-panel connections and diaphragm-to-wall connections, which are critical in maintaining the integrity of the structure under lateral load demands during seismic events.

Although tilt-up buildings are widely constructed, a number of buildings were damaged during previous earthquakes including the 1994 Northridge earthquake.

Typical damage includes collapse of roof diaphragms and wall panels due to connection failures, and concrete panel separation. There are still many existing structures that are considered to be vulnerable because they were not designed for the current seismic design provisions. This is particularly true in the Central U.S. where the national building codes have recently required that more stringent seismic design standards are needed to limit the potential damage in structures near the New Madrid Seismic Zone.

In order to assess seismic vulnerability of these structures including estimation of uncertainty, fragility analysis using a probabilistic approach can be performed. Seismic fragility is defined as the conditional probability of attaining or exceeding a specific performance level for a given earthquake intensity, such as spectral acceleration. A number of researchers have conducted studies on seismic performance evaluation of tilt-up concrete buildings (Carter et al. 1993, Wood and Hawkins 1994, Fonseca 1997, Johnson and Fonseca 1998, Wallace et al. 1999, Graf and Malley 2004, Chou 2007). However, there is limited understanding on nonlinear behavior under severe earthquakes as well as the development of seismic fragility curves for this type of building.

This section proposes a methodology to develop an analytical model using nonlinear properties to capture critical failure mechanisms of tilt-up concrete buildings. A typical one-story tilt-up concrete building with a 1.4:1 aspect ratio and metal deck diaphragm system similar to those constructed in Memphis, Tennessee, is selected as the case study structure. Nonlinear dynamic analyses using synthetic ground motions are conducted to assess the seismic performance of the building. In addition, probabilistic demand models are constructed to account for uncertainties. Sets of fragility curves with

appropriate capacity limits are developed to quantify seismic vulnerability of the case study building. Finally, a second tilt-up concrete building with a longer aspect ratio is selected and analyzed to show the influence of aspect ratio with respect to the building plan dimensions on the overall seismic performance and fragility estimates.

3.2. Damage to Tilt-Up Concrete Structures

Many tilt-up structures were damaged during previous earthquakes including the 1964 Alaska earthquake, the 1971 San Fernando earthquake, the 1987 Whittier Narrows earthquake, the 1989 Loma Prieta earthquake, and the 1994 Northridge earthquake (Hamburger et al. 1988, Adham et al. 1990, Carter et al. 1993, Shepherd 1990, EQE International 1994). Typical damage includes tearing and collapse of roof diaphragms, collapse of wall panels due to connection failures, and concrete panel separation. Based on previous research, the horizontal response of the diaphragm can be fairly large compared to that of the in-plane concrete wall panels (Wallace et al. 1999, Johnson and Fonseca 1998, SEAONC 2001). A large horizontal response of the diaphragm can cause damage, including large out-of-plane deflections of wall panels and separation of the panels and diaphragms. Therefore, the shear capacity of the diaphragm against the horizontal response and the capacity of connection between the diaphragm and out-of-plane walls are critical for acceptable seismic performance under severe lateral loads. In addition, typical damage observations have included splitting cracks in the pilasters at the glulam beam seats, out-of-plane bending cracks in the wall panels and pilasters,

leakage from separation of joints in the sprinkler pipes, failure of ties between the subdiaphragms and the wall panels, and failure of suspended ceilings.

Thurston (1990) summarized the major factors affecting the structural performance, as well as the potential failure mechanisms for tilt-up concrete buildings. According to Thurston (1990), because there is little or no structural redundancy for typical tilt-up buildings, ultimate strength and ductility of the connections between rigid walls and a flexible diaphragm are critical. It is noted that the required design capacity of diaphragm-to-wall connections was increased by the Uniform Building Code (ICBA 1991) after the damage to tilt-up concrete structures in the Western U.S. However, there are still many existing buildings designed according to the previous specifications such that the seismic design forces are lower than the current requirements

3.3. Seismic Performance Evaluation and Fragility Analysis

ASCE/SEI 41-06 (ASCE 2007) provides analytical procedures and criteria for a performance-based seismic evaluation of existing buildings. Based on the ASCE/SEI 41-06 criteria, three performance levels are identified: Immediate Occupancy (IO), Life Safety (LS), and Collapse Prevention (CP). In addition, the Basic Safety Objective (BSO) is defined as LS performance for the Basic Safety Earthquake 1 (BSE-1) earthquake hazard level and CP performance for the BSE-2 earthquake hazard level. BSE-1 is defined as the *smaller* of an event corresponding to 10% probability of exceedance in 50 years (10% in 50 years) and 2/3 of BSE-2, which is the 2% probability of exceedance in 50 years (2% in 50 years) event. ASCE/SEI 41-06 categorizes flexible

diaphragms, including bare metal deck and wood diaphragms, as force-controlled components that have acceptance criteria in terms of a lower-bound strength measure.

Seismic performance evaluations of structures are used to identify structural deficiencies and predict damage for particular structures, while seismic fragility analysis is used to quantify the vulnerability of a structure using probabilistic measures. Seismic fragility is defined as the conditional probability of attaining or exceeding a specific performance level for a given earthquake intensity, such as spectral acceleration S_a. To develop seismic fragility curves, structural capacity limits and demand models are needed. In general, the fragility can be written as

$$F(S_a;\boldsymbol{\Theta}) = P\left[g(S_a;\boldsymbol{\Theta}) \le 0 \middle| S_a\right] \tag{3.1}$$

where $g(S_a;\boldsymbol{\Theta}) = C - D(S_a;\ \boldsymbol{\Theta})$ is a limit state function used to define the failure event, C and D represent the capacity and demand of the building, respectively, and $\boldsymbol{\Theta}$ is a vector of unknown parameters in the demand model. Capacity limits are determined from the structural behavior and potential failure mechanisms based on the results of a structural analysis. For frame structures, demand models and capacity limits are frequently expressed in terms of limiting interstory drifts. However, it may be more appropriate to express demand models and capacity limits in terms of the forces of the structural members for tilt-up concrete buildings (Bai and Hueste 2006). In addition, because there can be several potential failure mechanisms to define a level of damage, those should be identified and considered as multiple limit state functions in the seismic fragility analysis.

3.4. Analytical Modeling Approach

3.4.1. Analytical Model Development

Several studies have focused on developing an analytical model for a flexible diaphragm and rigid wall system (Fonseca 1997, Cohen et al. 2004 a,b, Kim and White 2004, Graf and Malley 2004, Chou 2007). Previous studies indicate that the in-plane concrete panels exhibit stiff behavior, while the roof diaphragm is relatively flexible. Therefore, representing the nonlinear characteristics of the diaphragm system is important to predict reliable structural behavior under severe lateral movement. In addition, proper modeling of diaphragm-to-wall connections should be considered because these are critical based on previous studies. However, there has been little study to account for failure of individual connections, especially for a metal deck diaphragm system. In this study, an analytical model using nonlinear spring elements to represent failures of diaphragm connections (i.e. puddle welds) and diaphragm-to-wall connections is developed using the Abaqus program (Simulia 2007).

The superstructure of tilt-up concrete buildings consist of three fundamental components: perimeter tilt-up concrete wall panels, a roof diaphragm system, and connections. Previous studies indicate that the in-plane concrete panels exhibit stiff behavior, while the roof diaphragm is relatively flexible. Therefore, representing the nonlinear characteristics of the diaphragm system is important to more reliably predict structure behavior under severe lateral movement.

An analytical modeling approach is developed and implemented using the Abaqus program (Simulia 2007). To model the concrete walls and corrugated metal deck, eight-node shell elements (S8R) with nonlinear properties are used. For the metal deck model, a plain rectangular section that is equivalent to the corrugated shape of metal deck in terms of strength is used. The equivalent thickness of the plain rectangular section is computed based on the moment of inertia of the corrugated metal deck. In addition, the in-plane shear strength is derived from the effective shear modulus of the metal deck based on the Steel Deck Institute Diaphragm Design Manual (SDI 2004), which includes the torsional effect from the corrugation of the metal deck. Orthotropic material properties are used to allow the definition of two different stiffness values under axial and shear motions. Three-node beam elements (B32) with a rectangular cross section are used for the open web joist girders. In addition, Rayleigh damping is included in the model.

Proper modeling of diaphragm-to-wall connections was also considered because these connections are often critical based on previous studies. However, there has been little study to assess the failure of individual connections, especially for a metal deck diaphragm system. The proposed model uses nonlinear spring elements to represent failures of deck-to-joist diaphragm connections (i.e. puddle welds) and diaphragm-to-wall connections. To represent the diaphragm-to-wall connections and puddle welds, a 'translator' connector element (CONN3D2) with a failure criterion in terms of ultimate strength is used.

3.4.2. Verification of Analytical Modeling Approach

To verify the proposed analytical model approach using Abaqus, a shaking table test in the literature is selected and the analytical results are compared with the test data. Cohen et al. (2004a) conducted a shaking-table test of half-scale low-rise reinforced masonry buildings with flexible metal roof diaphragms. Although the wall system is not an exact match to the cast study structures, it is expected to exhibit similar behavior as a flexible diaphragm and concrete wall system. The test was performed at the United States Army Construction Engineering Research Laboratory, Engineering Research and Development Center (CERL). Two half-scale buildings were constructed with different roof systems; a roof diaphragm with a single layer of diagonal-lumber sheathing, and a roof diaphragm consisting of untopped, corrugated-metal deck on open-web steel joists. To verify the proposed analytical model for a metal deck diaphragm case, the test results from the second specimen are selected. The test specimen is a one-story reinforced masonry building with a length of 6.71 m (264 in.) and a width of 1.42 m (56 in.). The building is 2.13 m (84 in.) high and there are two openings (48 in. by 48 in.) only in one side of the out-of-plane walls. Four-inch concrete masonry unit (CMU) walls were grouted vertically at every 0.61 m (24 in.) with one #3 bar. The 203 mm (8 in.) deep open-web joists and 22-gage wide-rib metal decking were used with an equivalent of a 36/4 puddle weld pattern fasteners between the decking and the joists. Two ground motion records were scaled to match their periods with the half-scale structure and used for the tests. More details for the design and test data are provided by Cohen et al. (2004a).

Figure 3.1 shows the developed analytical model of the tested structure using Abaqus. It is noted that the ratio between length and width of the test building is 4:1, which is a relatively large plan aspect ratio. Material properties and other input data including strength and stiffness values are obtained from the Cohen et al.'s study and summarized in Table 3.1. Mechanical material properties such as Young's modulus are adopted from Cohen et al. (2004a) and Vulcraft manuals including "steel roof and floor deck" (Vulcraft 2008) and "steel joists and joist girders" (Vulcraft 2007). To estimate the shear modulus of the metal decking, and stiffness and strength values of puddle welds, the Steel Deck Institute Diaphragm Design Manual (SDI 2004) is used. It is noted that connections between joists and walls are assumed to be pinned connections for verification because there is no observed connection damage based on Cohen et al. (2004a).

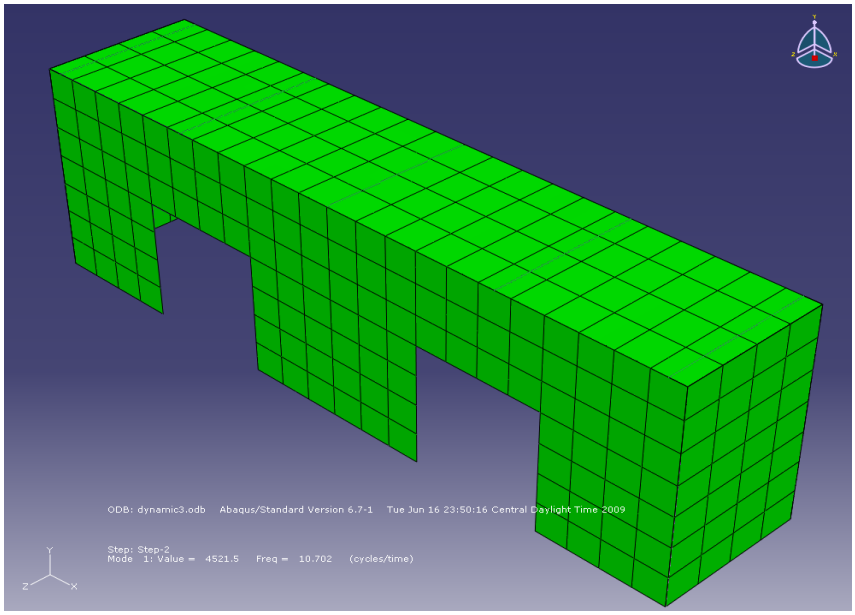

Fig. 3.1. Analytical model for verification

Table 3.1. Modeling parameters used in verification

Members	Parameters	Values
Metal deck (22WR, Type B)	Unit weight	8.04×10^{-5} N/mm^2 (1.68 psf)
	Moment of Inertia (I)	328,268 mm^4 (0.789 in^4)
	Equivalent thickness (t_E)	14.0 mm (0.553 in)
	Young's modulus (E)	199,948 N/mm^2 (29000 ksi)
	Hardening factor	0.03
	Effective shear modulus (G')	2156 N/mm (12.3 kip/in)
	Shear modulus ($G = G'/t_E$)	2878 N.mm^2 (417 ksi)
	Yield strength (f_y)	228 N/mm^2 (33 ksi)
	Ultimate strength (f_u)	310 N/mm^2 (45 ksi)
Reinforced masonry wall	Density	1.92×10^{-9} t/mm^3 (120 pcf)
	Thickness (t)	92.1 mm (3.63 in)
	Young's modulus (E)	3309 N/mm^2 (480 ksi)
	Usable strain	0.029
	Ultimate strength (f'_m)	9.65 N/mm^2 (1.4 ksi)
Open web joist (8K1)	Unit weight	0.0744 N/mm (5.1 lb/ft)
	Moment of Inertia (I)	2,764,925 mm^4 (6.64 in^4)
	Young's modulus (E)	199,948 N/mm^2 (29000 ksi)
	Hardening factor	0.03
	Yield strength (f_y)	345 N/mm^2 (50 ksi)
Puddle welds	Stiffness	26156 N/mm (149 k/in)
	Ultimate strength	7736 N (1.74 k)

The natural frequency of the structure using eigenvalue analysis is estimated. The natural frequency from the proposed model is 10.1 *Hz* (T_1 = 0.099 *s*). For comparison, the natural frequency from the Cohen's test was 12.0 *Hz* (T_1 = 0.083 *s*).

This natural frequency is used to estimate Rayleigh damping coefficients for dynamic analysis. In addition, dynamic analyses using three scaled ground motion records are conducted. Table 3.2 summarizes the maximum diaphragm drift ratio (DDR), which is a measure of diaphragm deformation relative to diaphragm length. The DDR is an indicator to evaluate the potential for seismic damage in structures with rigid walls and a flexible diaphragm, and is computed as follows (Cohen et al. 2004a).

$$DDR = \frac{\Delta_{diaphragm}}{L/2} \tag{3.2}$$

where $\Delta_{\text{diaphragm}}$ is in-plane displacement of the roof diaphragm relative to the supporting walls and L is the plan length of the diaphragm.

Table 3.2. Comparison of maximum DDR

Test No.	PGA (g)	Damage	Max. DDR (%)	
			Cohen's test	ABAQUS
5	0.4	Negligible	0.09	0.12
9	1.0	Extensive cracking	0.40	0.54
10	1.33	Extensive cracking, hinging	1.00	0.72

Based on the comparison in terms of the maximum DDR, the proposed model provides slightly larger deformations for tests 5 and 9, while the maximum DDR of the proposed model for test 10 is less than that from the experiments. The main reason for this difference is related to the highly nonlinear behavior of the structure due to failure of puddle welds. In the proposed model, the capacity of the puddle welds is estimated based on the SDI manual and used as the same value. Therefore, when the strength

reaches the maximum level of the shear capacity of the puddle welds, connector elements in the same row fail almost simultaneously. However, there are some variations in welding failures in the test structure because of the varying quality of the puddle welds (Cohen et al. 2004a).

The nonlinear behavior of the metal deck system is also compared with the quasistatic test results. Figure 3.2 shows the comparison between nonlinear behavior of the metal deck system and the quasistatic test results. The quasistatic test is conducted using the test protocol recommended by Cohen et al. (2004a). It provides a reasonable comparison in terms of stiffness and strength degradation from the failure of connections.

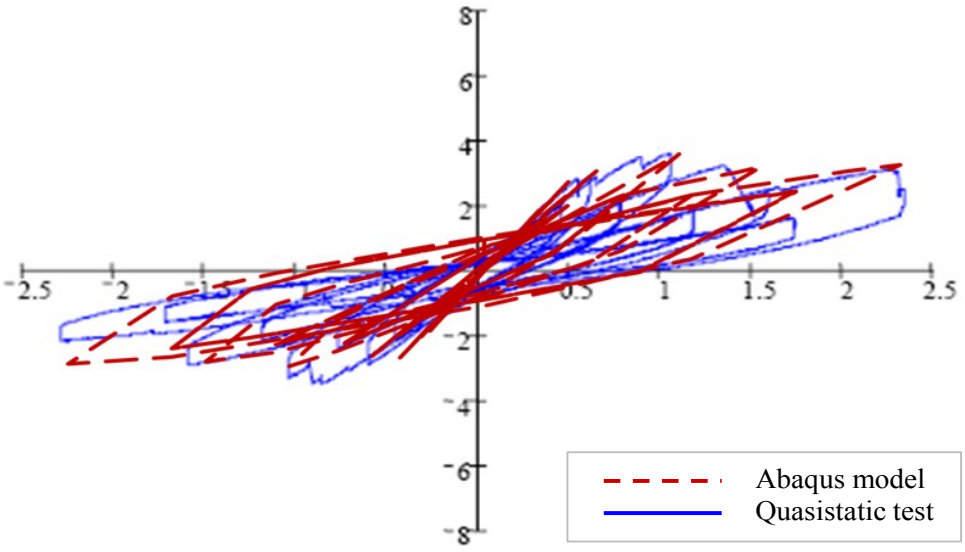

Fig. 3.2. Comparison between nonlinear behavior of analytical model and quasistatic test

3.5. Application Example

3.5.1. Case Study Structure

A typical one-story tilt-up concrete building with a metal deck roof diaphragm system is selected as an application example to assess the seismic vulnerability of existing tilt-up buildings in the Mid-America region. The building details are based on structural drawings for a tilt-up concrete structure located in St. Louis, Missouri. This structure was designed according to the Building Officials and Code Administrators (BOCA) National Building Code (1999), in which St. Louis is designated as seismic hazard exposure group I. It is noted that the seismic design level for St. Louis, Missouri, is the same as that for Memphis, Tennessee, based on the 1999 BOCA code. The seismic design forces are lower than what is now required by the IBC 2009 (ICC 2009) for the Mid-America region.

A plan and elevation view of the building is provided in Figure 3.3. The plan aspect ratio of the case study building is 1.4:1. The one-story structure with interior gravity load carrying steel columns and a steel joist and metal deck roof diaphragm is a common system for tilt-up construction in the Mid-America region. The roof system consists of metal deck [0.75 mm (0.0295 in.) thick with 38.1 mm (1.50 in.) rib height] spanning the short direction of the building, supported by open web metal joists placed on 2.0 m (80 in.) centers that span the long direction of the building. The metal deck is puddle welded to the supporting members [16 mm (0.625 in.) welds using a pattern of four welds per 914 mm (36 in.)] with a minimum of two screwed side lap connections

between joists. The roof joists are supported every 12.2 m (40 ft) by deeper steel joist girders that span the short direction of the structure. The joist girders are supported at each end by the perimeter concrete wall panels and every 12.2 m (40 ft) by interior steel columns.

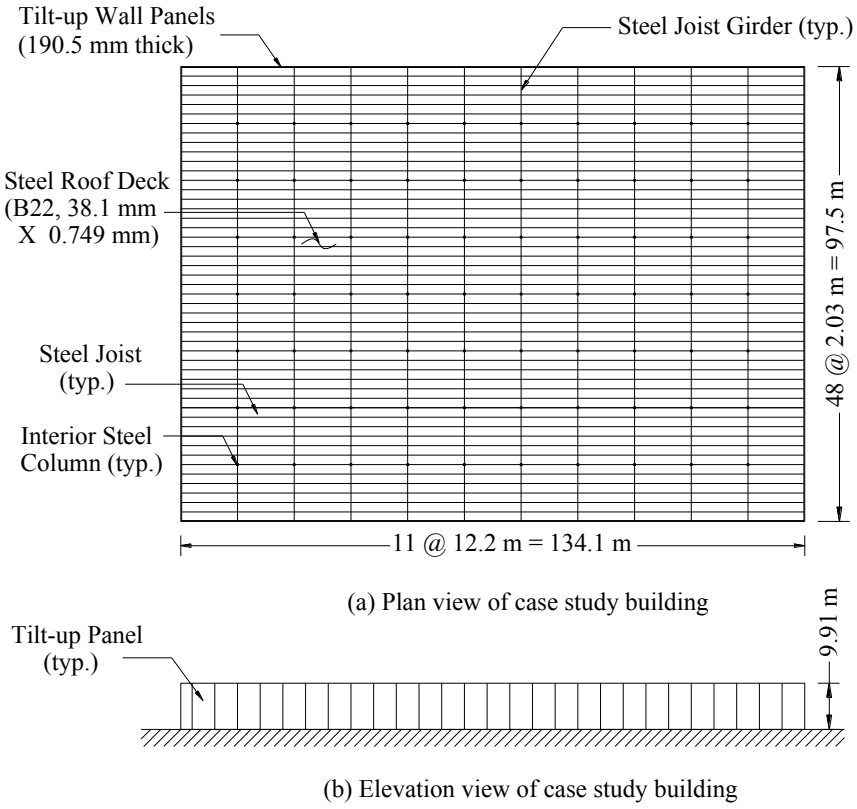

Fig. 3.3. Plan view and elevation view of case study building

The proposed analytical modeling approach is used to predict the structural behavior of the case study building under earthquake loads. It includes nonlinear material properties for metal deck and concrete walls, puddle welds using connector elements with failure criteria, and shear and tension connections between diaphragm and

wall panels with corresponding failure criteria. Table 3.3 summarizes the modeling parameters for the case study building.

Table 3.3. Modeling parameters for the case study building (1.4:1 aspect ratio)

Members	Parameters	Values
Metal deck (22WR, Type B)	Unit weight	8.04×10^{-5} N/mm^2 (1.68 psf)
	Moment of Inertia (I)	23100 mm^4 (0.169 in^4/ft)
	Thickness (t)	0.749 mm (0.0295 in)
	Equivalent thickness (t_E)	3.86 mm (0.152 in)
	Young's modulus (E)	199,948 N/mm^2 (29000 ksi)
	Effective shear modulus (G')	2546 N/mm (14.5 kip/in)
	Shear modulus ($G = G'/t_E$)	659 N.mm^2 (95.6 ksi)
	Yield strength (f_y)	228 N/mm^2 (33 ksi)
	Ultimate strength (f_u)	310 N/mm^2 (45 ksi)
Reinforced concrete wall	Density	2.40×10^{-9} t/mm^3 (150 pcf)
	Thickness (t)	191 mm (7.5 in)
	Young's modulus (E)	26436 N/mm^2 (3834 ksi)
	Ultimate strength (f'_c)	27.6 N/mm^2 (4 ksi)
Open web joist (26K6)	Unit weight	0.155 N/mm (10.6 lb/ft)
	Moment of Inertia (I)	1.09×10^{-8} mm^4 (262 in^4)
Joist girder (44G6N10K)	Unit weight	0.438 N/mm (30 lb/ft)
	Moment of Inertia (I)	1.19×10^{-9} mm^4 (2850 in^4)
Puddle welds	Stiffness	26156 N/mm (149 k/in)
	Ultimate strength	7736 N (1.74 k)

3.5.2. Ground Motion Records

To conduct nonlinear dynamic analysis, ground motion records in the Mid-America region are needed. Because strong ground motion records for this area are not available, synthetic ground motions for Memphis, Tennessee, developed by Rix and Fernandez (2006), are used for the dynamic analyses of the selected structures. A total of 40 ground motions are provided for each of two earthquake hazard levels: 2% in 50 years and 10% in 50 years. Each hazard level has 20 ground motions for each of two types of soil conditions (lowlands and uplands) for Memphis, Tennessee. Figure 3.4 shows the median of response spectra for the ground motion records used in this study.

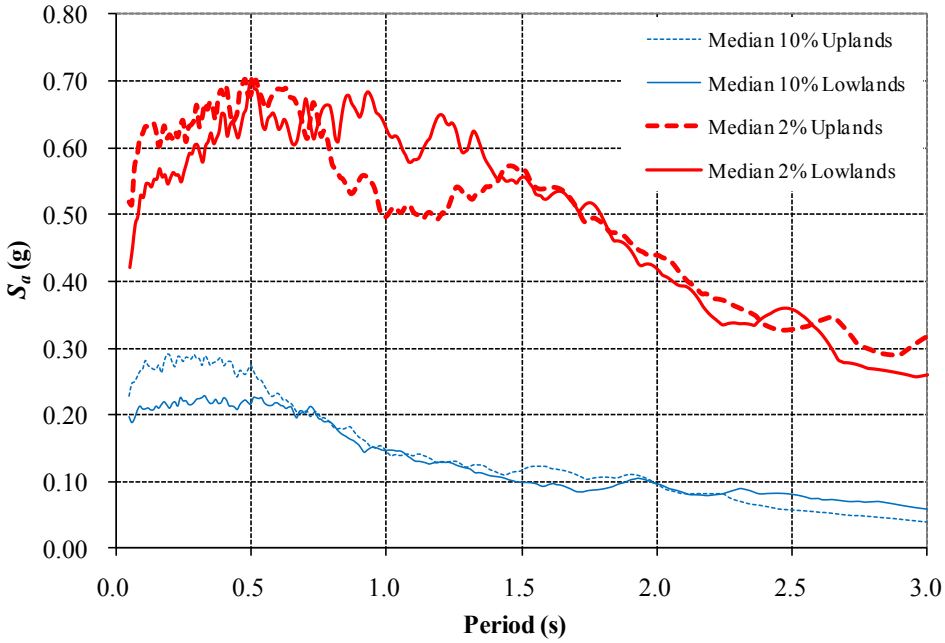

Fig. 3.4. Median of response spectra for Rix and Fernandez motions

3.5.3. Analytical Results

First, eigenvalue analysis is conducted to estimate the fundamental period of the structure. The fundamental period of the structure is 0.41 *s*. This value is close to the estimated period using the ASCE/SEI 41-06 approximate equation for a rigid wall-flexible diaphragm system, which gives 0.42 *s*. Equation (3.3) shows the ASCE/SEI 41-06 equation using Method 3, which is an approximate estimation for one-story buildings with single span flexible diaphragms, given as follows.

$$T = \left(0.1\Delta_w + 0.078\Delta_d\right)^{0.5} \tag{3.3}$$

where T is the fundamental period (s) in the direction under consideration, Δ_w and Δ_d are the in-plane wall and diaphragm displacements (inches), due to a lateral load in the direction under consideration equal to the weight of the diaphragm. For estimating the displacements of the transverse walls and roof diaphragm, the stiffness values found by Cohen's procedure are used. Figure 3.5 shows the corresponding mode shape of the case study building using the Abaqus model.

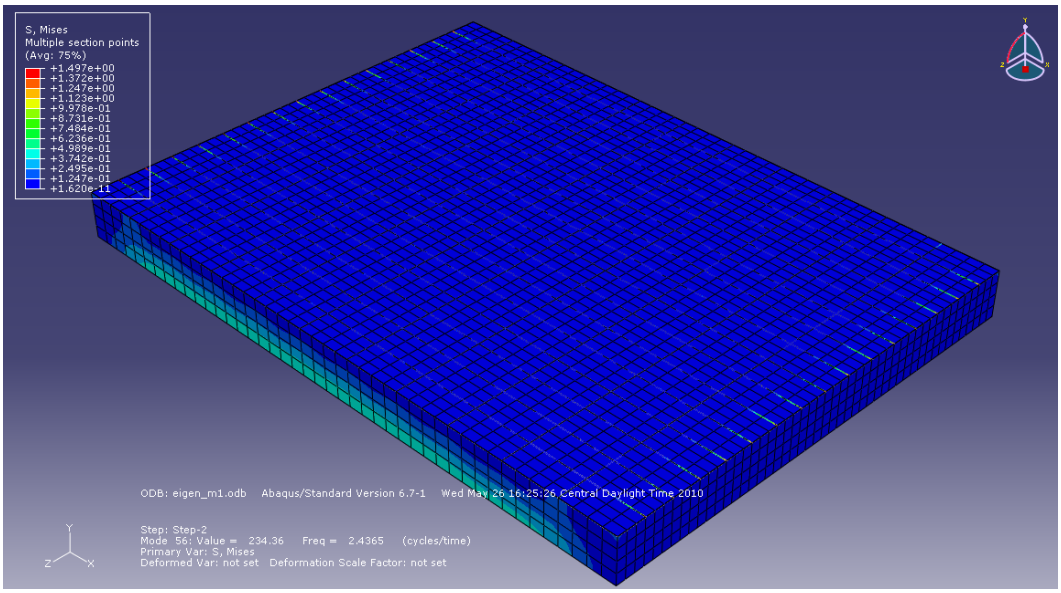

Fig. 3.5. First mode shape of the case study building (1.4:1 aspect ratio)

Push-over analysis is conducted to monitor the nonlinear behavior of the structure under monotonically increasing lateral loads. Figure 3.6 shows the relationship between the maximum DDR and the shear ratio, which is the base shear V as a percentage of the building weight W.

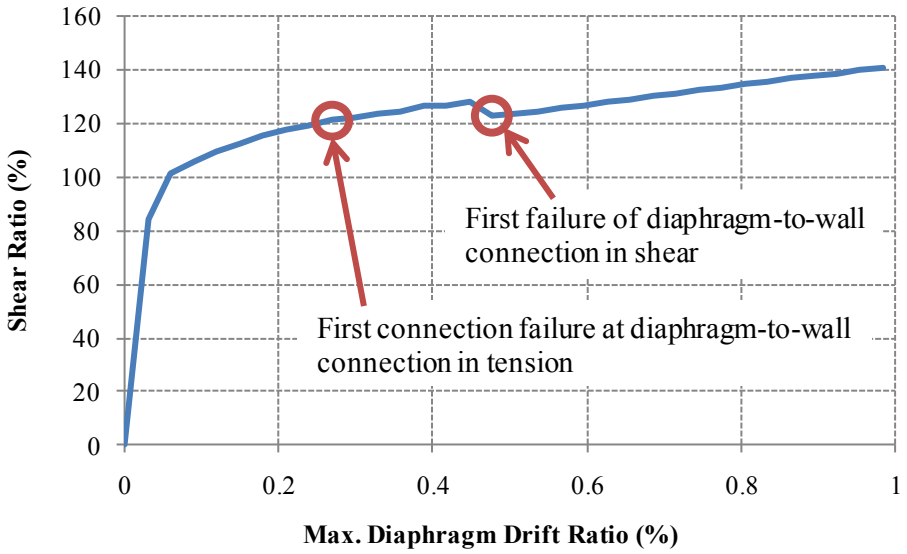

Fig. 3.6. Push-over curve for the case study building (1.4:1 aspect ratio)

The first failure of a diaphragm-to-wall connection is observed at a DDR of 0.24% (160 mm) in the out-of-plane direction. The base shear increases incrementally until the first failure of a diaphragm-to-wall connection in shear at a maximum DDR of 0.54% (360 mm). At that time step, 50% of the tension connections between the diaphragm and concrete walls have failed. When the maximum DDR reaches 0.98%, 10 out of 20 diaphragm-to-wall connections in tension, two out of 30 diaphragm-to-wall connections in shear, and none of puddle welds have failed. The corresponding base shear ratio is about 140%.

Nonlinear dynamic analyses are also conducted to assess the dynamic behavior of the case study building. Table 3.4 summarizes the maximum DDR for each ground motion record with the corresponding spectral acceleration. Figure 3.7 provides an example deflection (DDR) time history at the top of the case study building with the

corresponding ground motion record. It is noted that the ground motions are shortened for the nonlinear dynamic analysis at the time point where the energy reaches 95% of the total energy imparted by a particular ground motion record to reduce the computational time. This procedure is based on the methodology developed by Trifunac and Brady (1975). The dotted line on the ground motion record in Figure 3.7 indicates the 95% cut-off point.

Table 3.4. Maximum DDR and spectral acceleration from nonlinear dynamic analysis (1.4:1 aspect ratio case study building)

Ground Motion ID	10% in 50 years				2% in 50 years			
	Lowlands		Uplands		Lowlands		Uplands	
	S_a (g)	DDR (%)	S_a (g)	DDR (%)	S_a (g)	DDR (%)	S_a (g)	DDR (%)
1	0.20	0.05	0.28	0.07	0.49	0.21	0.52	0.24
2	0.20	0.06	0.30	0.06	0.76	0.18	0.69	0.12
3	0.21	0.05	0.34	0.08	0.52	0.15	0.69	0.16
4	0.26	0.05	0.24	0.06	0.70	0.25	0.68	0.19
5	0.22	0.05	0.33	0.04	0.58	0.24	0.64	0.17
6	0.21	0.04	0.25	0.06	0.53	0.23	0.78	0.23
7	0.25	0.06	0.24	0.05	0.71	0.23	0.66	0.25
8	0.27	0.07	0.29	0.08	0.69	0.31	0.54	0.20
9	0.27	0.10	0.29	0.05	0.53	0.22	0.78	0.18
10	0.16	0.03	0.28	0.05	0.74	0.26	0.72	0.28
Mean	0.22	0.05	0.28	0.06	0.63	0.23	0.67	0.20

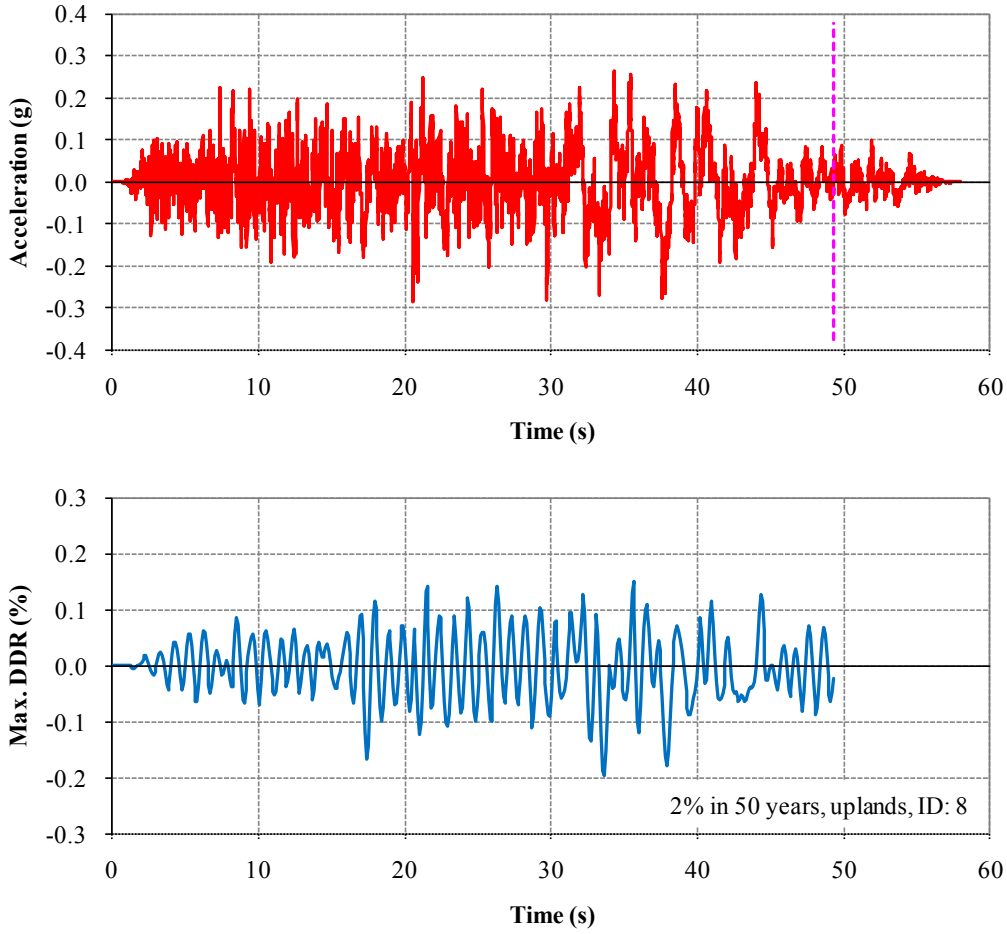

Fig. 3.7. Example of ground motion record and corresponding deflection (DDR) time history from nonlinear dynamic analysis (1.4:1 aspect ratio case study building)

Based on the dynamic analysis results, the maximum DDR values for 10% in 50 years motions ranges from 0.03% to 0.10%, while those for 2% in 50 years motions are between 0.12% and 0.31%. No connection failures are observed for all the nonlinear dynamic analyses using the 40 ground motion records. A failure based on the shear strength of metal deck is observed for 1 of 40 analyses.

3.5.4. Limit State Functions

To develop fragility relationships, limit state functions associated with capacity and demand need to be defined to cover potential failure mechanisms. From the previous studies, failure of connections between the diaphragm system and concrete walls is critical for tilt-up concrete buildings because this has caused significant damage in the past (Hamburger et al. 1988, Shepherd 1990, Thurston 1990). In addition, in-plane shear strength of the metal deck as a ratio between total shear through the connections and the ultimate shear strength of the metal deck is included as a limit state function because this parameter indicates the failure of the metal deck diaphragm system. Therefore, a total of four failure scenarios are considered for the case study structure: (1) failure of the metal deck based on in-plane shear strength (LS_1), (2) failure of the diaphragm-to-wall connections in shear (LS_2), (3) failure of the diaphragm-to-wall connections in tension (LS_3), and (4) failure of the deck-to-joist puddle weld connections in shear (LS_4 and LS_5). Because two different puddle welds patterns (36/4 and 36/7) are used within the diaphragm for the case study building, two limit state functions with separate capacity limits and demand models are developed for the last scenario (LS_4 and LS_5). The limit state functions used in this study are summarized in Table 3.5.

Table 3.5. Limit state functions for the case study building (1.4:1 aspect ratio)

Limit state functions	Description
LS_1	Failure due to lack of in-plane shear strength of metal deck
LS_2	Failure of diaphragm-to-wall connections in shear
LS_3	Failure of diaphragm-to-wall connections in tension
LS_4	Failure of deck-to-joist connection (puddle welds; 36/4 pattern)
LS_5	Failure of deck-to-joist connection (puddle welds; 36/7 pattern)

Unseating of open-web joists is another possible failure mechanism based on a displacement-controlled limit state. Displacements between the top of concrete walls and joists are checked separately, but are not included in the fragility estimates because they are marginal for this case.

3.5.5. Probabilistic Demand Models

Probabilistic demand models for each limit state function are developed to describe the relationship between earthquake intensity and the overall maximum force demands. In this study, a probabilistic linear model is used for developing demand models. Equation (3.4) shows the model form of a probabilistic linear model.

$$D(S_a;\boldsymbol{\Theta}) = \theta_0 + \theta_1 \ln(S_a) + \sigma\varepsilon \tag{3.4}$$

where $D(S_a;\boldsymbol{\Theta})$ is the natural logarithm of the force demand, $\boldsymbol{\Theta}$ is a vector of unknown parameters, ε is a random variable representing the error in the model with zero mean and unit standard deviation, and σ is the standard deviation of the model error. To estimate unknown parameters $\boldsymbol{\Theta}$, the Bayesian updating rule is used. For the posterior

statistics in the estimation of unknown parameters, an adaptive Markov Chain Monte Carlo (MCMC) simulation technique is used. More details about the Bayesian updating and MCMC techniques are found in Section 2.

Table 3.6 provides the posterior statistics of the unknown parameters of each demand models (D_i) corresponding to five limit state functions (LS_i) for the case study structure. Table 3.7 shows the posterior mean and standard deviation of the correlations ($\rho_{i,j}$) among the individual model error, which represent the potential dependence between the limit state functions. As shown in Table 3.6, correlations between model errors are approximately 0.3.

Table 3.6. Posterior statistics of parameters for the case study building (1.4:1 aspect ratio)

Limit state functions		θ_0	θ_1	σ
LS_1	Mean	4.80	1.29	0.24
	St. dev.	0.03	0.02	0.004
LS_2	Mean	4.10	1.24	0.22
	St. dev.	0.03	0.02	0.007
LS_3	Mean	3.25	1.29	0.21
	St. dev.	0.02	0.02	0.006
LS_4	Mean	1.75	1.29	0.21
	St. dev.	0.04	0.03	0.003
LS_5	Mean	1.18	1.17	0.17
	St. dev.	0.02	0.02	0.010

Table 3.7. Posterior mean and standard deviation of correlations for the case study building (1.4:1 aspect ratio)

Parameters	$\rho_{1,2}$	$\rho_{1,3}$	$\rho_{1,4}$	$\rho_{1,5}$	$\rho_{2,3}$	$\rho_{2,4}$	$\rho_{2,5}$	$\rho_{3,4}$	$\rho_{3,5}$	$\rho_{4,5}$
Mean	0.35	0.31	0.34	0.33	0.35	0.30	0.31	0.35	0.32	0.30
St. dev.	0.005	0.010	0.010	0.010	0.008	0.006	0.007	0.005	0.010	0.010

Figure 3.8 shows the demand models (D_i) corresponding to the five limit state functions (LS_i) for the case study building. The predicted demands (solid line) are shown along with the one standard deviation confidence interval (dashed lines) in the original space. In these figures, the dots (●) represent the equality data, while the triangles (▽) and the squares (□) represent the lower bound data. The triangles indicate the data exceeding 100% of capacity, and the squares indicate the corresponding lower bound data for the other limit state functions

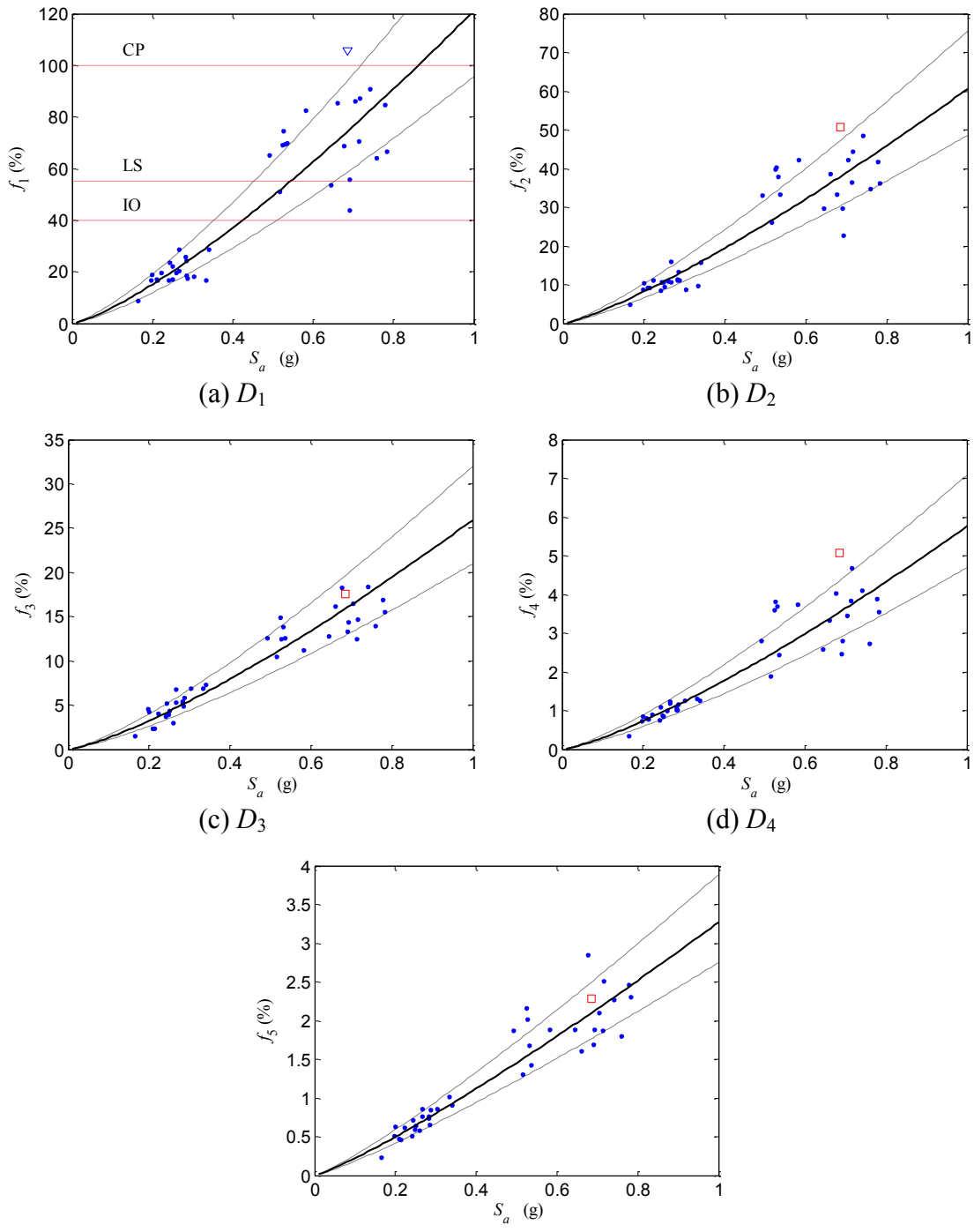

Fig. 3.8. Demand models (D_i) for the case study structure (1.4:1 aspect ratio)

Figure 3.8 shows that the force demands for LS_1 (f_1) associated with the in-plane shear strength provides the most critical failure mechanism among the five limit state functions. The ultimate capacity of the metal deck is exceeded during one of the 40 ground motions. The force demands for LS_2 (f_2) reach up to 50% of the connection capacity (shear), while those for LS_3 (f_3) reach up to 20% of their capacity (tension). Force demands in the deck-to-joist puddle weld connections (f_4 and f_5) reach less than 5% of their capacity for all 40 ground motions.

3.5.6. Probabilistic Capacity Limits

Capacity limits are determined for each of the selected limit state functions. For LS_1 associated with the in-plane shear strength of metal deck, capacity limits for three performance levels are used: Immediate Occupancy (IO), Life Safety (LS) and Collapse Prevention (CP). According to Luttrel (1967) and Cohen (2004), 40% of the ultimate strength is an indicator for minor damage of metal deck. Cohen (2004) discussed the relationship between shear forces and the corresponding DDR values. Based on previous experimental studies, nonlinear response begins at 40% of the ultimate strength to cause measurable damage. Therefore, this limit is used for IO. For the LS limit, 55% of the ultimate strength of the metal deck is used. This is based on the reduction factor for metal deck design under earthquake loads (SDI 2004) because most design practice targets LS performance level. Finally, 100% is used for defining the CP limit, which corresponds to the ultimate in-plane shear capacity of the metal deck (1010 kN) based on the SDI manual (SDI 2004).

For limit state functions LS_2 through LS_5, 100% of the ultimate strength of each individual connection is used for the CP limit, which is a conservative assumption in terms of the overall response of the structure. It is noted that the uncertainty associated with the capacity limits is assumed to be equal to 0.3 based on Wen et al. (2004). Table 3.8 summarizes the capacity limits and the corresponding force values for the case study building. For the capacities for LS_4 and LS_5, the sum of ultimate capacity of puddle welds within 12.2 m (40 ft), which is the dimension of a single panel, is used. The horizontal lines in Figure 3.9 indicate the mean capacity limits for each limit state function in terms of force.

Table 3.8. Capacity limits for the case study building (1.4:1 aspect ratio)

Limit state functions	Performance levels	Capacity limits (%)	Capacity (kN)
	IO	40	404
LS_1	LS	55	556
	CP	100	1010
LS_2	CP	100	59.7
LS_3	CP	100	41.8
LS_4	CP	100	413
LS_5	CP	100	722

3.5.7. Fragility Curves

The five demand models and corresponding capacity limits are used to estimate fragilities using Monte-Carlo simulations. It is noted that no modeling uncertainty is included in the Monte-Carlo simulation. Figure 3.9 shows the seismic fragility curves

with one standard deviation bounds for the case study building using the linear demand models. It is noted that the fragility curves are developed up to S_a of 1.0g to cover all the data points used in the development of demand models.

Approximate confidence bounds (dashed lines) are also constructed along with the fragility curves (solid lines) in Figure 3.9. Gardoni et al. (2002) proposed the approximate confidence bounds based on the relationship between reliability index and the corresponding fragility estimates. Bounds of the reliability index are computed using a first-order analysis and these are transformed back into the probability space to express confidence bounds of fragility. The dotted lines along with each fragility curve in Figure 3.9 show the one standard deviation bounds of fragility estimates. More information about the fragility bounds is provided by Gardoni et al. (2002).

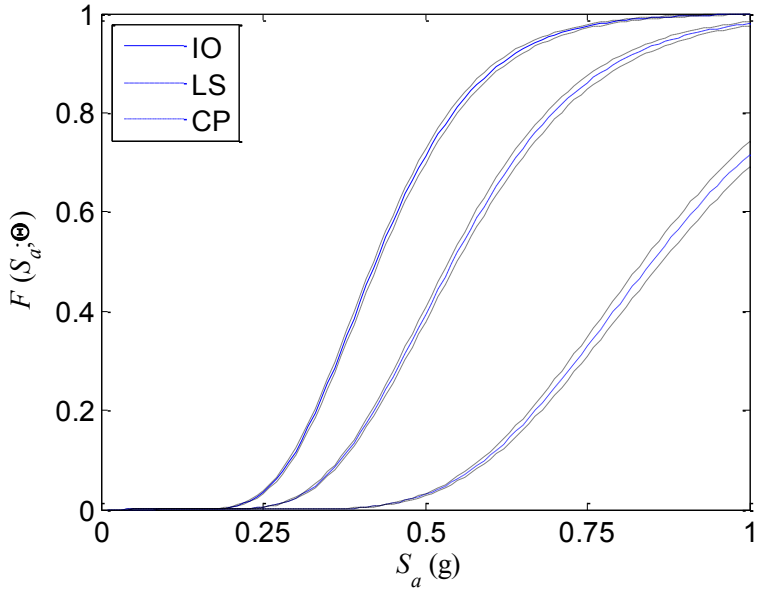

Fig. 3.9. Fragility curves for the case study structure (1.4:1 aspect ratio)

Table 3.9 shows fragility estimates for the median S_a computed over the synthetic ground motions for the 10% and 2% in 50 years records. As defined earlier, fragility estimates are the conditional probability of attaining or exceeding a specific performance level for a given earthquake intensity. As shown in Table 3.9, the corresponding S_a values for 10% and 2% in 50 years motions are 0.26g and 0.68g, respectively. For the 10% in 50 years motions, the fragility estimates for the three performance levels are low. However, the 2% in 50 years motions show a high probability of exceeding the IO and LS performance levels. Even for the CP limit, the fragility is estimated as 22%.

Table 3.9. Fragility estimates for the case study building (1.4:1 aspect ratio)

Ground motion	Median S_a(g)	Performance level	Mean fragility estimates
10% in 50 years	0.26	IO	0.05
		LS	0.01
		CP	0.00
2% in 50 years	0.68	IO	0.94
		LS	0.78
		CP	0.22

As discussed earlier, the limit state functions associated with connections (LS_2 to LS_5) use a conservative assumption of CP performance with the failure of one connection. Figure 3.10 shows the comparison of CP fragility curves with two different sets of limit state functions. One curve is developed based on all the limit state functions (LS_1-LS_5) for the case study building and the other is developed based only on LS_1. As

shown, there is only a marginal difference between fragilities because the first limit state function (LS_1) governs the estimation of the CP fragility. The assumption used in this study provides a slightly conservative result for the upper range of earthquake intensity (S_a values of 0.70g and larger).

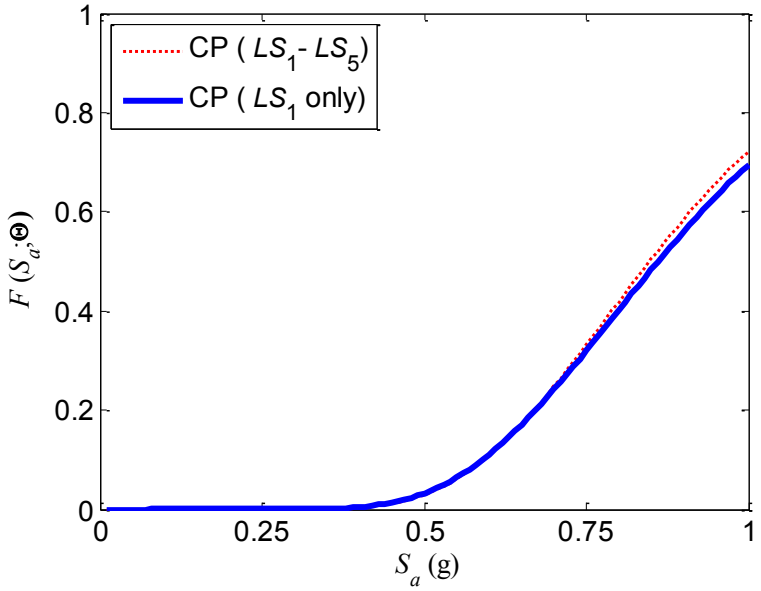

Fig. 3.10. Comparison of CP fragility curves (1.4:1 aspect ratio)

3.6. Influence of Different Aspect Ratios

3.6.1. Tilt-up Concrete Building with 4:1 Aspect Ratio

To see the influence of different aspect ratios, a ratio between length and width of 4:1 is selected for comparison. This aspect ratio is determined based on the maximum aspect ratio limit of untopped metal deck diaphragm by ASCE/SEI 31-03 (2003) to avoid high diaphragm shear demands. The building is designed and analyzed using the same

criteria. The same design codes are used as the 1.4:1 aspect ratio case study building and Table 3.10 shows the major differences in the design parameters.

Table 3.10. Comparison of design parameters for the tilt-up buildings with different aspect ratios

Members	Parameters	Values	
		1.4:1	**4:1**
Metal deck (22WR, Type B)	Thickness (t)	0.749 mm (0.0295 in)	0.909 mm (0.0358 in)
	Moment of Inertia (I)	23100 cm^4/m (0.169 in^4/ft)	29000 cm^4/m (0.212 in^4/ft)
	Effective shear modulus (G')	2550 N/mm (14.5 kip/in)	12400 N/mm (70.7 kip/in)
Concrete wall	Thickness (t)	190 mm (7.5 in)	240 mm (9.5 in)
Puddle welds	Pattern	36/4 and 36/7	36/7

3.6.2. Analytical Results for 4:1 building

Abaqus is used for eigenvalue, push-over and nonlinear dynamic analyses for the 4:1 building. For nonlinear dynamic analysis, the same ground motion records are used. Figure 3.11 shows the first mode shape of the 4:1 building using Abaqus. The fundamental period of the 4:1 building is 0.77 *s*.

Push-over analysis is also conducted to monitor nonlinear behavior of the structure under static loads. Figure 3.12 shows the relationships between shear ratio and maximum DDR for the 4:1 building.

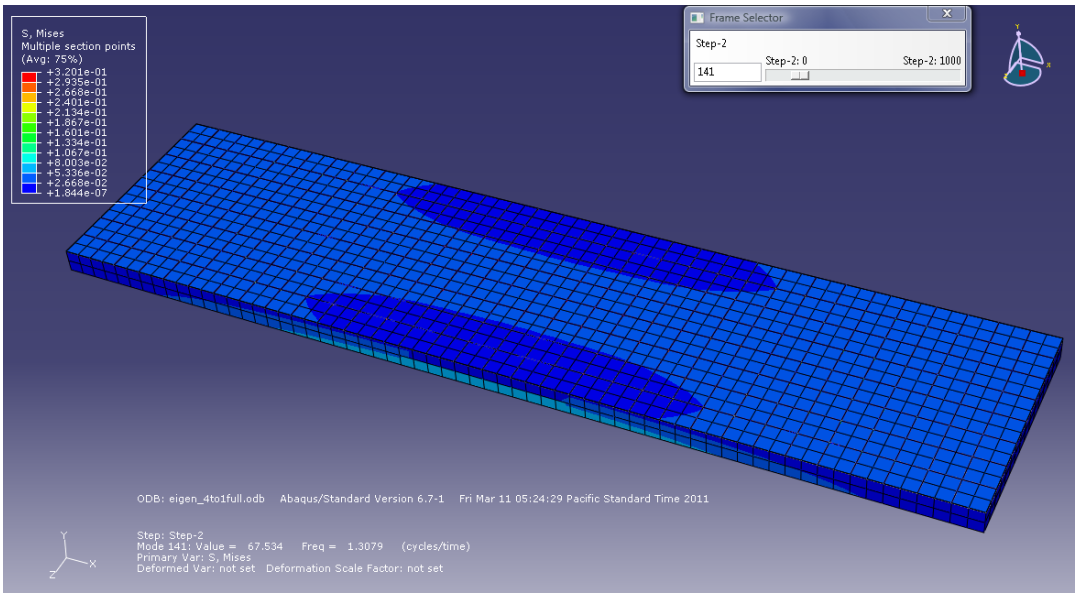

Fig. 3.11. First mode shape for the 4:1 building

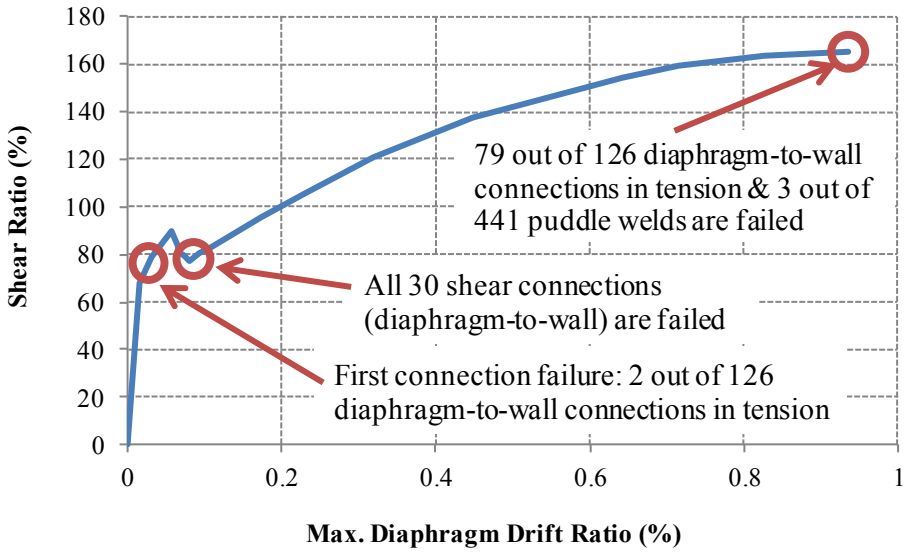

Fig. 3.12. Push-over curve for the 4:1 building

First failure of connection is observed at the maximum DDR of 0.06% (109 mm) in the diaphragm-to-wall connections in tension. After the first failure of diaphragm-to-

wall connections in tension, 83% of diaphragm-to-wall connections in shear (25 out of 30) are failed in the next time step at the maximum DDR of 0.07% (127 mm). Then the base shear is reduced until all the diaphragm-to-wall connections in shear are failed at the maximum DDR of 0.08% (158 mm). When the diaphragm-to-wall connections in shear are all failed, the base shear is increased again until most of connections including three puddle welds are failed. At the end of the analysis, all the diaphragm-to-wall connections in shear and 63% of diaphragm-to-wall connections in tension are failed. It is noted that the base shear after losing all the diaphragm-to-wall connections in shear might be overestimated since concrete panels are assumed to be connected firmly without any panel-to-panel connection models. Comparing with the 1.4:1 building, the overall behavior is similar: first connection failure is occurred at the diaphragm-to-wall connections in tension but after all more connections in shear are failed.

Nonlinear dynamic analysis is also conducted to provide dynamic behavior of the 4:1 building. Table 3.11 summarizes the maximum DDR for each ground motion data with the corresponding spectral acceleration.

Table 3.11. Maximum DDR and spectral acceleration from nonlinear dynamic analysis (4:1 aspect ratio)

Ground Motion ID	10% in 50 years				2% in 50 years			
	Lowlands		Uplands		Lowlands		Uplands	
	S_a (g)	DDR (%)	S_a (g)	DDR (%)	S_a (g)	DDR (%)	S_a (g)	DDR (%)
1	0.17	0.02	0.28	0.03	0.67	0.08	0.78	0.09
2	0.19	0.03	0.21	0.02	0.75	0.08	0.52	0.06
3	0.20	0.04	0.25	0.03	0.62	0.07	0.53	0.07
4	0.21	0.05	0.17	0.02	0.79	0.07	0.54	0.06
5	0.19	0.02	0.16	0.02	0.57	0.06	0.61	0.08
6	0.20	0.04	0.18	0.03	0.56	0.07	0.72	0.08
7	0.12	0.02	0.16	0.02	0.82	0.09	0.71	0.08
8	0.21	0.02	0.22	0.02	0.74	0.10	0.53	0.06
9	0.22	0.03	0.21	0.02	0.61	0.06	0.63	0.07
10	0.12	0.03	0.15	0.02	0.64	0.09	0.75	0.11
Mean	0.18	0.03	0.20	0.02	0.68	0.08	0.63	0.08

Based on the dynamic analysis results, the maximum DDR values for 10% in 50 years motions range from 0.02% to 0.05%, while those for 2% in 50 years motions are between 0.06% and 0.11%. There are no connection failures observed from all the dynamic analyses using 40 ground motion records. It is noted that the maximum DDR values for the 4:1 building are smaller than those for the 1.4:1 building because DDR is a function of the longitudinal dimension of the building. Most of the maximum displacements of the roof diaphragm relative to the supporting walls for the 4:1 building are close to or larger than those for the 1.4:1 building.

For constructing fragility curves, limit state functions are defined and corresponding capacity limits and demand models are developed for the 4:1 building. Probabilistic capacity limits in percentage are the same except for the last scenario of failure associated with puddle welds because the 4:1 building only has the 36/7 pattern for puddle welds. Therefore, a total of four capacity limits and corresponding demand models are developed. Using the Bayesian updating and the MCMC techniques, unknown parameters of the posterior statistics are determined for the demand models. Table 3.12 provides the posterior statistics of the unknown parameters of each demand model (D_i) corresponding to four limit state functions (LS_i) for the 4:1 building. Table 3.13 shows the posterior mean and standard deviation of the correlations ($\rho_{i,j}$) among the individual model errors, which represent the potential dependence between the limit state functions.

Figure 3.13 shows the demand models of four limit state functions for the 4:1 building. The predicted demands (solid line) are shown along with the one standard deviation confidence interval (dashed line) in the original space. In these figures, the dots (●) represent the equality data, while the triangles (▽) and the squares (□) represent the lower bound data. The triangles indicate the data exceeding 100% of capacity, and the squares indicate the corresponding lower bound data for the other limit state functions.

Table 3.12. Posterior statistics of parameters for the 4:1 building

Limit state functions		θ_0	θ_1	σ
LS_1	Mean	5.24	0.92	0.13
	St. dev.	0.02	0.01	0.009
LS_2	Mean	4.76	1.17	0.16
	St. dev.	0.02	0.02	0.012
LS_3	Mean	2.95	0.98	0.19
	St. dev.	0.02	0.01	0.004
LS_4	Mean	1.38	1.20	0.23
	St. dev.	0.02	0.01	0.009

Table 3.13. Posterior mean and standard deviation of correlations for the 4:1 building

Parameters	$\rho_{1,2}$	$\rho_{1,3}$	$\rho_{1,4}$	$\rho_{2,3}$	$\rho_{2,4}$	$\rho_{3,4}$
Mean	0.29	0.30	0.30	0.30	0.31	0.28
St. dev.	0.007	0.010	0.009	0.010	0.008	0.022

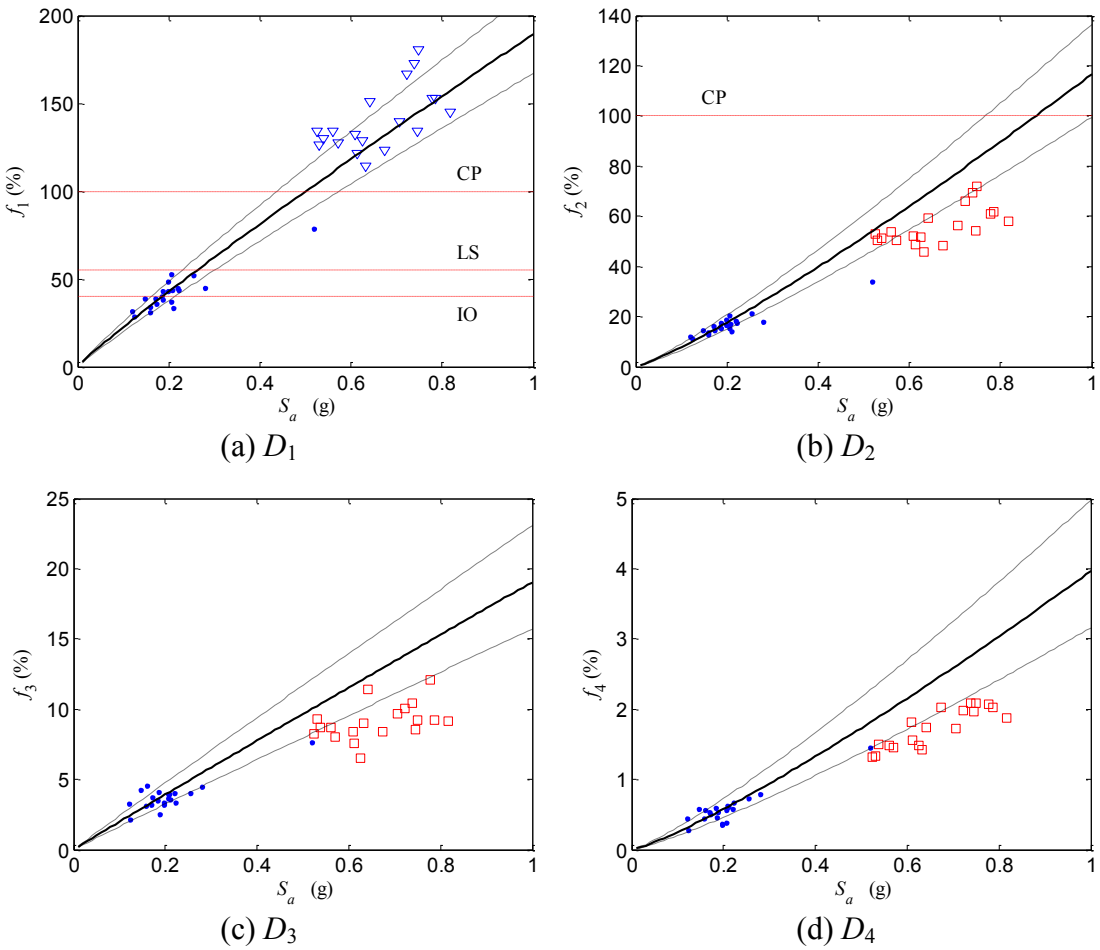

Fig. 3.13. Demand models (D_i) for the case study structure (4:1 aspect ratio)

As shown in Figure 3.13, the force demands for LS_1 (f_1) associated with the in-plane shear strength provides the most critical failure mechanism among the four limit state functions. The ultimate capacity of the metal deck is exceeded during 19 of 20 ground motion records of the 2% in 50 years motions. The force demands for LS_2 (f_2) reach up to 90% of the connection strength (shear), while those for LS_3 (f_3) reach around 15% of the capacity (tension). Force demands in puddle welds connections are less than 3% of the capacity.

3.6.3. Comparison of Fragility Estimates between 1.4:1 and 4:1 Aspect Ratios

Fragility curves for the 4:1 building are developed and compared with those for the 1.4:1 building. Figure 3.14 shows the seismic fragility curves (solid lines) with one standard deviation bounds (dashed lines) for the 4:1 building using the linear demand models. In addition, Table 3.14 shows fragility estimates along with one standard deviation bounds for the median S_a computed over the synthetic ground motions for the 10% and 2% in 50 years records.

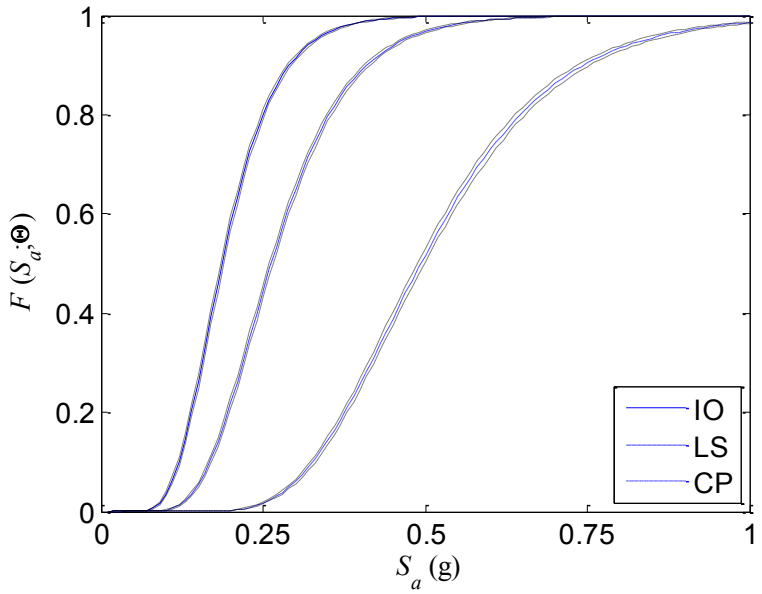

Fig. 3.14. Fragility curves for the 4:1 building

Table 3.14. Fragility estimates for the 4:1 building

Ground motion	Median S_a(g)	Performance level	Mean fragility estimates
10% in 50 years	0.19	IO	0.53
		LS	0.18
		CP	0.002
2% in 50 years	0.64	IO	1.00
		LS	1.00
		CP	0.79

Figure 3.14 and Table 3.14 show the seismic fragility estimates assessed using the linear demand model for the 4:1 building. As shown in Table 3.14, the corresponding spectral acceleration values for 10% and 2% in 50 years motions are 0.19g and 0.64g, respectively. For the motions with a 10% probability of exceedance in 50 years, the fragility estimates for three performance levels are larger than those for the 1.4:1 building. The 2% in 50 years motions provide significantly high probabilities of exceeding all the performance levels. In particular, for the CP limit, fragility is estimated as 79%. This indicates significant damage for the structure during a high intensity, but less frequent, earthquake event in the Central U.S.

Based on the comparison between Tables 3.9 and 3.14, 4:1 building has significantly higher fragilities than 1.4:1 building. It is noted that all the fragility estimates are developed based on the force-controlled limit states, particularly governed by the in-plane shear strength of metal deck. The 4:1 building has extremely high shear demands according to large aspect ratio, while the maximum DDR values are even less

than those for the 1.4:1 building. Therefore, larger aspect ratio provides higher shear demands which cause higher fragilities.

3.7. Summary

This section focuses on seismic vulnerability assessment for typical tilt-up concrete buildings in the Central U.S. Analytical modeling techniques using nonlinear properties to capture potential failure mechanisms are developed and verified with measured data in the literature. The developed modeling approach is applied to tilt-up concrete buildings for assessing seismic vulnerability of the structures. The influence of different aspect ratios (1.4:1 and 4:1) with respect to the building plan dimensions is also considered. Eigenvalue analysis and push-over analysis are conducted to have a better understanding of structural performance of the buildings. In addition, nonlinear dynamic analyses using synthetic ground motions for Memphis, Tennessee, are performed to assess dynamic behavior of the buildings. Then, probabilistic demand models for multiple limit states that represent potential failure mechanisms are developed with a Bayesian updating approach. These demand models are used in conjunction with appropriate capacity limits to develop fragility curves that provide a probabilistic measure of the seismic vulnerability of typical tilt-up concrete buildings. This study shows that the vulnerability of typical tilt-up structures in mid-America is significant when seismic hazards are high. In addition, it is found that aspect ratio of building geometry has a significant impact on the seismic performance and fragility estimates of buildings.

4. PROBABILISTIC FRAMEWORK FOR STRUCTURAL DAMAGE ASSESSMENT*

4.1. Introduction

Stakeholders like investors, city planners, and building owners in regions subject to seismic hazards need to know the expected losses due to seismic events. To estimate the losses due to structural damage, a probabilistic methodology is needed that accounts for available structural damage data and the prevailing uncertainties.

This section proposes a set of structural damage states and a procedure for calculating structural damage factors, defined as the cost of structural repairs as a percentage of the replacement value of the structural portion of a building, which is essential information to compute economic losses. This methodology provides a means to link the structural performance to a structural loss estimation that can be used for social and economic impact studies. Prediction and confidence bands are constructed to account for the prevailing uncertainties. Based on this developed methodology, the expected seismic structural damage for three types of building structures in the Mid-America region is assessed.

Several studies have been conducted to assess the structural damage due to a seismic event (Erberik and Elnashai 2006, Kircher et al. 2006a, Olshansky and Wu 2004,

---

*Reprinted with permission from "Probabilistic assessment of structural damage due to earthquakes for buildings in Mid-America" by Bai, J.-W., Hueste, M.B.D, and Gardoni, P., 2009, *Journal of Structural Engineering*, 135(10), 1155-1163, Copyright © 2009, ASCE.

Porter et al. 2002, King et al. 2005, Singhal and Kiremidjian 1996). Only a few studies have evaluated the expected seismic damage of buildings in the Central and Eastern United States, and those are based on a deterministic approach that does not consider the underlying uncertainties. However, proper accounting for the uncertainties is needed for a decision-making process focused on whether to repair a given building or collection of buildings.

The HAZUS (FEMA 2001) program can be used to estimate potential losses due to various hazards including floods, earthquakes, and hurricanes. The HAZUS methodology provides estimates of losses due to structural and nonstructural damage in terms of repair costs, expressed as a percent of building replacement costs. However, the repair costs, provided by building occupancy class and model building type, are deterministic. Moreover, HAZUS is intended to provide estimates at the regional scale.

4.2. Past Damage Records and Related Studies

The Applied Technology Council (ATC) conducted a survey on building structures after the Northridge, California, earthquake of January 17, 1994. The outcomes of this survey were documented in the ATC-38 report *Database on the Performance of Structures near Strong-Motion Recordings: 1994 Northridge, California, Earthquake* (ATC 2000). The ATC-38 document provides information related to the surveys, including the standardized form used, details about the procedures used, and a summary database. The database was developed by collecting 530 survey results from 31 strong motion recording stations in the Los Angeles area. In the database, the peak ground acceleration

(PGA) varies from 0.15g to 1.78g and the distances from the epicenter ranges from 2 to 39 km. The data was collected for 15 building types, categorized primarily by structural materials, and 20 occupancy types. Four categories of qualitative damage states were used for the overall damage inspection, as described in Table 4.1. In addition to the overall damage rating, the same group of engineers categorized the building damage using the damage states provided in ATC-13 *Earthquake Damage Evaluation Data for California* (ATC 1985). The ATC-13 damage states were developed as a function of the percentage of replacement cost (damage factor). The damage states and corresponding damage factor ranges were based on inputs from earthquake engineering experts who provided estimates for different classes of facilities. Table 4.2 shows the seven ATC-13 damage states and the corresponding ranges of the damage factors.

Table 4.1. ATC-38 damage state classification [adapted from ATC (2000)]

Damage state	Description
None (N)	None. No damage is visible, either structural or nonstructural.
Insignificant (I)	Damage requires no more than cosmetic repair. No structural repairs are necessary. For nonstructural elements this would include spackling, partition cracks, picking up spilled contents, putting back fallen ceiling tiles, and righting equipment.
Moderate (M)	Repairable structural damage has occurred. The existing elements can be repaired essentially in place, without substantial demolition or replacement of elements. For nonstructural elements this would include minor replacement of damaged partitions, ceilings, contents, and equipment or their anchorages.
Heavy (H)	Damage is so extensive that repair of elements is either not feasible or requires major demolition or replacement. For nonstructural elements this would include major or complete replacement of damaged partitions, ceilings, contents, equipment or their anchorages.

Table 4.2. ATC-13 damage states and corresponding damage factor ranges [adapted from ATC (1985)]

Damage state	Damage factor range (%)
1 – None	0
2 – Slight	0 – 1
3 – Light	1 – 10
4 – Moderate	10 – 30
5 – Heavy	30 – 60
6 – Major	60 – 100
7 – Destroyed	100

The ATC-13 (ATC 1985) methodology and preliminary ATC-38 damage data (which is slightly different from the final ATC-38 damage data [ATC 2000]) were used in a study conducted by the National Center for Earthquake Engineering Research. The study called "Loss Assessment of Memphis Buildings (LAMB)" estimated the economic losses due to structural damage in the Memphis region. The LAMB report (Abrams and Shinozuka 1997) provides the inventory of structures, ground motion data, structural analysis and response of reinforced concrete (RC) and masonry buildings, fragility curve development, and loss estimation.

The LAMB study developed average damage factors, defined as a percentage of replacement value, to estimate the direct economic losses from damage of reinforced concrete and unreinforced masonry buildings in Memphis/Shelby County, Tennessee, due to a magnitude 7.5 event with an epicenter at Marked Tree, Arkansas. The study used the ATC-38 preliminary database and determined the total number of buildings that were assigned to each combination of the ATC-13 and ATC-38 damage states. The

ATC-38 overall damage states were mapped onto the ATC-13 damage factor range for structural, nonstructural, and contents loss and the number of buildings in each combination was listed. The mapped results for structural damage using the final ATC-38 database are provided in Table 4.3. These values are similar to those summarized in the LAMB study based on the preliminary ATC-38 database. It may be observed that low damage states have significantly more data points than high damage states. Most buildings are categorized within the "None" and "Insignificant" overall damage states. This gives more confidence in the accuracy of these ranges. For the "Heavy" damage state, the number of buildings is only 10 (1.9 percent of the total number of buildings). Table 4.4 shows the damage factors for the repair cost as a percentage of replacement value used in the LAMB study based on the distribution of the damaged buildings shown in Table 4.3. These values were computed by summing the product of the central damage factor (mid-point of the damage factor range) and the percentage of damaged structures in each structural damage state. As shown in Table 4.4, average damage factors increase as the overall damage state becomes greater. However, for "Heavy" damage of nonresidential buildings, a loss factor of 41% seems to be quite low for the expected repair costs. This may be partly due to the fact that there were fewer data for the "Moderate" and "Heavy" damage states, and so the distribution of damage factors is less accurate than for the lower damage states. The LAMB study provides a procedure to compute average loss factors but it is a deterministic approach so that uncertainties in damage state definition and final damage factors are not considered. In addition, the

central damage factor for ATC-13 damage category 6 is 80%, which is a relatively small number for structures that may have up to 100% damage.

Table 4.3. Damage factor distributions by number of buildings in the ATC-38 database

ATC-13		ATC-38 structural damage state			
Damage state	**Damage factor range (%)**	**N**	**I**	**M**	**H**
1	0	86	113	3	·
2	0 – 1	10	198	17	·
3	1 – 10	·	8	32	1
4	10 – 30	·	·	16	1
5	30 – 60	·	·	4	3
6	60 – 100	·	·	·	4
Unknown		2	22	6	1
Total No. of buildings*		98	341	78	10
Percentage		18.5%	64.3%	14.7%	1.9%

* 3 unknown data are not included.

Table 4.4. LAMB damage factors for repair cost [adapted from Abrams and Shinozuka (1997)]

Type of loss	Overall damage state			
Major use of building	**N**	**I**	**M**	**H**
Structural				
Residential	0%	0%	9%	68%
Nonresidential	0%	1%	11%	41%

4.3. Probabilistic Assessment of Structural Damage

Many uncertain parameters play an important role in the damage assessment process. Sources of uncertainty include hazard definition, structural and nonstructural capacities, performance level definitions, damage state descriptions, repair and replacement costs, and other modeling assumptions. Uncertainties associated with analytical models of structures, capacity limits describing structural performance levels, and demand models, are included in the development of the structural fragility curves used in the damage assessment. To account for uncertainties in estimating building structural damage due to earthquakes, a probabilistic approach is developed in this section. This approach provides mean damage factors as a function of the intensity measure, along with prediction and confidence bands to describe the uncertainties in the damage assessment, thus providing refined information to decision makers.

The overall process for assessing structural damage includes five steps: (1) defining the damage state descriptions; (2) mapping between fragility curves and damage states; (3) defining damage factors associated with damage states; (4) calculating total damage factor; and (5) constructing prediction/confidence bands.

4.3.1. Damage State Descriptions

For this study, the ATC-13 damage factors, along with the ATC-38 damage state classifications and database of building damage, are used as a starting point for selecting damage factors for structural damage. This is because the ATC-38 study is unique with respect to the information provided for building damage following an earthquake. In addition, uncertainty is considered to account for the variability associated with the collection of the data, the selection of the damage factors, and the application of the data to construction in other regions. Table 4.5 shows the difference between the ATC-38 damage state classifications and the proposed damage states. The main changes are that the ATC-38 "None" and "Insignificant" damage states have been merged together to provide one low level damage state. It can be noted that for these lower damage levels, there is very little structural damage expected and the damage factor range is very small. As such, refinement in this range is not required for the structural damage assessment. In addition, a new category for complete damage ("Complete") has been added to provide more refinement for higher levels of damage where the damage factors have a larger range. This provides a total of four damage states for the proposed methodology: Insignificant (I), Moderate (M), Heavy (H), and Complete (C). This is considered to be a sufficient number of damage states for use in a structural damage assessment given the inherent uncertainty associated with such an analysis. The selected descriptions and number of damage states also relates well with the use of three structural fragility curves based on standard performance levels, as described in the following section. Table 4.6 provides a description of the damage associated with each damage state. The damage

states descriptions are based on those used in ATC-38 (Table 1) with the modifications described above.

Table 4.5. Comparison of ATC-38 and proposed damage states

ATC-38 damage states	Proposed damage states	Comments
None (N) / Insignificant (I)	Insignificant (I)	None (N) and Insignificant (I) damage states in ATC-38 are merged into Insignificant (I) damage state.
Moderate (M)	Moderate (M)	Same
Heavy (H)	Heavy (H) / Complete (C)	Heavy (H) damage state in ATC-38 is divided into Heavy (H) and Complete (C) damage states.

Table 4.6. Proposed damage state descriptions

Damage state	Description
Insignificant (I)	Damage requires no more than cosmetic repair. No structural repairs are necessary. For nonstructural elements, repairs could include spackling, partition cracks, picking up spilled contents, putting back fallen ceiling tiles, and righting equipment.
Moderate (M)	Repairable structural damage has occurred. The existing elements can be repaired essentially in place, without substantial demolition or replacement of elements. For nonstructural elements, repairs would include minor replacement of damaged partitions, ceilings, contents, and equipment or their anchorages.
Heavy (H)	While the damage is significant, the structure is still standing. Structural damage would require major repairs, including substantial demolition or replacement of elements. For nonstructural elements, repairs would include major replacement of damaged partitions, ceilings, contents, equipment or their anchorages.
Complete (C)	Damage is so extensive that repair of most structural elements is not feasible. Structure is destroyed or most of the structural members have reached their ultimate capacities.

4.3.2. Relationship between Fragility Curves and Damage States

Fragility curves are typically developed based on performance levels that reference the occurrence of various limit states within a structure. Recent studies on the seismic fragility assessment of buildings in the Central U.S. include Hueste and Bai (2007a,b), Kinali and Ellingwood (2007), Lee and Rosowsky (2006), Ramamoorthy et al. (2006), and Wen and Ellingwood (2005). The appropriate limit states can vary among structure types, depending on specific structural behavior and potential modes of failure during a seismic event.

Figure 4.1 and Table 4.7 illustrate a possible relationship between the performance levels used to define fragility curves and the damage state definitions. In

the developed methodology, three performance levels corresponding to structural limit states are defined generically as PL1, PL2, and PL3. For example, PL1, PL2, and PL3 could be three ASCE/SEI 41-06 (2007) performance levels: Immediate Occupancy (IO), Life Safety (LS), and Collapse Prevention (CP), respectively. The performance levels assigned to a set of fragility curves is mapped to the appropriate generic performance level based on the desired damage bounds.

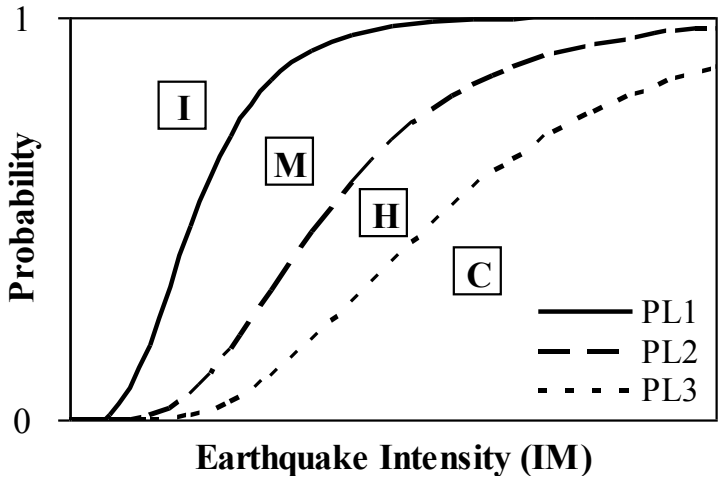

Fig. 4.1. Illustration of relationship between fragility curves and damage states

Table 4.7. Relationship between damage states and performance levels

Damage state	Performance level
Insignificant (I)	
Moderate (M)	← PL1
Heavy (H)	← PL2
Complete (C)	← PL3

4.3.3. Damage Factors Associated with Damage States

Structural damage factors are needed to quantify the cost of structural repairs as a percentage of the replacement value of the structural portion of a building. To calculate the damage factors for estimating the cost of repairing structural damage, a link is made between the ATC-13 damage categories and the developed damage states in this study. The numerical ATC-38 building data presented in Table 4.3 was used to determine an appropriate mapping strategy. Table 4.8 provides the relationship between the overall damage states and the ATC-13 damage categories, along with the ATC-13 damage factors. As determined from Table 4.3, "Insignificant" damage corresponds primarily to ATC-13 damage categories 1 and 2, while ATC-13 damage categories 3 and 4 are assigned to the majority of the structures with "Moderate" damage. For "Heavy" damage, ATC-13 damage category 6 (60 – 100%) is divided into two ranges (6a and 6b). A linear function is assumed for damage category 6 when it is separated.

Table 4.8. Relationship between proposed damage states and ATC-13 damage categories

Proposed damage state	ATC-13 damage category	ATC-13 damage factor range (%)
Insignificant (I)	1, 2	0, 0 – 1
Moderate (M)	3, 4	1 – 10, 10 – 30
Heavy (H)	5, 6a	30 – 60, 60 – 80
Complete (C)	6b, 7	80 – 100, 100

A probabilistic approach is necessary to account for the uncertainties in the data collection and the information used to select the damage factors. This uncertainty should be directly incorporated into the overall uncertainty for the structural damage assessment. To take into account variability in estimating the damage factors, the damage factor (L_k) for each damage state, *k*, is assumed to be a random variable that has a Beta distribution. Since L_k is bounded, a Beta distribution is selected to model its variability. Table 4.9 shows the Beta distribution range for each damage state, along with the proposed mean (μ_{L_k}) and standard deviation values (σ_{L_k}) for the corresponding damage factors. The means μ_{L_k} are calculated as median points within the ranges. To explore the effect of σ_{L_k} on the distribution of L_k, Figure 4.2 shows the probability distribution for each damage state for three different values of σ_{L_k} (0.15, 0.20, and 0.25 times the given range for each damage state). The Beta distribution for $\sigma_{L_k} = 0.25$ times the given range is fairly flat, reflecting that there is much uncertainty in the value of L_k. On the contrary, for σ_{L_k} = 0.15 times the given ranges provides distribution mode

concentrated around the mean value, implying that there is little uncertainty in the value of L_k. In the current study, a value of $\sigma_{L_k} = 0.20$ times the given range is assumed. As more earthquake damage data becomes available, these statistical parameters can be refined.

Table 4.9. Statistical description of damage factors, L_k

Damage state	Range of Beta distribution (%)	Mean of damage factor μ_{L_k} (%)	Standard deviation of damage factor σ_{L_k} (%)
Insignificant (I)	[0, 1]	0.50	0.2 × [0, 1] = 0.2
Moderate (M)	[1, 30]	15.5	0.2 × [1, 30] = 5.8
Heavy (H)	[30, 80]	55.0	0.2 × [30, 80] = 10
Complete (C)	[80, 100]	90.0	0.2 × [80, 100] = 4

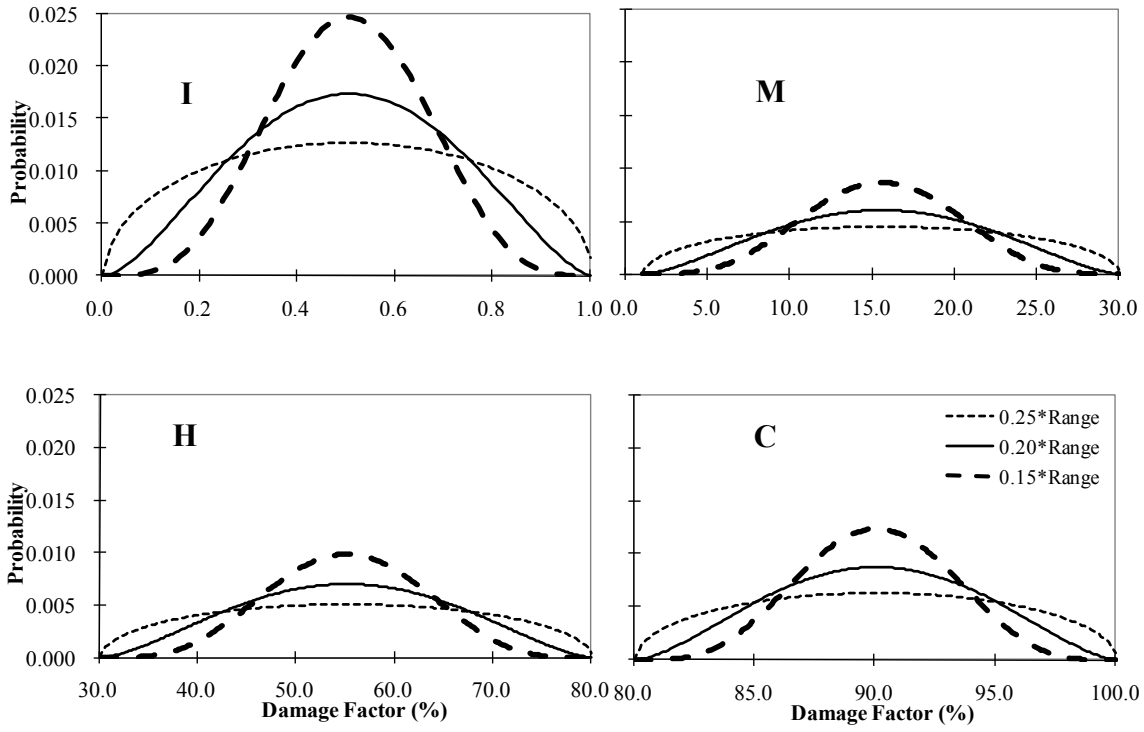

Fig. 4.2. Probability distribution for each damage factor, L_k

4.4. Estimation of Total Damage Factors

4.4.1. Total Damage Factors

After defining the damage factors associated with individual damage states, the total damage factor for a given intensity measure, $L|IM$, can be computed. The damage states are assumed to be bounded by the fragility curves, as illustrated in Figure 4.3. The probability of being in each damage state can be computed as the difference between the conditional probabilities of the bounding fragility curves. Conditional probability values (P_{PL1}, P_{PL2}, and P_{PL3}) that correspond to each performance level can be obtained for a given intensity measure from the fragility curves. These are the probability values of

attaining or exceeding a certain performance level conditioned on a measure of earthquake intensity.

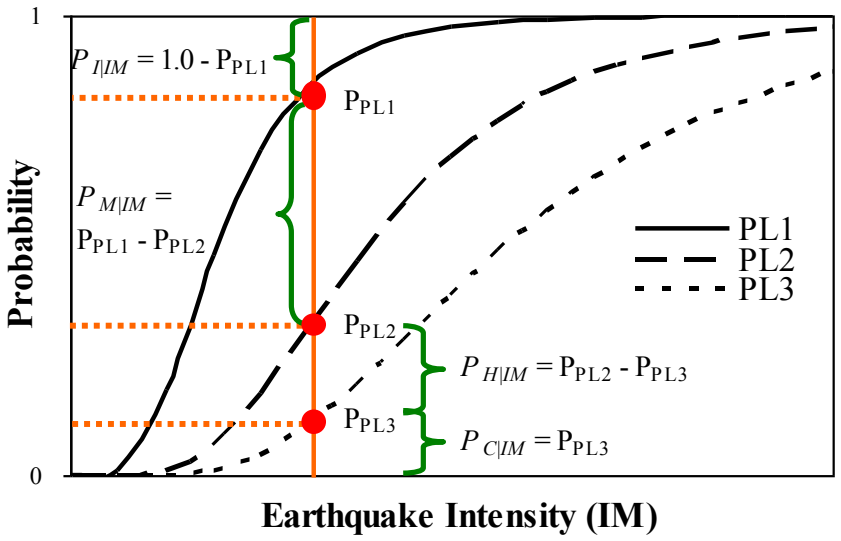

Fig. 4.3. Illustration for computing the probability of being in each damage state

Because $L\,|\,IM$ can only have a value between 0 and 1, it is assumed to have a Beta distribution as L_k. The following expressions are used to determine the conditional mean and variance of $L\,|\,IM$:

$$E\left[L\middle|IM\right]=\mu_{L|IM}=\sum_{k=1}^{4}\left(L_k\times P_{k|IM}\right) \tag{4.1}$$

$$Var\left[L\middle|IM\right]=\sigma^2_{L|IM}=\sum_{k=1}^{4}\left[\left(L_k-\mu_{L|IM}\right)^2\times P_{k|IM}\right] \tag{4.2}$$

where, $\mu_{L|IM}$ is the conditional mean of the total damage factor for a given intensity measure and $\sigma^2{}_{L|IM}$ is the conditional variance of the total damage factor for a given

intensity measure. One should note that since L_k in Equations (4.1) and (4.2) are random variables, $\mu_{L|IM}$ and $\sigma^2{}_{L|IM}$ are also random. Point estimates of $\mu_{L|IM}$ and $\sigma^2{}_{L|IM}$ can be computed by considering the mean values of L_k in Equations (4.1) and (4.2) as

$$\hat{\mu}_{L|IM} = \sum_{k=1}^{4} \left(\mu_{L_k} \times P_{k|IM} \right) \tag{4.3}$$

$$\hat{\sigma}^2_{L|IM} = \sum_{k=1}^{4} \left[\left(\mu_{L_k} - \hat{\mu}_{L|IM} \right)^2 \times P_{k|IM} \right] \tag{4.4}$$

where, $\hat{\mu}_{L|IM}$ is the point estimator of $\mu_{L|IM}$, μ_{L_k} is the mean of the damage factor for each damage state, and $\hat{\sigma}^2_{L|IM}$ is the point estimator of $\sigma^2{}_{L|IM}$.

4.4.2. Prediction and Confidence Bands

A prediction interval can be constructed to reflect the variability in $L \mid IM$ using its distribution (a Beta distribution, as assumed earlier, with mean and variance estimated according to Equations (4.3) and (4.4)). A series of prediction intervals can be generated by varying IM. This series of prediction intervals creates a prediction band. In addition, a confidence interval can be constructed for a given IM to capture the statistical uncertainty in $\mu_{L|IM}$. Based on Equation (4.1), it is noted that the confidence interval reflects the uncertainty in L_k, which in turn depends on the sample size used to assess L_k. In particular, to construct a confidence interval $\mu_{L|IM}$ is assumed to have a Beta distribution with mean $\hat{\mu}_{L|IM}$ and variance $\sigma^2_{\mu_{L|IM}}$, which can be calculated as

$$Var\left(\mu_{L|IM}\right)=\sigma^2_{\mu_{L|IM}}=\sum_{k=1}^{4}\sum_{l=1}^{4}\left[P_{k|IM}\times P_{l|IM}\times\rho_{kl}\times\sigma_{L_k}\times\sigma_{L_l}\right]$$
$$=\sum_{k=1}^{4}\left[P^2_{k|IM}\times\sigma^2_{L_k}\right]+2\sum_{k=1}^{3}\sum_{l=k+1}^{4}\left[P_{k|IM}\times P_{l|IM}\times\rho_{kl}\times\sigma_{L_k}\times\sigma_{L_l}\right] \quad (4.5)$$

where ρ_{kl} is the correlation coefficient between L_k and L_l. As for the prediction band, a confidence band can be generated by varying IM.

Figure 4.4 illustrates the expected total damage factor as a function of the intensity measure, along with the prediction and confidence bands. The prediction and confidence bands can be constructed using different percentiles to reflect different levels of confidence. The confidence band on $\mu_{L|IM}$ is, in general, contained in the corresponding prediction band for $L|IM$ because it is possible to predict the average response more precisely than an individual observation.

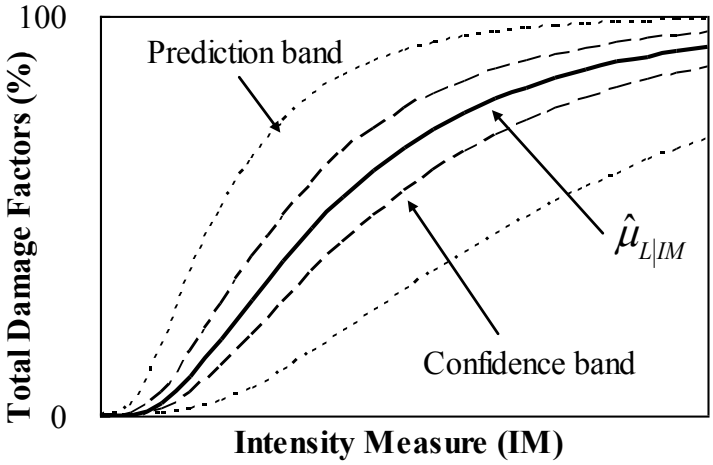

Fig. 4.4. Illustration of expected damage factor with prediction and confidence bands

4.5. Application of Developed Methodology to Three Case Studies

The proposed framework for estimating structural damage can be adapted to different approaches for conducting a regional damage assessment. One approach is to develop fragility curves that represent the building-to-building variability within a class of structures and to aggregate buildings within an inventory into relatively fewer classes of structures (for example, one class could be all RC frame buildings). A second approach is to develop fragility curves that correspond to more specific building characteristics within a class of structures and to aggregate buildings within an inventory into a more refined set of building classifications (for example, one class could be 3-5 story RC frame buildings). The selected approach for a particular regional loss assessment will depend on the availability of fragility curves and ground motion data. One benefit of the developed methodology is that it can be applied for either approach.

The developed methodology is illustrated for three case study buildings: a reinforced concrete (RC) building, a steel moment resisting frame (MRF) building, and an unreinforced masonry (URM) building. The buildings represent typical structures in the Mid-America region. Figure 4.5 shows the elevation views of the case study buildings.

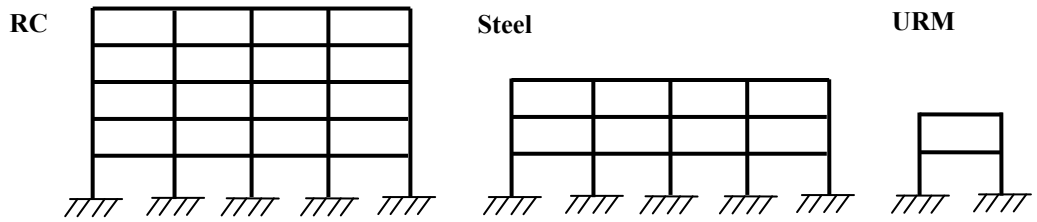

Fig. 4.5. Elevation of the case study structures

A set of synthetic ground motion data for Memphis, Tennessee, developed by Rix and Fernandez (2010), is used for the case studies. Both uplands and lowlands soil profiles are considered because Memphis has both soil types. The synthetic ground motion set contains suites of 20 ground motions each for 10% and 2% probabilities of exceedance in 50 years (10/50 and 2/50) motions. The selected earthquake intensity for each case study is the median value of spectral acceleration, S_a for a ground motion suite at the fundamental period of the building and it is calculated with 5% viscous damping.

Two levels of earthquake intensity are used to illustrate the calculations for each case study building, while the total damage factor is shown over the entire range of S_a. In addition, prediction and confidence bands are constructed to account for the inherent uncertainties.

4.5.1. Five-Story Reinforced Concrete (RC) Flat-Slab Structure

The first case study is a five-story RC flat-slab structure, designed for Memphis, Tennessee, based on building codes used in the mid-1980s (Hueste and Bai 2007a,b). This building has a moment frame system not specially detailed for ductile behavior. The floor system is composed of a flat-slab and perimeter moment-resisting frames with

spandrel beams. The fundamental period of the structure based on cracked section properties is 1.62 *s* and the corresponding median spectral acceleration values for 10/50 and 2/50 motions are 0.104g and 0.535g, respectively. Figure 4.6a shows fragility curves for this structure, determined using 1%, 2%, and 2.9% drift limits based on the FEMA 356 (ASCE 2000) global-level performance levels IO, LS, and CP.

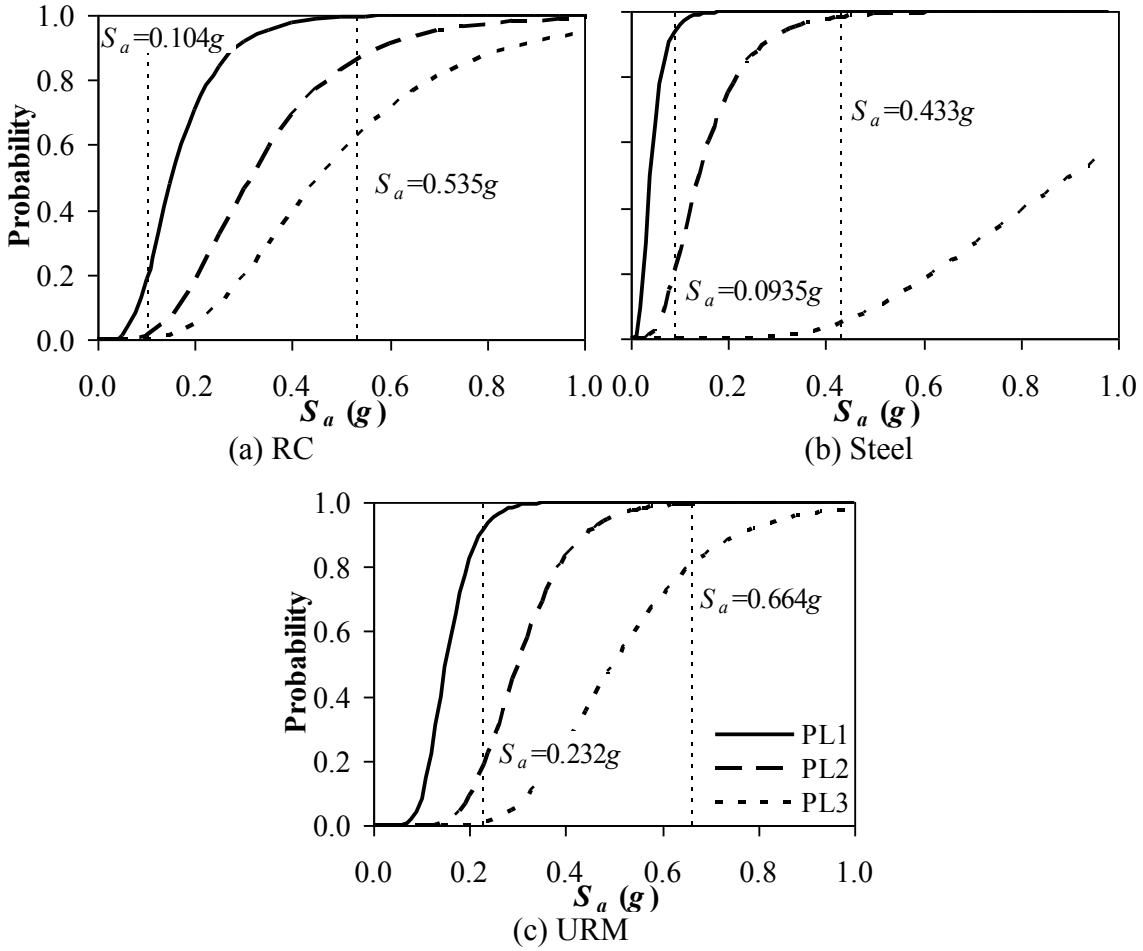

Fig. 4.6. Fragility curves for case study structures

4.5.2. Three-Story Steel Moment Resisting Frame (MRF) Structure

The second case study is a three-story, four-bay steel MRF building, which is typical of steel frames in the Central and Eastern U.S. and designed based on building codes used in the mid-1990s (Kinali and Ellingwood 2007). The moment connection for the case study building was assumed as fully restrained. The fundamental period of the structure is 2.01 *s* and the corresponding median spectral acceleration values for the 10/50 and 2/50 motions are 0.0935g and 0.433g, respectively. Kinali and Ellingwood (2007) developed fragility curves using interstory drift angle (ISDA) limits of 0.8%, 2%, and 8.6% for Immediate Occupancy (IO), Structural Damage (SD), and Collapse Prevention (CP) performance levels, respectively. Figure 4.6b shows the fragility curves for the three performance levels.

4.5.3. Two-Story Unreinforced Masonry (URM) Structure

The third case study is a two-story URM structure typical of those built in the 1930s in Memphis, Tennessee (Wen et al. 2004, MAE Center 2006). For nonlinear structural analysis, four wall damage modes including diagonal tension, bed-joint sliding, toe crushing, and rocking were considered. The fundamental period of the structure based on cracked section properties is 0.55 *s* and the corresponding median spectral acceleration values for the 10/50 and 2/50 motions are 0.232g and 0.664g, respectively. Figure 4.6c shows fragility curves for this structure, determined using 0.3% and 0.6% drift limits based on the FEMA 356 (ASCE 2000) performance levels IO and LS. For

PL3, Wen et al. (2004) used incremental dynamic analysis to define Incipient Collapse (IC).

4.5.4. Structural Damage Estimates

Table 4.10 describes the mapping of the damage states to the performance levels used to develop the fragility curves. Figure 4.7 shows the probabilities of each damage state as a function of S_a for the case study structures. The RC building has a higher probability range of Insignificant damage for S_a<0.2g, Moderate damage for 0.2g< S_a<0.4g, and Complete damage for S_a>0.4g. The URM building has a higher probability range of Insignificant damage for S_a<0.1g, Moderate damage for 0.1g<S_a<0.3g, Heavy damage for 0.3g<S_a<0.5g, and Complete damage for S_a>0.5g. For the steel building, the higher probability range for Insignificant and Moderate damage ends at $S_a \approx 0.15g$ and Heavy damage governs up to $S_a \approx 0.9g$. Table 10 lists the mean damage factors for each damage state and the probability values corresponding to the 10/50 and 2/50 motions.

Table 4.10. Data for case study structures

Performance level	Damage State	Damage factors μ_{L_k} (%)	Probability, $P_{k\|IM}$ (%)					
			RC		Steel		URM	
			10/50	2/50	10/50	2/50	10/50	2/50
PL1 → PL2 → PL3 →	I	0.50	81.4	0.425	5.46	0.00	7.64	0.00
	M	15.5	17.7	11.9	72.2	1.66	73.1	0.421
	H	55.0	0.820	22.7	22.3	93.4	18.2	19.1
	C	90.0	0.0851	65.0	0.00	4.94	0.997	80.5

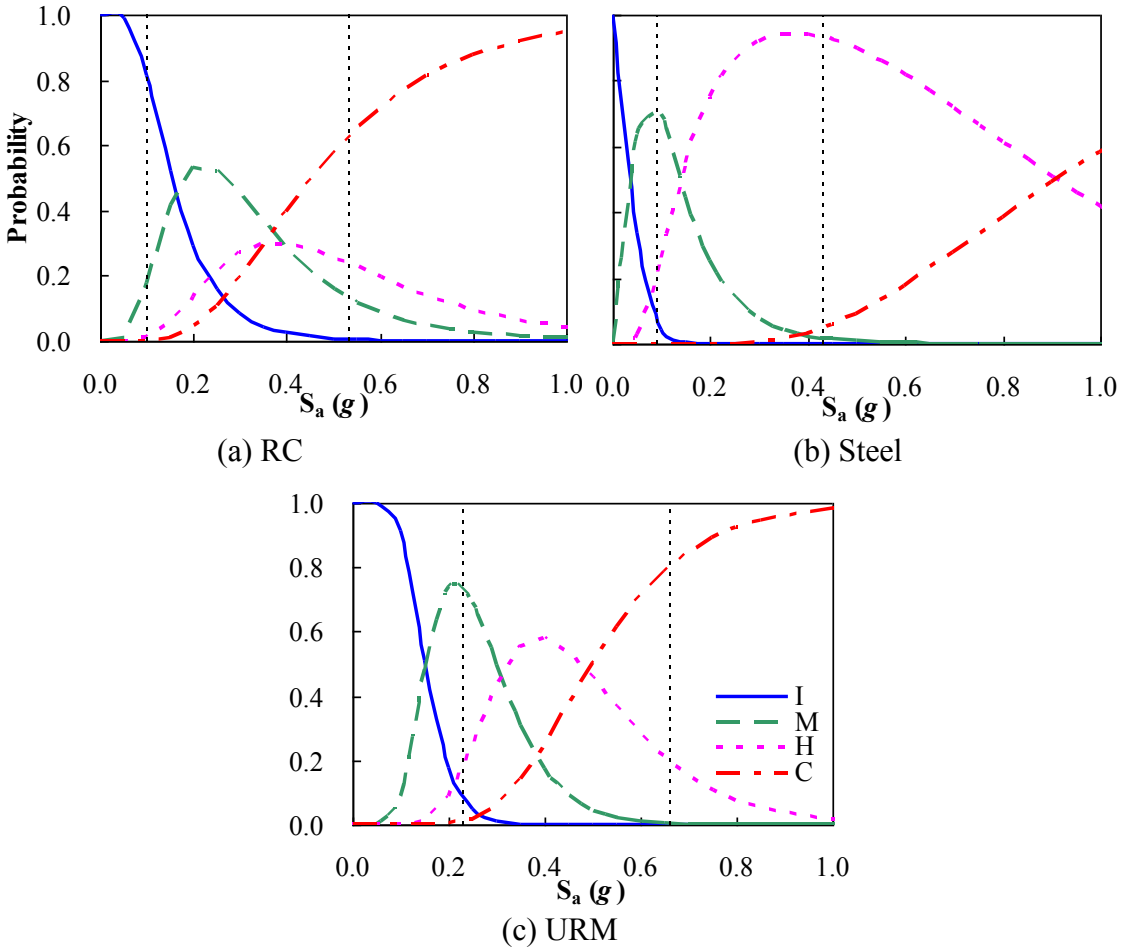

(a) RC (b) Steel

(c) URM

Fig. 4.7. Probabilities of each damage state as a function of S_a for case study structures

Figures 4.8 and 4.9 show the expected total damage factor $\hat{\mu}_{L|IM}$ (solid line) for each structure as a function of S_a, along with the 50% to 90% prediction bands (dotted lines) and confidence bands (dashed lines), respectively. The change in slope and values of $\hat{\mu}_{L|IM}$ for the RC and URM buildings are similar over the provided S_a range, while the steel building has a higher slope and values of of $\hat{\mu}_{L|IM}$ for S_a<0.2g and a lower slope and values of $\hat{\mu}_{L|IM}$ for S_a>0.2g. However, it should be noted that the S_a values of interest for each building vary due to differences in their fundamental periods. The two vertical dotted lines in each graph indicate the S_a values of interest, with the lower S_a corresponding to the 10/50 motions and the higher S_a corresponding to the 2/50 motions (each being the median S_a for the ground motion set at the corresponding fundamental period of the building). The width of the prediction bands for the steel building is narrows around 0.4g. This is because the Heavy damage state governs around these regions and so the standard deviation of $\hat{\mu}_{L|IM}$ reflects the uncertainty in L_H. For the comparison of the total damage factor for each structure, the values corresponding to the median S_a are selected.

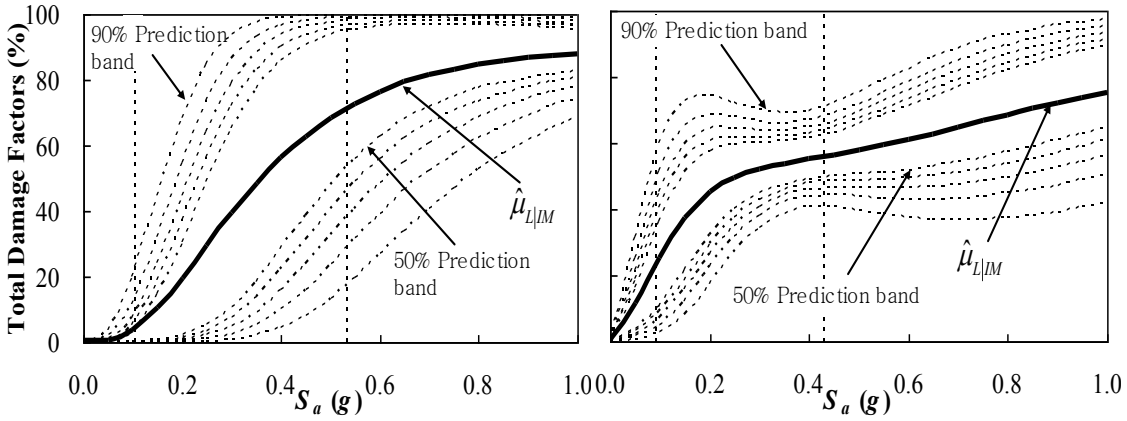

(a) RC (b) Steel

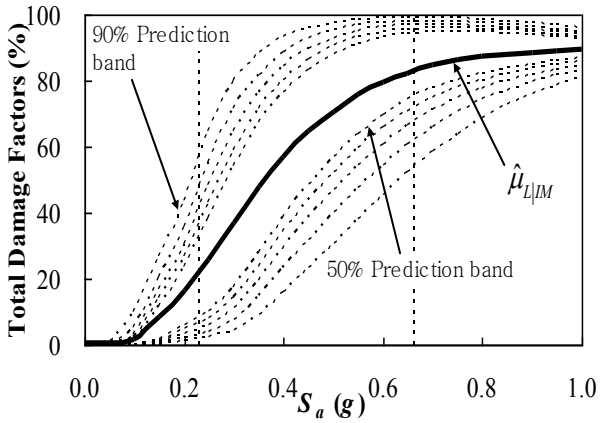

(c) URM

Fig. 4.8. Expected total damage factor with prediction bands for case study structures

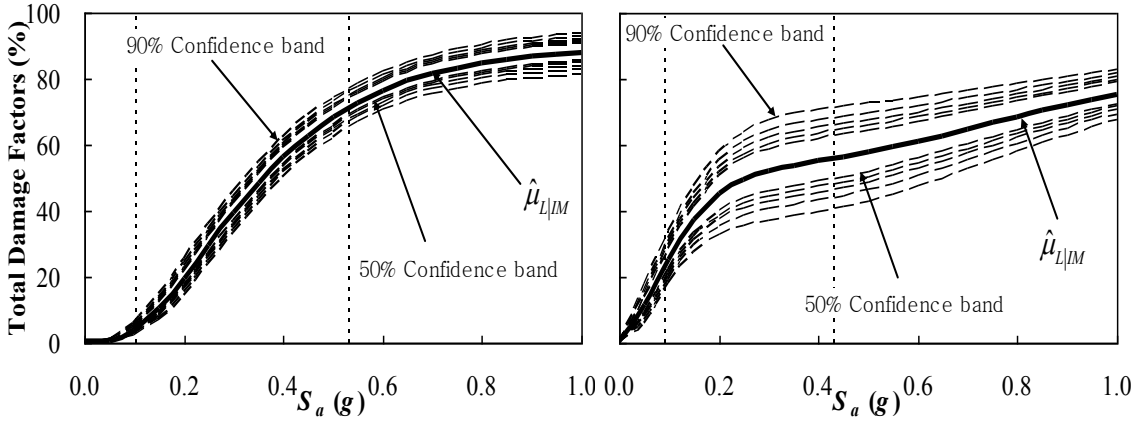

(a) RC (b) Steel

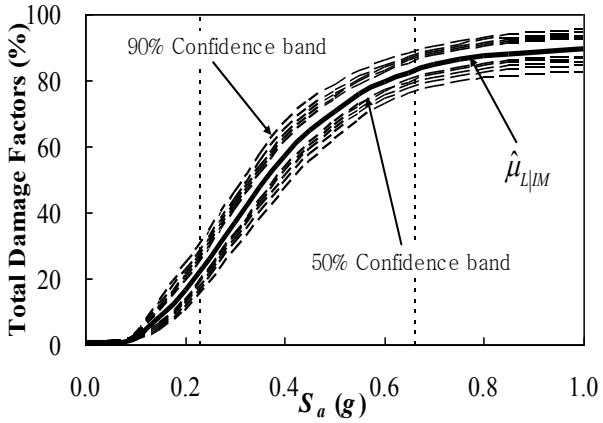

(c) URM

Fig. 4.9. Expected total damage factor with confidence bands for case study structures

For the case studies, the variance of the expected damage factor is computed as follows using Equation (4.5) and the additional assumption that the damage factors are uncorrelated:

$$Var\left(\mu_{L|IM}\right) = \sigma^2_{\mu_{L|IM}} = \sum_{k=1}^{4}\left[P^2_{k|IM} \times \sigma^2_{L_k}\right] \tag{4.6}$$

Table 4.11 provides the statistics of the total damage factors $L|IM$ for both levels of earthquake intensities. Based on the results, all the case study structures are within the Moderate damage range for the 10/50 motions. For the 2/50 motions, the RC and steel buildings are in the Heavy damage range, while the URM building is in the range of Complete damage.

Table 4.11. Statistics of total damage factors for case study structures

Parameter	RC		Steel		URM	
	10/50	**2/50**	**10/50**	**2/50**	**10/50**	**2/50**
Mean, $\hat{\mu}_{L\|IM}$ (%)	3.68	72.8	23.5	56.1	22.3	83.0
Standard deviation, $\hat{\sigma}_{L\|IM}$ (%)	7.81	26.0	17.2	9.23	17.6	14.4
Coefficient of variation (COV), $\hat{\sigma}_{L\|IM} / \hat{\mu}_{L\|IM}$	2.12	0.357	0.733	0.165	0.791	0.174

For the 10/50 motions, the values of the expected total damage factor $\hat{\mu}_{L|IM}$ for the steel and URM buildings are 23.5% and 22.3%, respectively; while $\hat{\mu}_{L|IM}$ for the RC building is less than 3.68%. This difference occurs because the RC building has an 81.4% probability of being in the Insignificant damage state for the 10/50 motions, so contributions coming from other damage states are relatively small. One might expect more damage for the URM building as compared to the steel building for the 10/50 motions. If one looks more closely at Table 4.10, it can be observed that the steel building has a slightly higher probability of being in the Heavy damage state. The damage estimates are impacted by differences in the structural fragility curves and in the

S_a values corresponding to the fundamental periods of the structures. In such cases, the prediction and confidence bands are a useful tool because they provide a measure of the uncertainty in the estimates of $\hat{\mu}_{L|IM}$.

For the 2/50 motions, the URM and RC buildings have higher values of $\hat{\mu}_{L|IM}$ (83.0% and 72.8%, respectively) than the steel building (56.1%). As shown in Figure 4.7, the steel building has a larger contribution from the Heavy damage state for the 2/50 motions, while the RC and URM buildings have a greater contribution from the Complete damage state. The coefficients of variation (COVs) for the total damage factor vary from 0.165 to 0.791, except that the RC building has a COV of 2.12 for the 10/50 motions. This is because this building has a small value of $\hat{\mu}_{L|IM}$ for the 10/50 motions.

4.5.5. Sensitivity Analysis

A sensitivity analysis for the value of σ_{L_k} selected for L_k is conducted for each case study. As an initial point, σ_{L_k} are assumed to be equal to 0.2 times the given range for each damage state, as proposed in Table 4.9. Table 4.12 provides the upper and lower values of the 90% confidence bands for σ_{L_k} equal to 0.15, 0.20 and 0.25 times the given damage state range, for 10/50 and 2/50 motions. The values of $\hat{\mu}_{L|IM}$ are not changed because $\hat{\mu}_{L|IM}$ is not affected by σ_{L_k}. As shown in Table 4.12, the differences in the confidence bands vary between 0.8% and 16%, in general. The difference for lower

bounds is always larger than that for upper bounds. The highest difference comes from the lower bounds for the RC building with 10/50 motions. Similar considerations can be made for the sensitivity of the prediction bands.

Table 4.12. Results of the sensitivity analysis for the total damage factor for case study structures

Structure	Earthquake level	Bounds	Values for 90% confidence bands (Difference, %)		
			Standard deviation of damage factor, σ_{L_k} (%)		
			0.15 × Range	0.20 × Range	0.25 × Range
RC	10/50	Upper	5.05 (9.01%)	5.55	6.05 (9.01%)
		Lower	2.49 (16.4%)	2.14	1.82 (15.0%)
	2/50	Upper	77.7 (0.893%)	78.4	79.8 (1.79%)
		Lower	68.4 (2.24%)	66.9	65.3 (2.39%)
Steel	10/50	Upper	31.4 (6.27%)	33.5	35.7 (6.57%)
		Lower	19.5 (10.2%)	17.7	15.9 (10.2%)
	2/50	Upper	67.8 (5.18%)	71.5	75.2 (5.18%)
		Lower	44.9 (9.52%)	41.0	37.0 (9.76%)
URM	10/50	Upper	32.0 (5.88%)	34.0	36.1 (6.18%)
		Lower	20.4 (9.68%)	18.6	16.8 (9.68%)
	2/50	Upper	86.8 (1.59%)	88.2	89.5 (1.47%)
		Lower	77.5 (2.24%)	75.8	74.0 (2.38%)

4.6. Summary

This section provides an approach to conduct a probabilistic assessment of structural damage due to seismic events with an application to typical building structures in Mid-America. The developed methodology includes modified damage state classifications

based on the ATC-13 and ATC-38 damage states and the ATC-38 database of building damage. Damage factors are assigned to each damage state to quantify structural damage as a percentage of structural replacement cost. To account for the inherent uncertainties, these factors are expressed as random variables with a Beta distribution. A set of fragility curves, quantifying the structural vulnerability of a building, is mapped onto the developed methodology to determine the expected structural damage. The total structural damage factor for a given seismic intensity is then calculated using a probabilistic approach. Prediction and confidence bands are also constructed to account for the prevailing uncertainties. The expected seismic structural damage is assessed for three types of building structures in the Mid-America region using the developed methodology. In addition, a sensitivity analysis for the probabilistic parameters is conducted. The developed methodology provides a transparent procedure, where the structural damage factors can be updated as additional seismic damage data becomes available.

5. SCENARIO-BASED LOSS ESTIMATION OF STRUCTURAL DAMAGE UNDER SEISMIC LOADING

5.1. Introduction

Earthquake events can cause extensive direct and indirect economic losses. It is not possible to forecast the exact time when a damaging earthquake of a specific magnitude will occur in a particular region. Only limited predictions can be done for well-understood faults on a statistical basis. While structures located near a seismically active geologic setting are at risk of being damaged during a potential seismic event, it is possible to mitigate future structural damage by identifying vulnerable structures and applying appropriate retrofit or replacement strategies. As such, seismic loss estimation is an important tool for developing a plan for seismic hazard mitigation.

Earthquakes are of concern to cities in the Central United States (U.S.) because of the history of seismic activity around the New Madrid Seismic Zone (NMSZ). In particular, a significant seismic event affecting a densely populated area, such as the city of Memphis, Tennessee, could lead to severe damage and significant economic losses. Therefore, there is a significant need for research on seismic loss estimation in this region. In this study, a scenario-based assessment is conducted for moderate to high intensity earthquakes in the Central U.S. Three scenario earthquake magnitudes from moderate to high (5.5, 6.5, and 7.5) are used to provide a better understanding of the expected losses due to different seismic hazard levels for decision makers to expect structural damage and consider mitigation strategies in particular for concrete structures.

There have been a number of studies related to seismic loss estimation framework and supporting software tools. For example, Porter (2003) developed a modular framework to assess seismic losses based on the performance-based earthquake engineering methodology. It includes four stages: hazard analysis, structural analysis, damage analysis, and loss analysis. This framework provides the frequency with which levels of decision variable are exceeded so that decision makers can determine whether the structural system is safe or has low expected damage for potential earthquakes. Elnashai and Hajjar (2006) developed the consequence-based risk management (CRM) paradigm which is used to assess economic losses and alternatives with the goal of reducing the expected losses to an acceptable level. Based on this framework, MAEviz, open-source seismic loss assessment software, was developed by the MAE Center. HAZUS-MH (2010) was developed by Federal Emergency Management Agency for estimating potential losses from natural disasters including floods, hurricane winds, and earthquakes.

Using various seismic loss estimation frameworks, a number of studies on scenario-based assessment have been conducted for regional and building-specific losses (Eguchi et al. 1997, Karaka 2005, Kircher et al. 2006b, Kappos et al. 2007, Steelman et al. 2007, Muto et al. 2008, Tantala et al. 2008, Ramirez and Miranda 2009, Lynch et al. 2011). Because of the potential earthquake risk near the NMSZ, there also have been studies on regional seismic loss assessment for the buildings near Memphis, Tennessee, including CUSEC (1985) and Abrams and Shinozuka (1997). They performed comprehensive loss estimations using various hazard levels, inventories and fragilities.

Recently, Steelman and Hajjar (2008) conducted the Memphis testbed capstone project using MAEviz. They conducted loss assessment covering direct and indirect losses such as business interruption losses, casualties, and short term shelter requirements. For seismic vulnerability of building structures, fragility curves for various types of buildings based on the traditional maximum interstory drift demand model were used.

The main contribution is that seismic losses for typical concrete buildings in the Central U.S. are estimated using a probabilistic approach. Recently, there have been several studies on a probabilistic loss estimation (Ergonul 2005, Yucemen et al. 2006, Baker and Cornell 2008, Bradley and Lee 2010) that takes account of uncertainties in the loss estimation process. However, there are few case studies on building structures in the region near NMSZ with the fragility relationships based on the design practices in the Central U.S. The buildings considered in this study are typical reinforced concrete (RC) moment frame buildings and tilt-up concrete buildings in the case study region. For RC moment frame buildings, fragility curves that are developed in Section 2 using story-specific demand models are used to represent the seismic vulnerability of the buildings. Story-specific demand models provide a refined approach that includes more building response information than typical demand models, allowing for more accurate estimates of the seismic fragility of multi-story buildings. When only the maximum interstory drift of a building is considered, as is the case for traditional fragility curve development, the fragility tends to be underestimated; particularly if the interstory drifts for one or more stories are close to the maximum value. For tilt-up concrete buildings,

fragility curves developed in Section 3 using force-controlled limit state functions are used to provide seismic vulnerability of the corresponding buildings.

Steelman and Hajjar (2009) found that regional loss estimates can be significantly influenced by various nonlinear seismic modeling methods, which can cause differences in fragility. Therefore, fragility relationships that have been recently developed using more refined demand models are used in this study to provide more accurate seismic loss estimates. Throughout this study, it provides a better understanding of seismic loss estimates for decision makers in this region to expect structural damage and consider mitigation strategies in particular for concrete structures. It is shown from the results that the framework used in this study is successful to evaluate seismic vulnerability of concrete structures and effective in estimating uncertainties related to the structural losses of the buildings.

5.2. Scenario-Based Assessment of Structural Damage

For scenario-based assessment of structural damage, MAEviz, the seismic loss assessment software developed by the Mid-America Earthquake (MAE) Center is used. All the required input data including building inventory, seismic hazard, fragility curves, and damage assessment framework is implemented into MAEviz.

5.2.1. Case Study Region

Existing structures located in the Central United States (U.S.) near the New Madrid Seismic Zone (NMSZ) are at risk of being damaged during a potential seismic event. In

particular, a significant seismic event affecting a densely populated area, such as the city of Memphis, Tennessee, could lead to severe damage and significant economic losses. Based on the high seismic risk in the Central U.S., Shelby County, Tennessee, is selected as a case study region. Shelby County is the largest county in Tennessee not only in terms of population, but also geographic area. It contains the city of Memphis and is also a part of the Memphis Metropolitan area which is the 41st largest among similarly designated areas in the U.S. Therefore, a significant seismic event affecting a densely populated area like Shelby County could lead to severe damage and significant economic losses

5.2.2. Scenario Earthquakes

Three levels of scenario earthquakes (5.5, 6.5, and 7.5) near Shelby County, Tennessee, are selected. Blytheville, Arkansas (35.927ºN, 89.919ºW), which is a city approximately 60 miles (96.7 km) from the city of Memphis, with a focal depth of 10 km is selected as the point source epicenter. It is noted that the epicenter and the focal depth are selected based on the Memphis testbed project (Steelman and Hajjar 2008). To create seismic hazard in the MAEviz, NEHRP and CEUS characteristic models are used for period spectrum and attenuation calculations, respectively.

5.2.3. Building Inventory Data

The building inventory used in the scenario-based assessment is based on data obtained from the Shelby County Tax Assessor's database (French and Muthukumar 2006).

Because the focus of this study is limited to low- to mid-rise RC moment frame buildings and tilt-up concrete buildings, a total of 1564 building are selected from the entire building stock dataset of 292,438 records. It is noted that the concrete moment-resisting frame (building type C1) is the second largest type among concrete structures after concrete tilt-up structures (building type PC1). Figure 5.1 shows the case study region in the MAEviz with the selected C1 building inventories which are shown as dots.

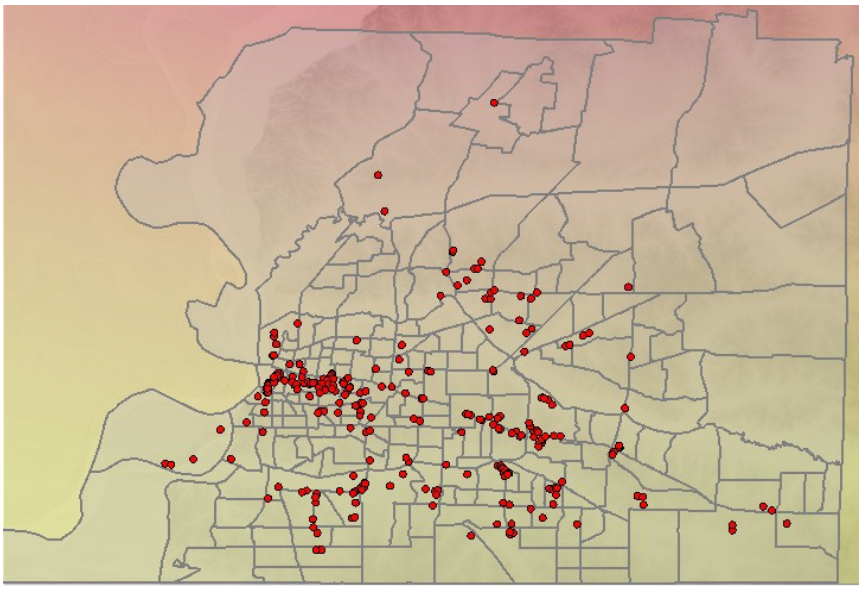

Fig. 5.1. Case study region with selected C1 building inventory locations

Table 5.1 shows the number of each type of building and the corresponding total appraised value for this study. As shown in Table 5.1, there are two types among the C1 buildings: low-rise (C1L) and mid-rise (C1M) concrete moment-resisting frame buildings. In addition, Tables 5.2 and 5.3 provide more detailed information for the buildings in the building inventory, such as general occupancy and year built.

Table 5.1. Number of concrete buildings and appraised value (MAEviz)

Building Type	Number	Total Appraised value (million dollars)
C1L (1-3 stories)	400	504
C1M (4-7 stories)	86	328
PC1	1078	2112
Total	1564	2944

Table 5.2. Number of buildings by general occupancy and building type

General occupancy	C1L	C1M	PC1
Retail trade	44	21	99
Wholesale trade	55	1	564
Light industrial	6	1	133
Office commercial	60	45	40
Health care	4	5	3
Food and entertainment	9	0	26
Education	1	0	3
Heavy industrial	15	5	171
Places of worship	1	0	0
Multi-family residential	205	8	39
Total	400	86	1078

Table 5.3. Number of buildings by year built and building type

Year built	C1L	C1M	PC1
Pre-1939	37	41	0
1940 – 1949	12	2	1
1950 – 1959	12	2	38
1960 – 1969	39	1	168
1970 – 1979	55	9	255
1980 – 1989	155	18	364
1990 – 1999	86	9	207
Post-2000	4	4	45
Total	400	86	1078

As shown in Table 5.2, the main occupancy of the C1 buildings is multi-family residential and office commercial buildings, while more than half of the PC1 buildings in this region are used as wholesale trade buildings. In addition, most of the C1L and PC1 buildings were constructed between 1970 and 1999, while 41 of 86 C1M buildings were constructed before 1940's. Therefore, typical low- to mid-rise RC office buildings and single story tilt-up concrete buildings for wholesale trade constructed with older seismic design provisions are selected as representative structures in the case study region

5.2.4. Seismic Fragility Curves

Since the scenario-based assessment is limited to two types of concrete buildings, RC frame buildings and tilt-up concrete buildings in the case study region, the most

appropriate fragility curves are used from available literatures. For RC frame buildings, this study uses the fragility curves in Section 2. The sets of curves were developed using story-specific demand models, which provide a refined description of the drift demand that accounts for the individual story responses of multi-story buildings. In particular, this approach is more accurate when the responses of multiple stories are close to the maximum value; whereas the traditional demand models capture only the overall maximum story response. For tilt-up concrete buildings, the fragility curves developed in Section 3 are used.

For the development of fragility curves for RC frame buildings, two representative structures were selected: a two-story and a five-story RC office building typical of those in the Central U.S. The particular features of these buildings include an interior flat slab gravity system with a perimeter moment resisting frame designed to resist lateral loads. These fragility curves describe the vulnerability of a significant number of low- to mid-rise concrete buildings constructed in this region. The buildings were designed for the code requirements during the early 1980s, which included relatively low seismic design forces. For the development of fragility curves for tilt-up concrete buildings, two aspect ratios of building dimension based on the literature were considered: 1.4:1 and 4:1. In this study, sets of curves for the 1.4:1 building are used since the 4:1 building is an extreme example of large aspect ratio.

Figures 5.2 and 5.3 show the seismic fragility curves used in this scenario-based assessment, adopted from Sections 2 and 3. Mean of the fragility estimates (F) were plotted along with the spectral acceleration (S_a) as an earthquake intensity measure. For

C1 buildings, three performance levels were used in the fragility curve development including first yield (FY) as a first performance level (PL1), life safety (LS) as a second performance level (PL2), and collapse prevention (CP) as a third performance level (PL3). More information about the demand models and capacity limits used in the fragility curve development is provided in Section 2. The equivalent fragility curves are described using a nonlinear fitting algorithm in MATLAB and implemented into the MAEviz software. For PC1 buildings, three performance levels adopted by ASCE/SEI 41-06 (ASCE 2007) were used: immediate occupancy (IO) as PL1, life safety (LS) as PL2, and collapse prevention (CP) as PL3

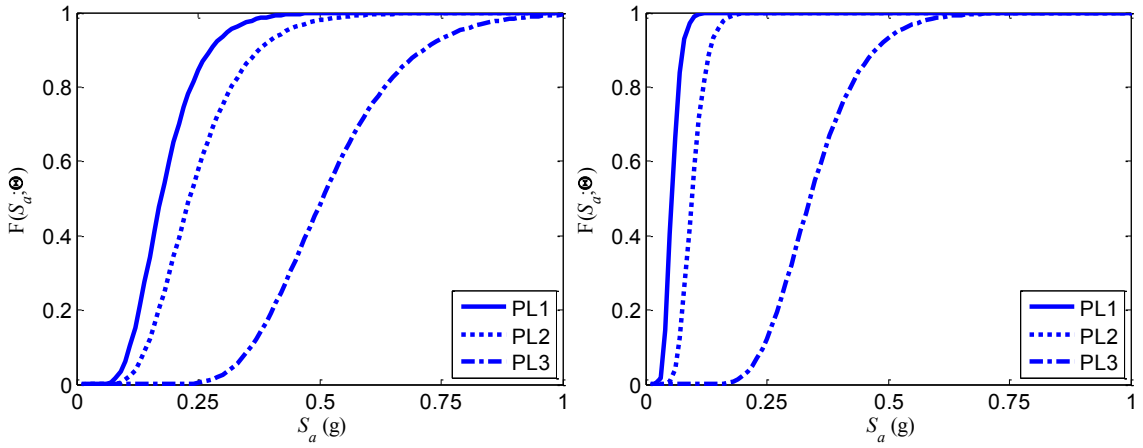

(a) C1L (b) C1M

Fig. 5.2. Seismic fragility curves implemented into MAEviz analysis (C1 buildings)

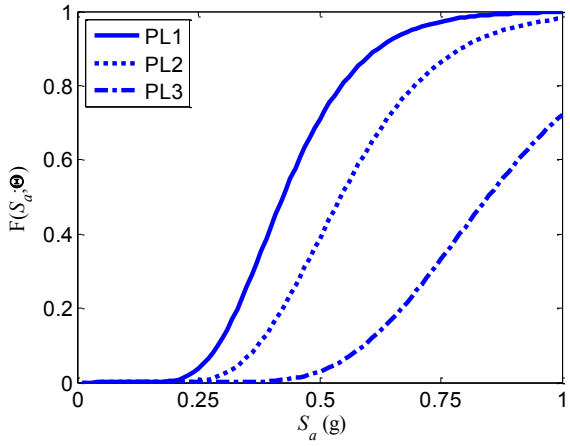

Fig. 5.3. Seismic fragility curves implemented into MAEviz analysis (PC1 buildings)

The probability of exceeding a given performance level is calculated based on the spectral acceleration (S_a). The appropriate value of S_a for a given building is determined by the approximate fundamental period based on the number of stories. Seismic hazard is estimated at a location as a function of the magnitude assumed for the scenario, distance from a specified epicenter, and soil data. Using a specified attenuation model, S_a for each building at the appropriate structural period is estimated.

5.2.5. Structural Damage Assessment Framework

To estimate direct losses due to structural damage, a damage assessment framework that provides a mapping relationship between fragility curves and damage states is necessary. This study uses a probabilistic damage assessment framework developed in Section 4. Structural damage factors are used to quantify the cost of structural repairs as a percentage of the replacement value of the structural portion of a building. The

uncertainty in the structural damage factors for each damage state is described using a Beta distribution, and suggested mean and standard deviation values are provided.

The framework provides a total of four damage states: Insignificant (I), Moderate (M), Heavy (H), and Complete (C). Table 5.4 shows the Beta distribution range for each damage state, along with the proposed mean (μ_{Lk}) and standard deviation (σ_{Lk}) values for the corresponding damage factors. It is noted that damage state factor (L_k) for each damage state, k, is assumed to be a random variable that has a Beta distribution. The mean damage factors μ_{Lk} are calculated as median points within the selected ranges. The standard deviation σ_{Lk} for each damage state is assumed to be 0.20 times the given range. For example, the damage factor for the moderate damage level (M) is described by a Beta distribution with a range of 1%-30%, a mean (μ_{Lk}) of 15.5%, and a standard deviation (σ_{Lk}) of 5.8%. More information about the damage assessment framework is provided in Section 4.

Table 5.4. Statistical description of damage factors, L_k

Damage state	Range of Beta distribution (%)	Mean of damage factor μ_{L_k} (%)	Standard deviation of damage factor σ_{L_k} (%)
I	[0, 1]	0.50	0.2 × [0, 1] = 0.2
M	[1, 30]	15.5	0.2 × [1, 30] = 5.8
H	[30, 80]	55.0	0.2 × [30, 80] = 10
C	[80, 100]	90.0	0.2 × [80, 100] = 4

Figure 5.4 illustrates a mapping relationship between the performance levels used to define fragility curves and the damage state definitions. For example, based on the selected fragility curves for concrete frame buildings (C1), PL1 is taken as FY, PL2 is taken as LS, and PL3 is taken as CP. For the earthquake intensity (IM), S_a was used. As such, insignificant damage corresponds to the range of damage less than that bounded by the FY fragility curve. Moderate damage corresponds to the range of damage bounded by FY and LS. Heavy damage is bounded by LS and CP. Complete damage is the range of damage greater than that bounded by the CP fragility curve.

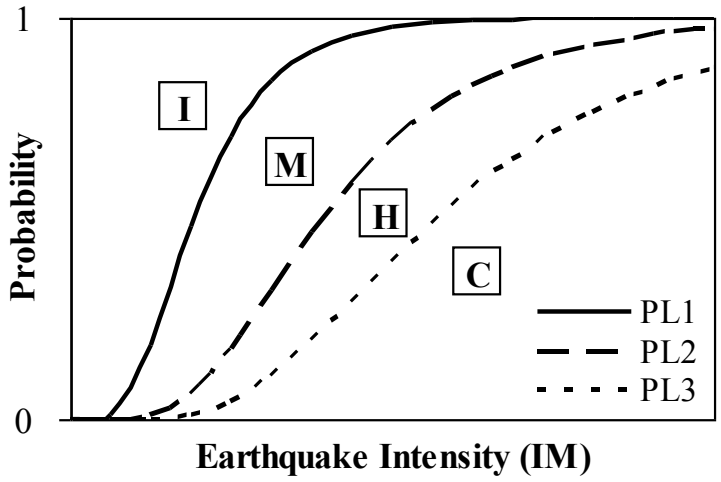

Fig. 5.4. Illustration of relationship between fragility curves and damage states

5.3. Structural Loss Estimation Using MAEviz

5.3.1. Results of MAEviz Analysis

To estimate structural losses for the selected buildings, all the input data including building inventory, seismic hazard, fragility curves, and damage assessment framework are implemented into MAEviz. The scenario events described earlier and the inventory information for concrete frame buildings and tilt-up concrete buildings in Shelby County, Tennessee, are used to estimate the damage state for each concrete building considered. It is noted that the fundamental period of structures is estimated using the relationship for period of case study building based on the number of stories. For tilt-up concrete buildings, the same fundamental period is applied to all the tilt-up concrete buildings since there is no detailed information for the building inventories on aspect ratio.

Figure 5.5 visualizes the structural damage states for a portion of the selected C1 buildings under the magnitude of 7.5 scenario earthquake in MAEviz as an example. A three-dimensional bar graph is generated for each building structure with four color codes representing the four damage states (I, M, H, and C). The bar graphs provide the relative probabilities of being in each damage state for a given structure. These probabilities are computed as the difference between the conditional probabilities of the bounding fragility curves. The bar graphs indicate that the buildings shown have the highest probability of being in the moderate to heavy damage range.

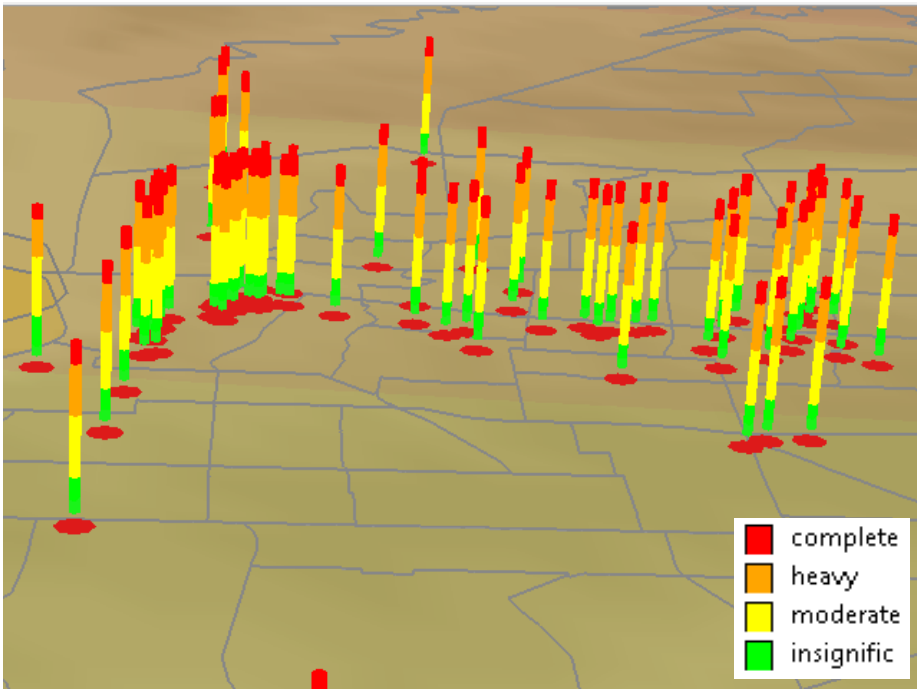

Fig. 5.5. 3D bar graphs illustrating structural damage states for specific buildings (M 7.5 scenario earthquake)

After determining the probability of being in each of the four damage states, the total damage factor for a given building can be determined using Equation (5.1).

$$\hat{\mu}_{L|IM} = \sum_{k=1}^{4} \left(\mu_{L_k} \times P_{k|IM} \right) \tag{5.1}$$

where, $\hat{\mu}_{L|IM}$ is the point estimator of the conditional mean of the total damage factor for a given intensity measure($\mu_{L|IM}$), μ_{L_k} is the mean of the damage factor for each damage state, and $P_{k|IM}$ is the probability of being in each damage state. Table 5.5 presents the expected values of the total damage factors for the 486 RC moment frame buildings and the 1078 tilt-up concrete buildings.

Table 5.5. Number of buildings versus expected damage factor

Scenario Event	Type	Expected Total Damage Factor (%)			
		0-1	1-30	30-80	80-100
M 5.5	C1L	400	0	0	0
	C1M	86	0	0	0
	PC1	1078	0	0	0
M 6.5	C1L	36	231	133	0
	C1M	50	36	0	0
	PC1	162	916	0	0
M 7.5	C1L	0	1	396	3
	C1M	0	11	75	0
	PC1	0	837	241	0

The ranges for the total damage factors in Table 5.5 match the damage ranges provided in Table 5.4 for the individual damage states. However, it is noted that each of

the buildings has a probability of being in each of the four damage states, as shown in Figure 5.5. The expected *total* damage factors are computed using the probabilities for each damage state and the corresponding mean damage factors in Section 4 using Equation (5.1).

Several observations can be made based on the expected total damage factors shown in Table 5.5. For the magnitude of 5.5 event, all the concrete buildings are expected to have insignificant damage. The severity of the expected damage increases for the magnitude of 6.5 event. Most C1L buildings (364 of 400) are expected to have moderate to heavy damage, with the remainder expected to experience insignificant damage. Of the 86 C1M buildings, 58% (50 of 86) are expected to have insignificant damage and the remaining 36 buildings are expected to have moderate damage. For the PC1 buildings, 85% (916 of 1078) are expected to have moderate damage while the remaining 162 buildings are expected to have insignificant damage.

For the highest intensity earthquake, 1% (3 of 400) of the C1L buildings is expected to have complete damage (collapse). The majority of C1L buildings are expected to have heavy damage (396 of 400). C1M buildings are also expected to primarily experience heavy damage (75 of 86) and the remaining 11 buildings are expected to have moderate damage. For the PC1 buildings, 77.6% (837 of 1078) are expected to have moderate damage and the remaining 241 buildings are expected to have heavy damage. Complete damage is not predicted for the C1M and PC1 buildings.

Mean total damage factors are found by summing the total damage factors for individual building structure and dividing by the number of the buildings in each census

tract which is defined by the Shelby County Tax Assessor's database. Equation (5.2) shows how to calculate the mean total damage factors for each census tract.

$$E(\mu_j) = \frac{\sum_{i=1}^{n} \hat{\mu}_i}{n} \tag{5.2}$$

where, $E(\mu_j)$ is the mean total damage factor in j^{th} census tract, $\hat{\mu}_i$ is the point estimator of $\mu_{L|IM}$ from Equation (5.1), and n is the total number of buildings in the j^{th} census tract. Average damage ranges are then overlaid on the census tract map for Shelby County, as shown in Figure 5.6 as an example. This presents the variation of the damage over the region. Such information can help prioritize locations that need mitigation or emergency response plans that address a higher risk of significant structural damage. The darkest shade indicates locations where the cost to repair structural damage is highest relative to the replacement value of the structural portion of the buildings.

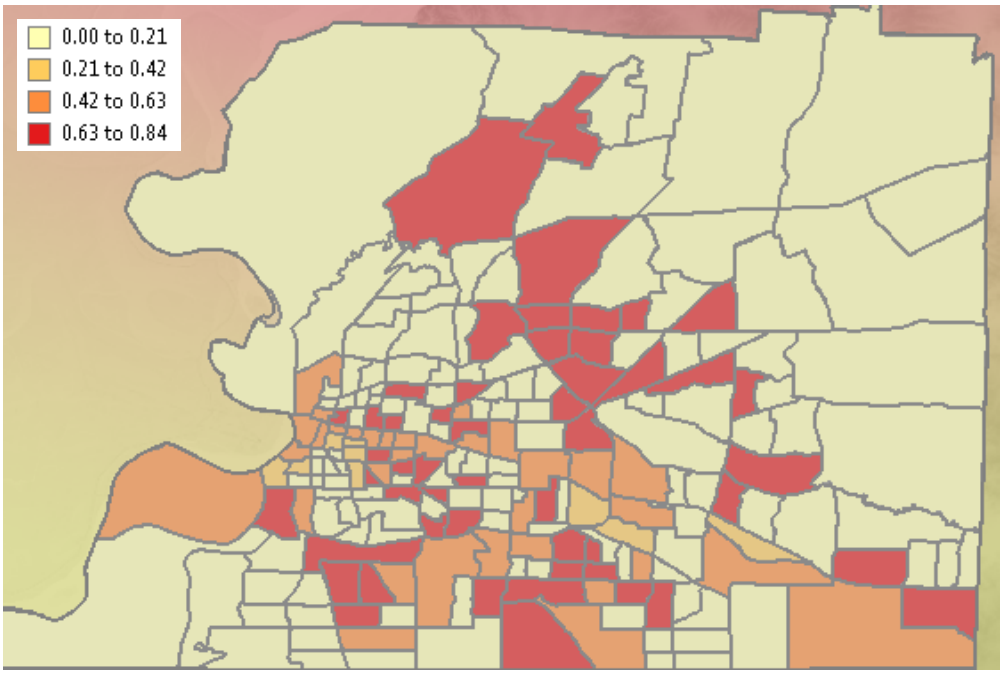

Fig. 5.6. Mean total damage factors for structural damage of C1 buildings plotted on census tracts for the magnitude of 7.5 scenario earthquake

It is noted that the mean total damage factors provide information about the average level of damage in an area. However, it is possible that areas with lower mean damage factors may have larger total repair costs than areas with higher mean damage factors due to differences in the building inventories when comparing census tracts. For example, a particular census tract may have more buildings or buildings with higher replacement values.

5.3.2. Structural Loss Estimation

Based on the structural damage assessment, direct losses related to the structural damage for the selected buildings are also estimated. These losses are calculated based on the

dollar value exposure of the individual inventory item. The expected total structural losses from both structural types for the magnitude of 5.5, 6.5, and 7.5 scenario events are 14.8 million, 95.5 million, and 793 million dollars for all 1564 concrete buildings, respectively. The expected total losses for the buildings are shown in Table 5.6. It is noted that the mean and standard deviation of expected total are calculated using the first-order approximation (Ang and Tang 2006). Equations (5.3) and (5.4) show how to calculate the approximate mean and standard deviation of the expected total losses:

$$E(Y) \cong g\left(\mu_{X_1}, \mu_{X_2}, \ldots, \mu_{X_n}\right) \tag{5.3}$$

and

$$Var(Y) \cong \sum_{i=1}^{n} {\sigma_{X_i}}^2 \left(\frac{\partial g}{\partial X_i}\right)^2 \tag{5.4}$$

where, $Y = g\left(X_1, X_2, \ldots, X_n\right)$ is a function of several random variables, μ_{X_i} and σ_{X_i} are the mean and standard deviation for each random variable, X_i, and it is assumed that X_i and X_j are statically independent for all i and j.

Table 5.6. Structural losses for scenario earthquakes (millions of dollars)

Earthquakes	Type	Mean of expected total	St. dev. of expected total
M 5.5	C1L	2.56	0.209
	C1M	1.64	0.121
	PC1	10.6	0.448
M 6.5	C1L	49.7	7.76
	C1M	5.39	2.58
	PC1	40.4	7.54
M 7.5	C1L	260	18.6
	C1M	135	11.5
	PC1	398	28.9

As shown in Table 5.6, a similar trend is observed between damage factors and structural losses. However, the differences among C1L, C1M and PC1 are substantial not only because of differences in the level of damage, but also because there are differences in number of buildings (400 C1L buildings, 86 C1M buildings, and 1078 PC1 buildings) and the corresponding total appraised value of the buildings. It is also observed that the upper limit of expected losses for the magnitude of 6.5 event is much higher than that for other events compared to the mean value.

5.4. Summary

The focus of this section is the estimation of structural damage and corresponding structural repair costs for concrete buildings due to scenario earthquakes. To have a better understanding of potential losses due to different levels of seismic events near the

New Madrid Seismic Zone, moderate to high intensity earthquakes are applied as the seismic hazard. Typical RC frame buildings and tilt-up concrete buildings in the case study region (Shelby County, Tennessee) are selected and the seismic vulnerability of structures is assessed. Finally, direct losses related to structural damage are estimated.

Based on the scenario-based assessment using MAEviz, for the magnitude of 5.5 scenario event, all the concrete buildings are expected to have limited structural damage with low total damage factors. The severity of the expected damage increases for higher events. For the magnitude of 6.5 event, the majority of the low-rise concrete frame buildings are expected to have moderate to heavy damage, while the mid-rise concrete frame buildings and the tilt-up concrete buildings are expected to have insignificant to moderate damage. The expected total cost to repair structural damage to the 1564 concrete structures for the magnitude of 7.5 event is 793 million dollars. A major concern for this scenario event is that most concrete buildings are expected to have heavy damage, with several buildings expected to be in the complete damage range.

6. SUMMARY, CONCLUSIONS, AND RECOMMENDATIONS

6.1. Summary

The focus of this study is to develop a methodology to assess seismic vulnerability of concrete structures and to estimate economic losses related to structural damage due to future seismic events. Mid-America is selected as a case study region and the most common types of concrete structures in this area are identified based on the building inventory data: reinforcedconcrete (RC) frame buildings and tilt-up concrete buildings. Nonlinear time history analyses using synthetic ground motion records are conducted to have better understanding of the structural behavior of the case study buildings. Using more detailed demand models and the corresponding capacity limits, analytical fragility curves are developed based on appropriate failure mechanisms while considering different structural parameters including different heights of RC frame buildings and different aspect ratios of tilt-up concrete structures. In particular, for multi-story RC frame buildings, story-specific demand models using a bilinear formulation are developed to account for the response of each story during earthquake excitation. Story-specific demand models provide a refined prediction of the drift demand over the building height and give a better account of the underlying uncertainties when compared to the traditional linear model. The developed models are demonstrated by estimating the seismic fragility of typical low- to mid-rise RC buildings in the Central U.S. A probabilistic methodology is used to estimate the seismic vulnerability of the case study structures reflecting the uncertainties in the structural demand and capacity, analytical

modeling, and the information used for structural loss estimation. To estimate structural losses, a set of damage states and the corresponding probabilistic framework to map the fragility and the damage state are proposed and scenario earthquakes are applied to assess structural losses to demonstrate the proposed methodology. It is shown from the results of this study that the proposed methodology provides a probabilistic framework that can be readily applied to evaluate seismic vulnerability of concrete structures and is effective in quantifying the uncertainties in the loss estimation process.

6.2. Conclusions

6.2.1. Seismic Vulnerability Assessment for Reinforced Concrete Frame Building Structures

Seismic fragility curves for multi-story reinforced concrete (RC) frame buildings are derived using the developed story-specific demand models that consider the maximum interstory drift of each story. Then these refined fragility estimates are compared with fragility estimates based on demand models for the overall maximum interstory drift. The following conclusions are made based on the results of this study.

1. The story-specific demand models provide a refined prediction of the drift demand to account for the complex story responses of multi-story buildings. In particular, it is more accurate when the responses of multiple stories are close to the maximum value so that the traditional demand model only using the overall

maximum interstory drift cannot capture the contribution from the story responses other than the largest one.

2. The results show that traditional fragility estimates may underestimate the actual vulnerability of a building, especially when the interstory drifts for one or more stories are close to the maximum value. The developed models are demonstrated by computing the seismic fragility of typical low- to mid-rise RC buildings in the Central U.S. The fragility estimates based on the traditional demand model tend to be lower than those based on the proposed story-specific demand models for severe earthquakes and can be higher for lower intensity earthquakes. In addition, the proposed methodology shows that the selected buildings are significantly vulnerable to ground motions with a 2% probability of exceedance in 50 years.
3. The proposed story-specific demand models give a better account of the underlying uncertainties when compared to the traditional model. The fragility curves developed using story-specific demand models have steeper slopes than those developed using the traditional demand models for both structures. This is because the story-specific demand models and the corresponding fragility estimates provide better predictions based on the reduced uncertainty.

6.2.2. Seismic Vulnerability Assessment for Tilt-Up Concrete Building Structures

Seismic vulnerability for one-story tilt-up concrete structures is assessed in terms of fragility estimates. Using the analytical model, seismic fragility curves are developed and the influence of different aspect ratios (1.4:1 and 4:1) with respect to the building

plan dimensions is also considered. The following conclusions are made based on the results of this study:

1. Based on the fragility analysis, tilt-up concrete buildings are vulnerable to potential earthquakes in the Central U.S. In particular, buildings with larger aspect ratios have significantly higher fragilities for both moderate and extreme earthquakes.
2. In-plane shear strength of metal deck diaphragms is the most critical parameter to assess seismic vulnerability of the tilt-up concrete structures with metal deck diaphragms considered in this study. It is noted that the seismic demand to capacity ratio for puddle welds are much lower than the demand to capacity ratios for the limit states assessing the diaphragm and diaphragm connections. However, in this study, all of puddle welds are assigned the same ultimate strength, which does not consider significant variations in the welds. Potential puddle weld failures can lead to changes in the stress distribution over the diaphragm and impact the structural response.
3. For tilt-up concrete structures, force-controlled parameters including in-plane shear strength of metal deck are more reasonable to be used as indicators to define limit state functions than displacement-controlled parameters. The maximum diaphragm drift ratio (DDR), which is based on diaphragm displacements, does not predict vulnerability as well as force demands in the connections and metal deck. However, it is important to monitor the maximum

diaphragm displacement and evaluate the potential for unseating of the joist girder.

4. Seismic performance of tilt-up buildings in the Mid-America region having large aspect ratios (approaching 4:1) needs improvement to reduce vulnerability against potential earthquakes. Possible retrofit techniques may include the addition of interior braced frames or shear walls, improvement of welding, and addition of connections between the diaphragm and walls.

6.2.3. Probabilistic Framework for Structural Damage Assessment

A probabilistic framework to assess structural damage due to seismic events is proposed and applied to typical building structures in Mid-America. Using damage factors that quantify structural damage as a percentage of structural replacement cost, the total structural damage factor for a given seismic intensity is calculated. The following conclusions are made based on the results of this study:

1. The probabilistic framework for estimating structural damage provides a transparent procedure that accounts for uncertainties and allows damage factors to be updated as additional seismic damage data becomes available.
2. Based on the calculation of structural damage factors for three example building types common in the Mid-America region, the selected steel and unreinforced masonry buildings are expected to have higher structural damage factors than the reinforced concrete building for 10% in 50 years motions for Memphis, with

moderate structural damage predicted. The selected unreinforced masonry and reinforced concrete buildings have the highest structural damage factors for the 2% in 50 years motions for Memphis, with heavy to complete structural damage predicted.

6.2.4. Scenario-based Loss Estimation of Structural Damage under Seismic Loading

Seismic losses for concrete buildings in the Mid-America region are estimated using a probabilistic framework. The scenario earthquakes under consideration have three magnitudes (5.5, 6.5, and 7.5) and Shelby County, Tennessee, is selected as the case study region. The structural damage of the selected buildings is assessed with a probabilistic approach that uses empirical structural damage factors and accounts for the prevailing uncertainties. Through this scenario-based approach, critical structures that might be expected to have extensive damage are identified. The following conclusions are made based on the results of this study:

1. Based on the scenario-based assessment, for the M 5.5 scenario event, all the concrete buildings are expected to have limited structural damage with low total damage factors. The severity of the expected damage increases for higher magnitude events.
2. For the M 6.5 event, the majority of the low-rise concrete frame buildings are expected to have moderate to heavy damage, while the mid-rise concrete frame

buildings and the tilt-up concrete buildings are expected to have insignificant to moderate damage.

3. The expected total cost to repair structural damage to the 1564 concrete structures for the M 7.5 event is $793 million dollars. A major concern for this scenario event is that most concrete buildings are expected to have heavy damage, with several buildings expected to be in the complete damage range.

6.3. Recommendations for Future Research

This study proposed a general framework to assess direct losses for any structural system with a specific focus on developing refined fragility curves for concrete structures typical of those in the Mid-America region. Recommendations for potential extended studies and selected future research needs related to seismic fragility analysis and loss estimation are listed below:

1. Development of seismic fragility curves and evaluation of seismic performance could be conducted for other types of concrete buildings including concrete shear wall and precast concrete buildings. In addition, seismic loss estimates could be extended to contents and nonstructural components using the refined fragility relationships. This could provide complete direct loss estimates for concrete buildings in the case study region.
2. Possible seismic mitigation options could be investigated further based on critical failure mechanisms for concrete structures. In addition, the corresponding cost-

benefit analysis of rehabilitation versus new construction could be beneficial for decision makers.

3. Loss estimation using other software such as HAZUS with more refined and updated information could be conducted to assess vulnerability in terms of the expected losses. In order to do this, detailed input data such as building inventories, hazard models, and fragility relationships should be provided for consistency.

REFERENCES

Abrams, D.P. and Shinozuka, M., eds. (1997). *Loss assessment of Memphis buildings*, Technical Report NCEER-97-0018, National Center for Earthquake Engineering Research, State Univ. of New York, Buffalo, NY.

ACI Committee 318. (1983). *Building code requirements for reinforced concrete (ACI 318-83)*, American Concrete Institute, Detroit, MA.

Adham, S., Anderson, R.W., and Kariotis, J.C. (1990). *Survey of tilt-up-wall structural systems affected by the Whittier narrows Earthquake of October 1, 1987*, Agbabian Associates, Report No. R-8820-6296.

Adham, S., Tabatabi, H., Brooks, H., Brugger, L., and Dick, G. et al. (1996). "Tilt-up-wall buildings, 1994 Northridge Earthquake reconnaissance report II," *Earthquake Spectra*, 12(S1), 99-123.

ASCE. (2000). *Prestandard and commentary for the seismic rehabilitation of buildings (FEMA 356)*, Prepared by American Society of Civil Engineers for the Federal Emergency Management Agency, Washington D.C.

ASCE/SEI. (2003). *Seismic evaluation of existing buildings, ASCE/SEI 31-03*, American Society of Civil Engineers, Reston, VA.

ASCE/SEI. (2007). *Seismic rehabilitation of existing buildings, ASCE/SEI 41-06*, American Society of Civil Engineers, Reston, VA.

ATC. (1985). *Earthquake damage evaluation data for California*, ATC-13 Report, Applied Technology Council, Redwood City, CA.

ATC. (1996). *Seismic evaluation and retrofit of concrete buildings*, ATC-40 Report, Applied Technology Council, Redwood City, CA.

ATC. (2000). *Database on the performance of structures near strong-motion recordings: 1994 Northridge, California, earthquake*, ATC-38 Report, Applied Technology Council, Redwood City, CA.

Atkinson, G. and Boore, D. (1995). "New ground motions relations for eastern North America," *Bulletin of the Seismological Society of America*, 85, 17-30.

Ay, B.O. and Erberik, M.A. (2008). "Vulnerability of Turkish low-rise and mid-rise reinforced concrete structures," *Journal of Earthquake Engineering*, 12(S2), 2-11.

Bai, J.-W. and Hueste, M.B.D. (2006). "Seismic fragility of a tilt-up concrete building in the Central United States," *Proceedings*, 8th U.S. National Conference on Earthquake Engineering.

Bai, J.-W., Hueste, M.B.D., and Gardoni, P. (2009). "Probabilistic assessment of structural damage due to earthquakes for buildings in Mid-America," *Journal of Structural Engineering*, 135(10), 1155-1163.

Bai, J.-W., Gardoni, P., and Hueste, M.B.D. (2011). "Story-specific demand models and seismic fragility estimates for multi-story buildings," *Structural Safety*, 33, 96-107.

Bartoletti, S.B. and Pierepiekarz, M.R. (2006). "Seattle earthquake scenario – performance of buildings and essential facilities," *Proceedings*, 8th US National Conference on Earthquake Engineering, Earthquake Engineering Research Institute, San Francisco, CA.

BOCA. (1987). *Building Officials and Code Administrators (BOCA) Basic/National Code/1987*, Building Officials and Code Administrators International, Inc., Country Club Hills, IL.

BOCA. (1999). *The BOCA National Building Code*, Building Officials and Code Administrators International, Country Club Hills, IL.

Box, G.E.P. and Tiao, G.C. (1992). *Bayesian inference in statistical analysis*, Addison-Wesley, Reading, MA.

Carter, J.W., Hawkins, N.M., and Wood, S.L. (1993). *Seismic response of tilt-up construction*, Structural Research Series No. 581, University of Illinois at Urbana-Champaign, Urbana, IL.

Central United States Earthquake Consortium (CUSEC). (1985). *An Assessment of Damage and Casualties for Six Cities in the Central United States Resulting from Earthquakes in the New Madrid Seismic Zone*, Internal Report, Federal Emergency Management Agency, Washington, DC.

Chou, H.F. (2007). *Seismic responses of a tilt-up building with segmented walls*, Ph.D. Dissertation, University of Southern California, Los Angeles, CA.

Cohen, G.L., Klingner, R.E., Hayes, J.R. Jr., and Sweeney, S.C. (2004a). "Seismic evaluation of low-rise reinforced masonry buildings with flexible diaphragms: I. Seismic and quasi-static testing," *Earthquake Spectra*, 20(3), 779-801.

Cohen, G.L., Klingner, R.E., Hayes, J.R. Jr., and Sweeney, S.C. (2004b). "Seismic evaluation of low-rise reinforced masonry buildings with flexible diaphragms: II. Analytical modeling," *Earthquake Spectra*, 20(3), 803-824.

Cornell, C.A., Jalayer, F., Hamburger, R.O., and Foutch, D.A. (2002). "Probabilistic basis for 2000 SAC Federal Emergency Management Agency steel moment frame guidelines," *Journal of Structural Engineering*, 128(4), 526-533.

Ditlevsen, O. and Madsen, H.O. (1996). *Structural reliability methods*, Wiley, New York, NY.

Dooley, K.L. and Bracci, J.M. (2001). "Seismic evaluation of column-to-beam strength ratios in reinforced concrete frames," *ACI Structural Journal*, 98(6), 843-851.

Dumova-Jovanoska, E. (2000). "Fragility curves for reinforced concrete structures in Skopje (Macedonia) Region," *Soil Dynamics and Earthquake Engineering*, 19, 455-466.

Ellingwood, B.R., Celik, O.C., and Kinali, K. (2007). "Fragility assessment of building structural systems in Mid-America," *Earthquake Engineering and Structural Dynamics*, 36(13), 1935-1952.

Elnashai, A.S. and Hajjar, J.F. (2006). "Mid-America Earthquake (MAE) Center program in seismic risk management," *Proceedings*, 8th U.S. National Conference on Earthquake Engineering, San Francisco, California.

Elnashai, A.S., Papanikolaou, V., and Lee, D.H. (2002). *ZEUS-NL user manual*, Mid-America Earthquake Center, University of Illinois at Urbana-Champaign.

Elwood, K.J. and Moehle, J.P. (2002). "Discussion of seismic evaluation of column-to-beam strength ratios in reinforced concrete frames," *ACI Structural Journal*, 99(5), 710-713.

EQE International Inc. (1989). *The October 17, 1989 Loma Prieta Earthquake, EQE Engineering catastrophe reports*, <http://www.absconsulting.com/catastropheReports.html>, August 15, 2011.

EQE International Inc. (1994). *The January 17, 1994 Northridge Earthquake, EQE Engineering catastrophe reports*, <http://www.absconsulting.com/catastropheReports.html>, August 15, 2011.

EQE International Inc. (2001). *Seattle (Nisqually), Washington Earthquake of February 28, 2001, EQE Engineering catastrophe reports*, <http://www.absconsulting.com/catastropheReports.html>, August 15, 2011.

Erberik, M.A. and Elnashai, A.S. (2006). "Loss estimation analysis of flat-slab structures," *Natural Hazards Review*, 7(1), 26-37.

ESRI. (2009). *ArcGIS ver. 9.3.1*, Economic and Social Research Institute, Redlands, CA.

FEMA. (2001). *HAZUS99 User's manual, Service release 2*, Federal Emergency Management Agency, Washington D.C.

FEMA. (2010). *HAZUS-MH MR5 Users and Technical Manual*, Federal Emergency Management Agency, Washington, D.C.

Fonseca, F.S. (1997). *Cyclic loading response of reinforced concrete tilt-up structures with plywood diaphragms*, Ph.D. Dissertation, University of Illinois, Urbana, IL.

Fonseca, F.S., Wood, S.L., and Hawkins, N.M. (1996). "Measured response of roof diaphragms and wall panels in tilt-up systems subjected to cyclic loading," *Earthquake Spectra*, 12(4), 783-802.

Frankel, A., Mueller, C., Barnhard, T., Perkins, D., Leyendecker, E., and Dickman, N. (1996). "National seismic hazard maps: Documentation," USGS open-file report 96-532.

French, S. (2004). *Memphis Test-Bed project summer report*, Mid-America Earthquake Center Project DS-2 Report, Georgia Institute of Technology, Atlanta, GA.

French, S. (2008). *EE-6: Memphis Test-Bed Inventory Data (version 5.0)*, Mid-America Earthquake Center Project, Georgia Institute of Technology, Atlanta, GA.

French, S.P. and Muthukumar, S. (2006). *Memphis Testbed inventory data, Version 4*, Center for Geographic Information Systems, Georgia Institute of Technology, Atlanta, Georgia.

Gardoni, P., Der Kiureghian, A., and Mosalam, K.M. (2002). "Probabilistic capacity models and fragility estimates for RC columns based on experimental observations," *Journal of Engineering Mechanics*, 128(10), 1024-1038.

Gardoni, P., Mosalam, K.M., and Der Kiureghian A. (2003). "Probabilistic seismic demand models and fragility estimates for RC bridges," *Journal of Earthquake Engineering*, 7(S1), 79-106.

Geweke, J. (1992). "Evaluating the accuracy of sampling-based approaches to the calculation of posterior moments," *Bayesian Statistics*, 4, 164-193.

Graf T. and Malley, J.O. (2004). *Evaluation and application of concrete tilt-up assessment methodologies*, PEER report 2004/03, Pacific Earthquake Engineering Research Center, University of California, Berkeley, CA.

Hamburger, R.O., McCormick, D.L., and Hom, S. (1988). "The Whittier Narrows Earthquake of October 1, 1987 - Performance of tilt-up buildings," *Earthquake Spectra*, 4(2), 219-254.

Hueste, M.B.D. and Bai, J.-W. (2007a). "Seismic retrofit of a reinforced concrete flat-slab structure: Part I – Seismic performance evaluation," *Engineering Structures*, 29(6), 1165-1177.

Hueste, M.B.D. and Bai, J.-W. (2007b). "Seismic retrofit of a reinforced concrete flat-slab structure: Part II – Seismic fragility analysis," *Engineering Structures*, 29(6), 1178-1188.

Hueste, M.B.D., Browning, J., Lepage, A., and Wallace, J.W. (2007). "Seismic design criteria for slab-column connections," *ACI Structural Journal*, 104(4), 448-458.

ICBA. (1991). *Uniform building code*, International Conference of Building Officials, Whittier, CA.

ICC. (2006). *International Building Code*, International Code Council, Falls Church, VA.

Johnson, M.A. and Fonseca, F.S. (1998). "Seismic response of reinforced concrete tilt-up wall panels," *Proceedings*, 6th U.S. National Conference on Earthquake Engineering.

Johnston, A.C. (1996). "Seismic moment assessment of earthquakes in stable continental regions; III, New Madrid 1811-1812, Charleston, 1886 and Lisbon 1755," *Geophysical Journal International*, 126(2), 314-344.

Kappos, A., Lekidis, V., Panagopoulos, G., Sous, I., Theodulidis, N., Karakostas, Ch., Anastasiadis, T., Salonikios, T., and Margaris, B. (2007). "Analytical estimation of economic loss for buildings in the area struck by the 1999 Athens Earthquake and comparison with statistical repair costs," *Earthquake Spectra*, 23(2), 333-355.

Karaka, E. (2005). *Regional earthquake loss estimation: role of transportation network, sensitivity and uncertainty, and risk mitigation*, Ph.D. dissertation, Massachusetts Institute of Technology, Massachusetts.

Kim, S.C. and White, D.W. (2004). "Nonlinear analysis of a one-story low-rise masonry building with a flexible diaphragm subjected to seismic excitation," *Engineering Structures*, 26(14), 2053-2067.

Kinali, K. and Ellingwood, B.R. (2007). "Seismic fragility assessment of steel frames for consequence-based engineering: A case study for Memphis, TN," *Engineering Structures*, 29(6), 1115-1127.

King, S.A., Kiremidjian, A.S., Sarabandi, P., and Pachakis, D. (2005). *Correlation of observed building performance with measured ground motion*, The John A. Blume Earthquake Engineering Center Report No. 148, Stanford University.

Kircher, C.A., Seligson, H.A., Bouabid, J. and Morrow, G.C. (2006a). "When the big one strikes again – Estimated losses due to a repeat of the 1906 San Francisco earthquake," *Earthquake Spectra*, 22(S2), S297-S339.

Kircher, C.A., Whitman, R.V., and Holmes, W.T. (2006b). "HAZUS earthquake loss estimation methods," *Natural Hazards Review*, 7(2), 45-59.

Laine M. (2008). *Adaptive MCMC methods with applications in environmental and geophysical models*, Ph.D. dissertation; Lappeenranta University of Technology, Lappeenranta (Finland).

Lee, K.H. and Rosowsky, D.V. (2006). "Fragility analysis of woodframe buildings considering combined snow and earthquake loading," *Structural Safety*, 28(3), 289-303.

Luttrel, L.D. (1967). *Strength and behavior of light-gage steel shear diaphragms*, Engineering Research Bulletin 67-1, Cornell University, Ithaca, NY.

MAE Center (2006). *Earthquake Risk Assessment Using MAEviz 2.0: A tutorial*, Mid-America Earthquake Center, University of Illinois at Urbana-Champaign.

Moehle, J.P. (2000). "State of research on seismic retrofit of concrete building structures in the US," US-Japan Symposium and Workshop on Seismic Retrofit of Concrete Structures.

Muto, M., Krishnan, S., Beck, J.L. and Mitrani-Reiser, J. (2008). "Seismic loss estimation based on end-to-end simulation," *Proceedings*, 2008 IALCCE: First international symposium on life-cycle civil engineering, Varenna, Lake Como, Italy.

Olshansky, R.B. and Wu, Y. (2004). "Evaluating earthquake safety in Mid-American communities," *Natural Hazards Review*, 5(2), 71-81.

Osteraas, J. and Somers, P. (1996). "Reinforced concrete buildings, 1994 Northridge Earthquake reconnaissance report II," *Earthquake Spectra*, 12(S1), 49-74.

Park, Y.J., Ang, A.H.-S., and Wen, Y.K. (1985). "Seismic damage analysis of reinforced concrete buildings," *Journal of Structural Engineering*, 111(4), 740-757.

Porter, K.A. (2003). "An overview of PEER's performance-based earthquake engineering methodology," *Proceedings*, 9th International Conference on Applications of Statistics and Probability in Civil Engineering, San Francisco, California.

Porter, K.A., Beck, J.L., and Shaikhutdinov, R.V. (2002). "Sensitivity of building loss estimates to major uncertain variables," *Earthquake Spectra*, 18(4), 719-743.

Ramamoorthy, S.K., Gardoni, P., and Bracci, J.M. (2006). "Probabilistic demand models and fragility curves for reinforced concrete frames," *Journal of Structural Engineering*, 132(10), 1563-1572.

Ramamoorthy, S.K., Gardoni, P., and Bracci, J.M. (2008). "Seismic fragility and confidence bounds for gravity load designed reinforced concrete frames of varying height," *Journal of Structural Engineering*, 134(4), 639-650.

Ramirez, C.M. and Miranda, E. (2009). *Building-specific loss estimation methods and tools for simplified performance-based earthquake engineering*, Technical Report No. 171, The John A. Blume Earthquake Engineering Center.

Rix, G.J. and Fernandez, J.A. (2004). *Earthquake ground motion simulation*, <http://www.ce.gatech.edu/research/mae_ground_motion>, September 1, 2004.

Rix, G.J. and Fernandez, J.A. (2010). *Probabilistic ground motions for selected cities in the upper Mississippi embayment*, <http://geosystems.ce.gatech.edu/soil_dynamics/research/groundmotionsembay/>, August 15, 2011.

Rossetto, T. and Elnashai, A. (2003). "Derivation of vulnerability functions for European-type RC structures based on observational data," *Engineering Structures*, 25, 1241-1263.

SDI. (2004). *Diaphragm design manual (3rd Edition)*, Steel Deck Institute, INC., Canton, OH.

SEAONC. (2001). *Guidelines for seismic evaluation and rehabilitation of tilt-up buildings and other rigid wall/flexible diaphragm structures*, Structural Engineers Association of Northern California, San Francisco, CA.

Shepherd, R., Holmes, W.T., Lizundia, B., Aiken, I.D., De Angelis, C.A. et al. (1990). "Buildings, Loma Prieta Earthquake reconnaissance report," *Earthquake Spectra*, 6, 127-149.

Shinozuka, M., Feng, M.Q., Lee, J., and Naganuma, T. (2000). "Statistical analysis of fragility curves," *Journal of Engineering Mechanics*, 126(12), 1224-1231.

Simulia. (2007). *ABAQUS/Standard, version 6.7*, Providence, RI.

Singhal, A. and Kiremidjian, A.S. (1996). "Method for probabilistic evaluation of seismic structural damage," *Journal of Structural Engineering*, 122(12), 1459-1467.

Steelman J. and Hajjar, J.F. (2008). *Capstone scenario applications of consequence-based risk management for the Memphis Testbed*, Technical Report, Mid-America Earthquake Center.

Steelman, J. and Hajjar, J.F. (2009). "Influence of inelastic seismic response modeling on regional loss estimation," *Engineering Structures*, 31, 2976-2987.

Steelman, J., Song, J. and Hajjar, J.F. (2007). *Integrated data flow and risk aggregation for consequence-based risk management of seismic regional losses*, Technical Report, Mid-America Earthquake Center.

Thurston, H.M. (1990). "Seismic damage evaluation of tilt-up buildings," *Journal of Computing in Civil Engineering*, 4(4), 349-369.

Vamvatsikos, D. and Cornell, C.A. (2002). "Incremental dynamic analysis," *Earthquake Engineering and Structural Dynamics*, 31(3), 491-514.

Vulcraft. (2007). *Steel joists and joist girders*, A division of Nucor Corporation.

Vulcraft. (2008). *Steel roof and floor deck*, A division of Nucor Corporation.

Wallace, J.F., Stewart, J.P., and Whittaker, A.S. (1999). "Building vulnerability studies: modeling and evaluation of tilt-up and steel reinforced concrete building," PEER report 1999/13, Pacific Earthquake Engineering Research Center, University of California, Berkeley, CA.

Wen, Y.K. and Ellingwood, B.R. (2005). "The role of fragility assessment in consequence-based engineering," *Earthquake Spectra*, 21(3), 861-877.

Wen, Y.K., Ellingwood, B.R., and Bracci, J. (2004). *Vulnerability function framework for consequence-based engineering*, Report DS-4, Mid-America Earthquake Center, University of Illinois at Urbana-Champaign.

Wood, S.L. and Hawkins, N.M. (1994). "Seismic response of concrete tilt-up systems," *Proceedings*, Structures Congress XII, Atlanta, GA, 1994.

Yucemen, M.S., Ozturk, N.Y., and Deniz, A. (2006). "Probabilistic seismic loss estimation for Eskisehir, Turkey," *Proceedings*, 2006 ECI Conference on Geohazards, Lillehammer, Norway.

APPENDIX A

INCREMENTAL DYNAMIC ANALYSIS FOR LOW-RISE AND MID-RISE RC FLAT SLAB BUILDINGS

Introduction

Incremental dynamic analysis (IDA) is an analysis method to describe a wide range of structural responses based on multiple nonlinear dynamic analyses using one or more scaled ground motion records (Vamvatsikos and Cornell 2002). Through this method, one or more curves of structural responses corresponding to multiple levels of intensity can be developed. Because there is a correlation between transition points from IDA and seismic demand models, in this section, IDA is conducted for the 2-story and 5-story RC flat slab buildings with one selected ground motion record. In addition, the IDA curves are compared with traditional push-over curves and the dynamic analysis results using unscaled synthetic ground motions. Based on the comparison of the results, it is observed that the IDA curves match well with the results from the nonlinear dynamic analyses used in the demand model. In addition, correlation between transition points from the demand models and push-over curves is also investigated.

Ground Motion Record for IDA

One of ground motion records developed by Rix and Fernandez (2010) is selected for the IDA. This set of ground motions consists of a suite of synthetic records for two earthquake hazard levels, one with 2% and one with 10% probability of exceedance in

50 years. Based on the responses of the structures, the ground motion that provides the closest response to the median response among twenty 10% in 50 years motions is selected (Lowlands, ground motion ID #1). Figures A.1 and A.2 show the acceleration time history and the response spectrum of the selected ground record, respectively. The peak ground acceleration (PGA) of this record is 0.157*g*. The spectral acceleration values corresponding to the fundamental periods for the two-story (T_1 = 0.914 *s*) and five-story (T_1 = 1.62 *s*) buildings are 0.137*g* and 0.09*g*, respectively.

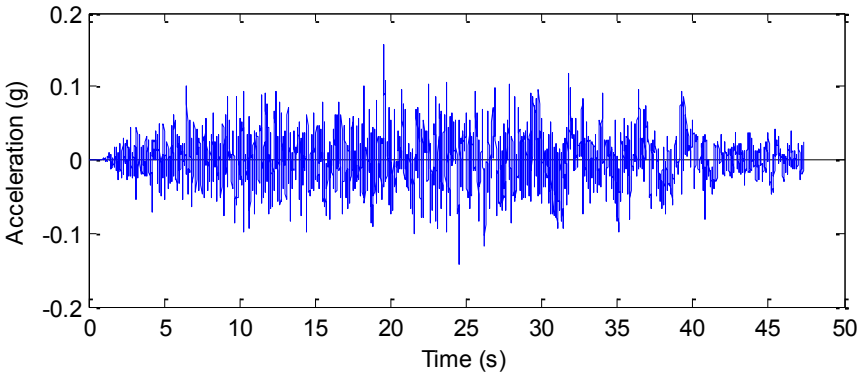

Fig. A.1. Acceleration time history of the selected ground motion

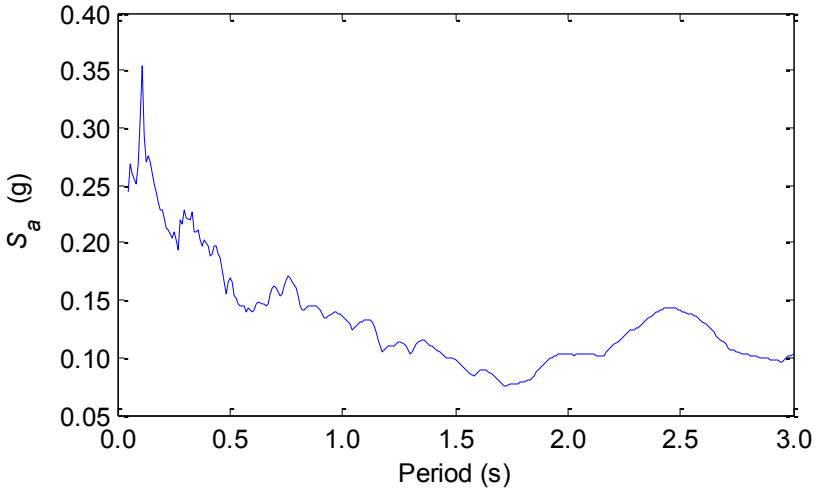

Fig. A.2. Response spectrum for the selected ground motion

IDA Curve Development

IDA curves are developed using the selected ground motion with scaling factors. The ground motion is scaled with factors varying from 1 (original) to 10 every in increments of 0.2. A total of 46 nonlinear time-history analyses are conducted and the corresponding maximum responses are estimated. Therefore, each IDA curve covers structural responses from the ground motion records having PGA of 0.157*g* to 1.57*g*. To be consistent with the demand model development of this study, the IDA curves are developed based on the overall maximum response and the story-specific responses, compared with the corresponding demand models for both case study buildings.

Comparison between IDA and Nonlinear Dynamic Analyses Results

The IDA curves are developed based on the overall maximum and the story-specific responses for the two-story and five-story buildings. Using the selected ground motion

with scaling factors, the maximum drifts and shear ratios are estimated. Then those data points are connected with linear lines to complete IDA curves. To compare with the results from the nonlinear dynamic analyses using a suite of unscaled ground motions, the maximum drifts and shear ratios using 160 ground motion records are also plotted.

Figure A.3 shows one of the comparisons between the IDA curve and the results from the nonlinear dynamic analyses. This comparison is for the first story behavior of the two-story building based on the story-specific responses as an example. Both the IDA curve and the nonlinear dynamic results are in a logarithmic scale. The vertical axes for IDA curves are based on the spectral acceleration values corresponding to the fundamental period of the structure on the left, and the PGA values on the right. It is noted that the results from the nonlinear dynamic analyses are plotted based on the spectral acceleration (y-axis) and the maximum drift in percentage (x-axis). Other comparisons in a logarithmic scale based on the overall maximum responses and the story-specific responses are provided in Figures A.5 to A.7. In addition, for the IDA curves in a real space based on the overall maximum and the story-specific responses are provided in Figures A.8 to A.10. In these figures, the dots (•) represent the equality data, while the triangles (▽) and the squares (□) represent the lower bound data. The triangles indicate the data exceeding 5% drift, and the squares indicate the corresponding lower bound data for the other stories. The vertical dotted lines represent the valid limit of estimated data points, which is identified as 5% drift based on the potential for punching shear at the interior slab-column connections (see Section 2). More details for describing the data points are found in Section 2.

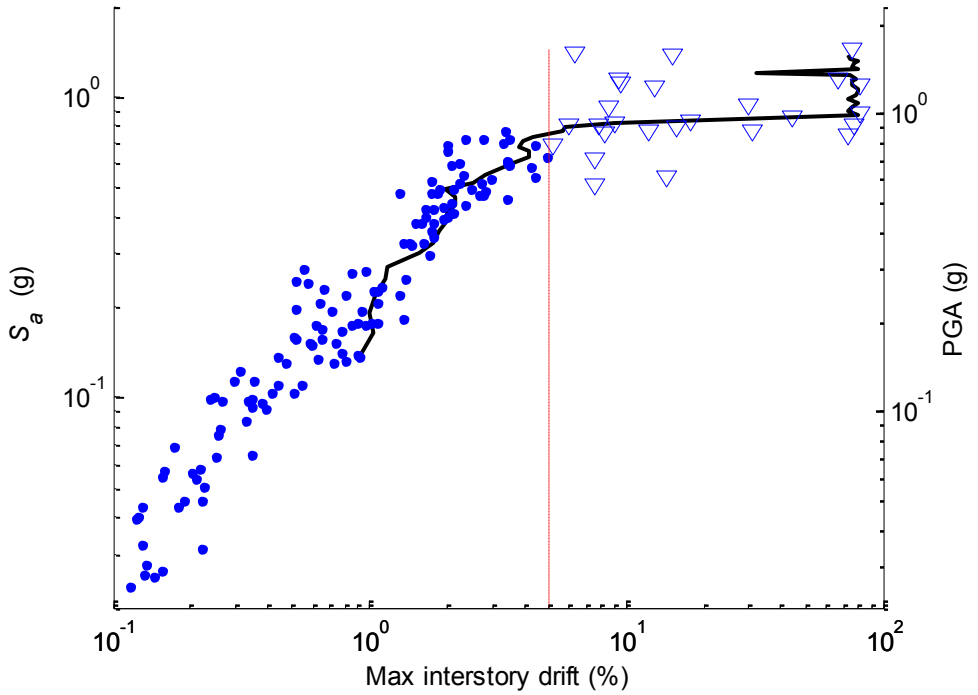

Fig. A.3. Comparison between IDA and nonlinear dynamic analysis results in a logarithmic scale

As shown in Figure A.3 and the other comparisons in Figures A.5 to A.10, the IDA curves and the results from the nonlinear dynamic analyses match well in terms of the responses of the two-story and five-story buildings. Initially, the slope of the IDA curves is similar to the elastic range of data points. Then it is clearly seen that at a certain level of earthquake intensity, the trend changes to a nonlinear response. The corresponding transition point from the IDA also matches well with that of the nonlinear dynamic analyses.

The complex behavior due to nonlinearity can be observed more clearly when the IDA curves and the results from the nonlinear dynamic analyses are in a real space (see

Figures A.8 to A.10). As shown, the IDA curves have fluctuating behavior when the earthquake intensity is beyond a certain level. There are several reasons for the fluctuating behavior of the IDA, such as a change in the building period due to stiffness degradation. In addition, the structural behavior at higher intensities is more complicated for the five-story building. This is because the response from the first story governs the overall behavior for the two-story building, while the story responses are more complex for the five-story building.

Comparison between IDA and Traditional Push-Over Curves

To compare structural behavior through two different analytical methods, the traditional push-over (nonlinear static) curves are developed for the case study buildings. To be consistent with the probabilistic demand models, push-over curves based on the overall maximum and the story-specific responses are developed. All the comparisons are provided in Figures A.11 to A.13. Figure A.11 shows the IDA curves and the push-over curves based on the overall maximum responses for the case study buildings. In addition, the comparisons based on the story-specific responses are provided in Figures A.12 and A.13. The results from the nonlinear dynamic analyses are also provided for a comparison purpose. Spectral acceleration on the left vertical axis is used for dynamic results and IDA curves, while shear ratio on the right is used for push-over curves. Because the measures on the vertical axes are different, the initial stiffness of the push-over curve is adjusted to be the same as that of the IDA suggested by Vamvatsikos and Cornell (2002). Figure A.4 shows the one of comparisons between IDA and the

traditional push-over curves. This comparison is for the second story behavior of the five-story building based on the story-specific responses as an example.

As shown in Figure A.4 and the other comparisons in Figures A.11 to A.13, the inflection point of the push-over curves generally correlates with the transition point of IDA curves. In general, when the slope of push-over curve is changed to negative, there is a change in the slope of the IDA curves. This observation is also provided by Vamvatsikos and Cornell (2002). If the push-over curves from the overall maximum and the story-specific responses are supposed to be the responses from the "equivalent single degree-of-freedom" system, then the initial slope can be comparable to the "elastic" region and the transition can be the "yield" point of the equivalent single degree-of-freedom system.

Table A.1 shows the comparison of the maximum building drifts at the transition points from the bilinear demand models with the results of nonlinear dynamic analyses, IDA, and push-over curves based on the overall maximum responses. It is noted that the transition points of bilinear demand models are determined by the Bayesian updating process. Because the formulation of lower bound data is different from that of equality data the transition points are slightly shifted to smaller ones. This is the reason why there are differences between the values from dynamic analysis and IDA even though they have a good match.

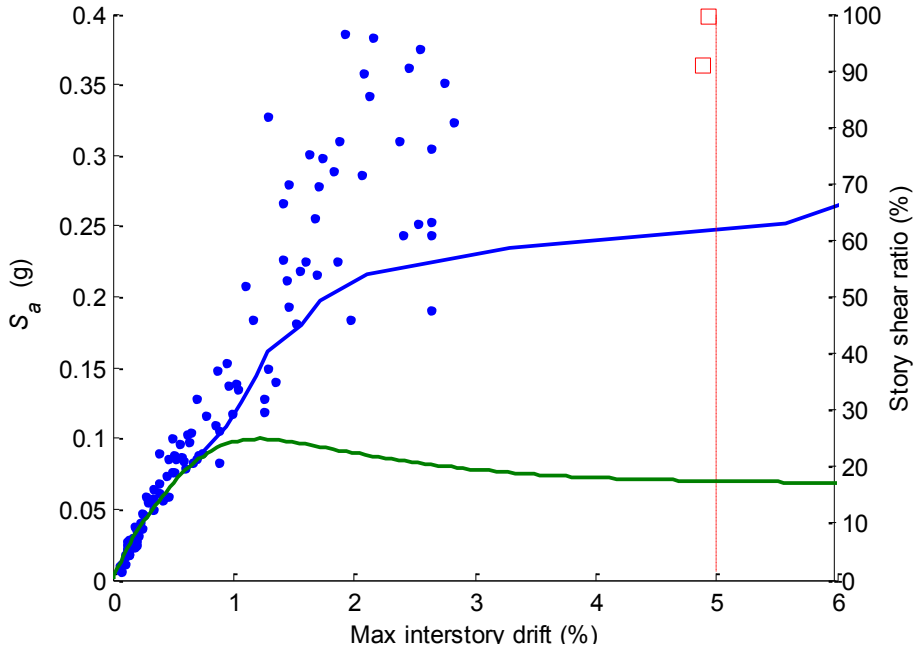

Fig. A.4. Comparison between IDA and push-over curves

Table A.1. Comparison of overall maximum building drift at transition points

Buildings	Demand model (bilinear)	IDA	Push-over
Two-story building	2.13%	2.36%	1.32%
Five-story building	2.67%	3.11%	1.77%

There is also a difference between IDA and push-over coming from the nature of two different analytical methods. Even though these curves represent demand of the same structure, push-over curves are developed with static lateral load applied to the structure cumulatively, while the results from IDA and nonlinear analyses are more record dependent because these are the results from the nonlinear dynamic analysis using scaled ground motions.

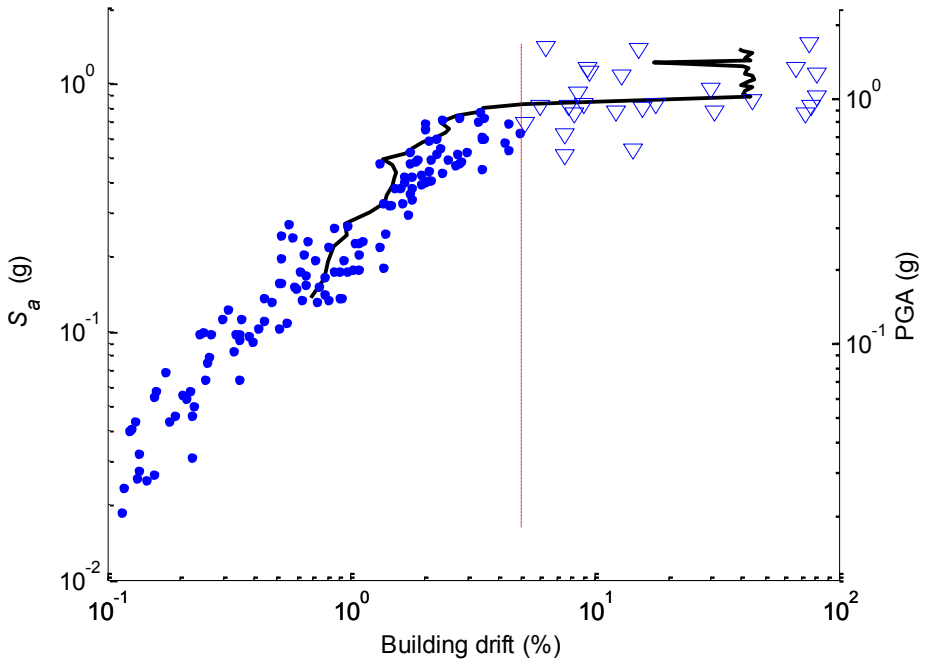

(a) 2-story building

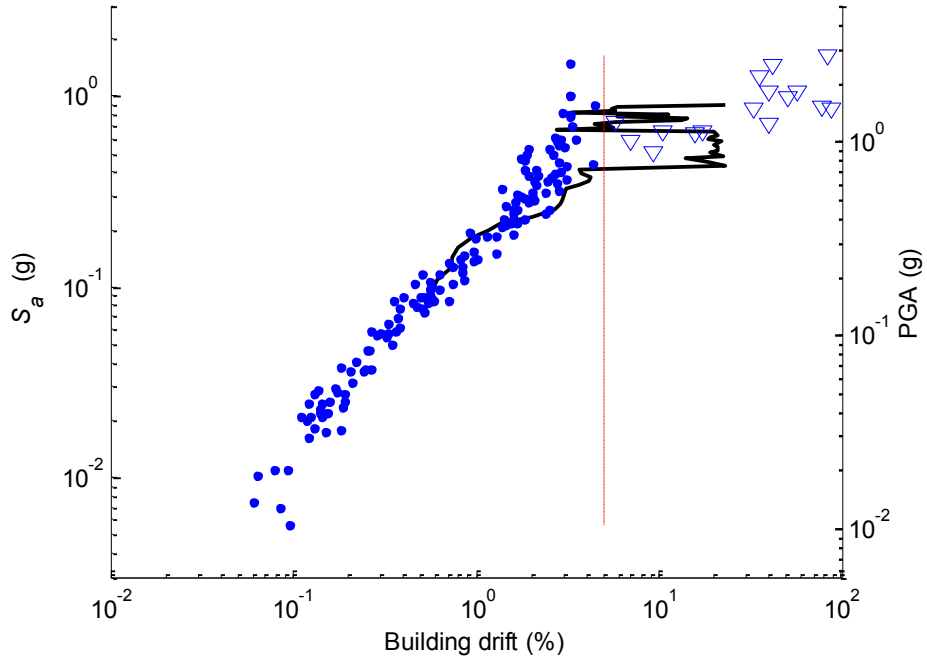

(b) 5-story building

Fig. A.5. IDA and nonlinear dynamic analysis results based on the overall maximum responses in a logarithmic scale

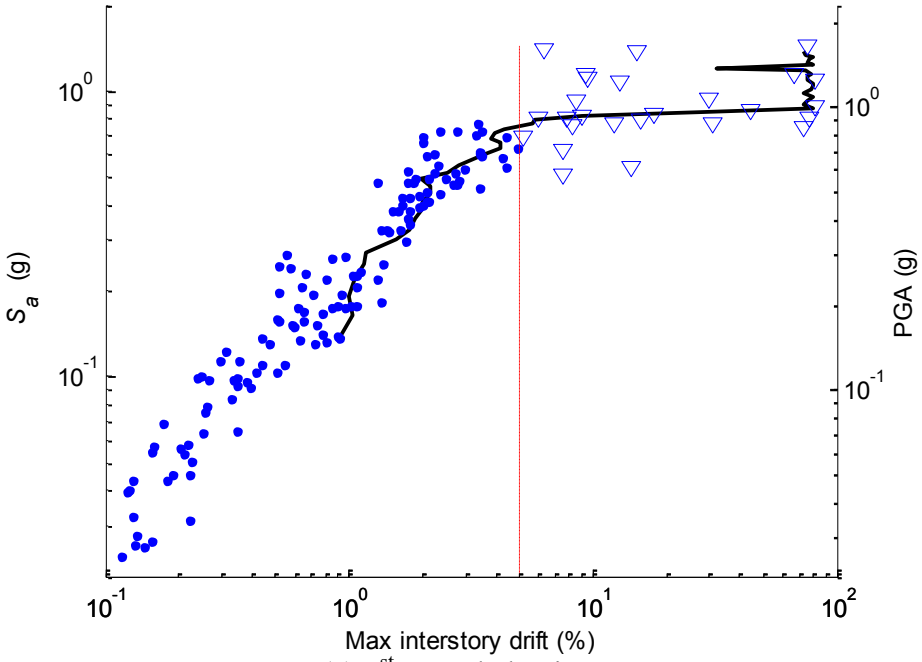

(a) 1st-story behavior

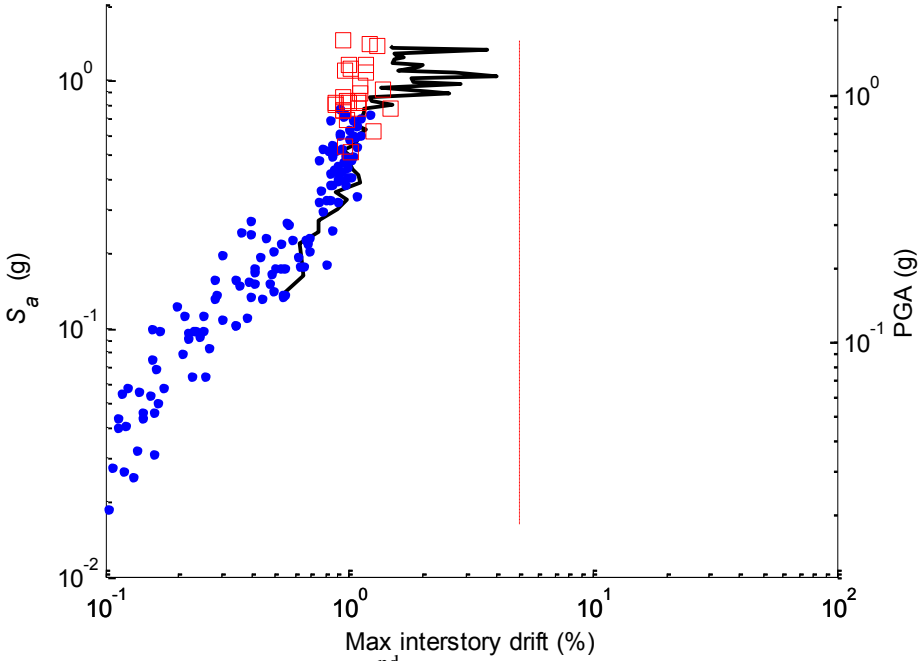

(b) 2nd-story behavior

Fig. A.6. IDA and nonlinear dynamic analysis results based on the story-specific responses in a logarithmic scale (2-story building)

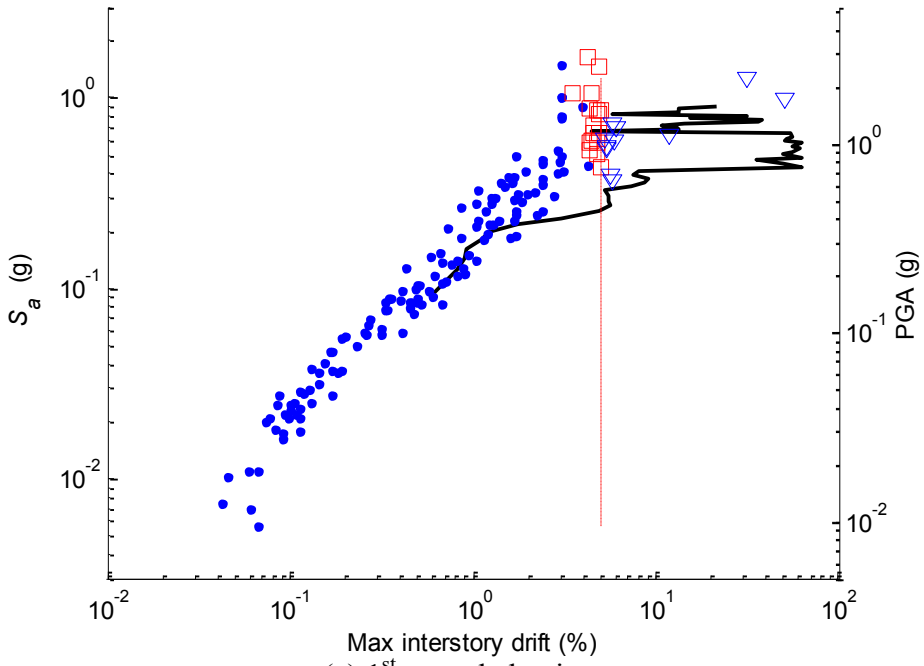

(a) 1st-story behavior

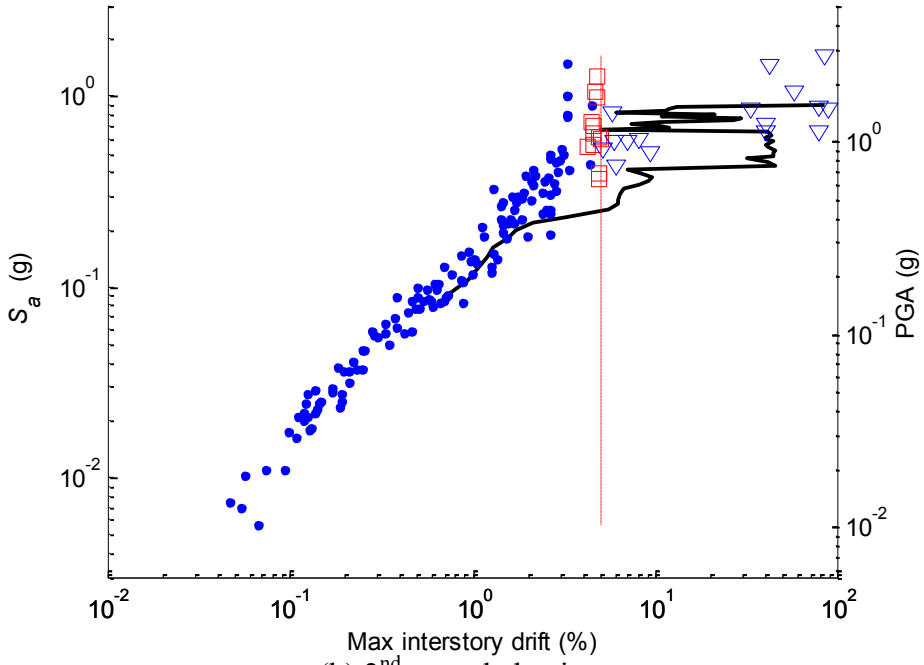

(b) 2nd-story behavior

Fig. A.7. IDA and nonlinear dynamic analysis results based on the story-specific responses in a logarithmic scale (5-story building)

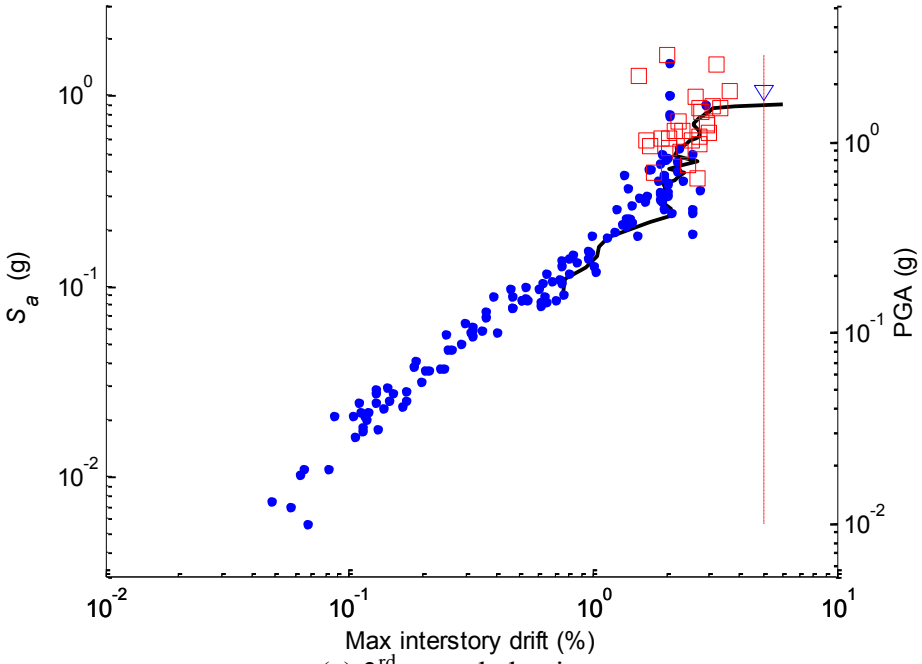

(c) 3rd-story behavior

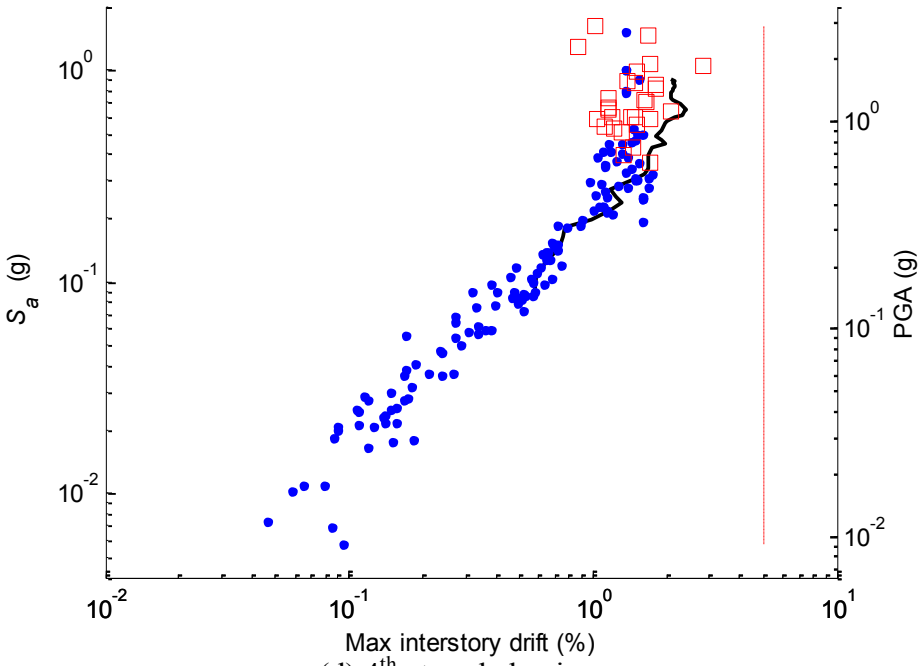

(d) 4th-story behavior

Fig. A.7. Continued

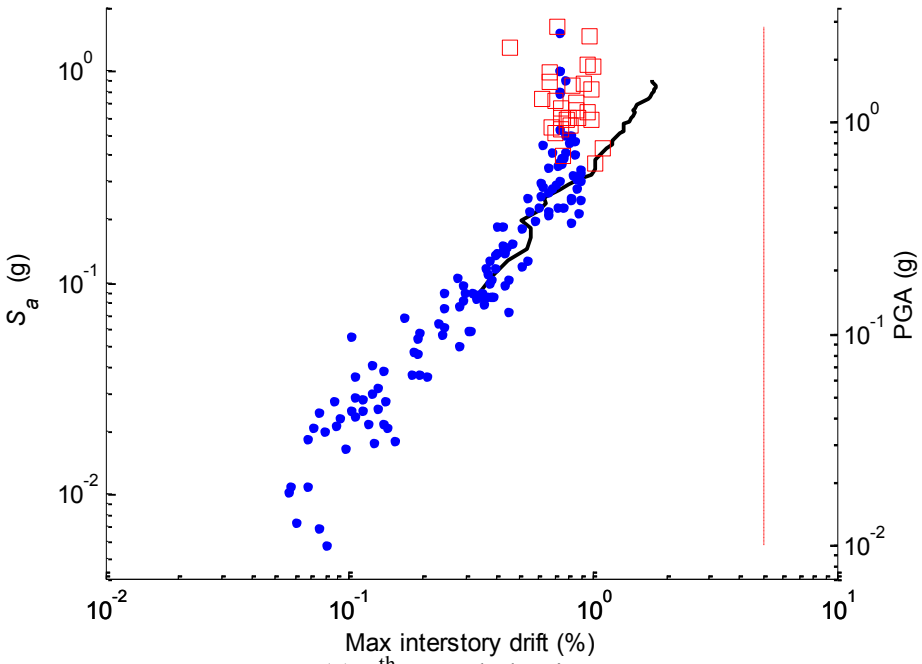

(e) 5th-story behavior

Fig. A.7. Continued

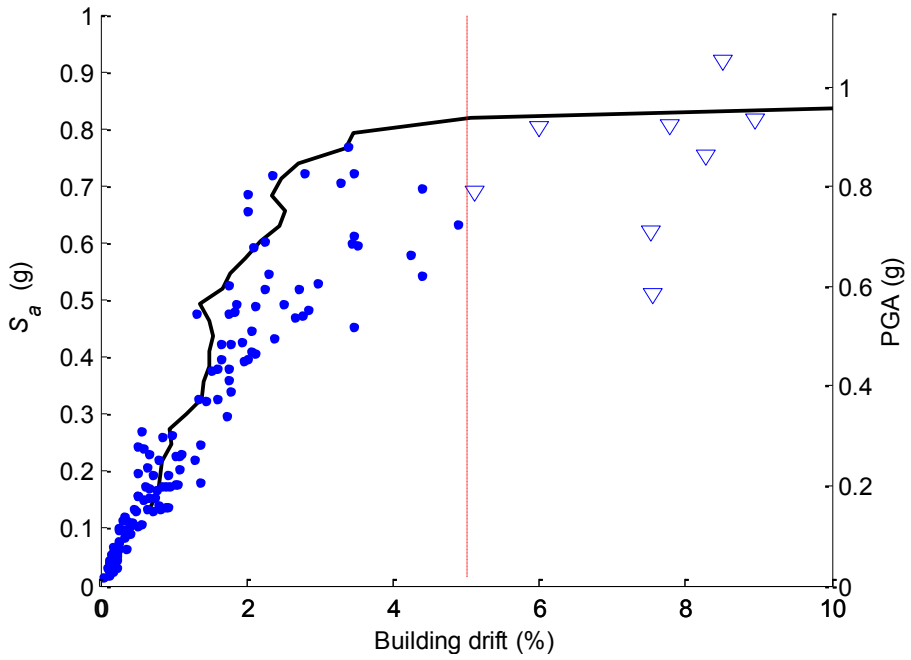

(a) 2-story building

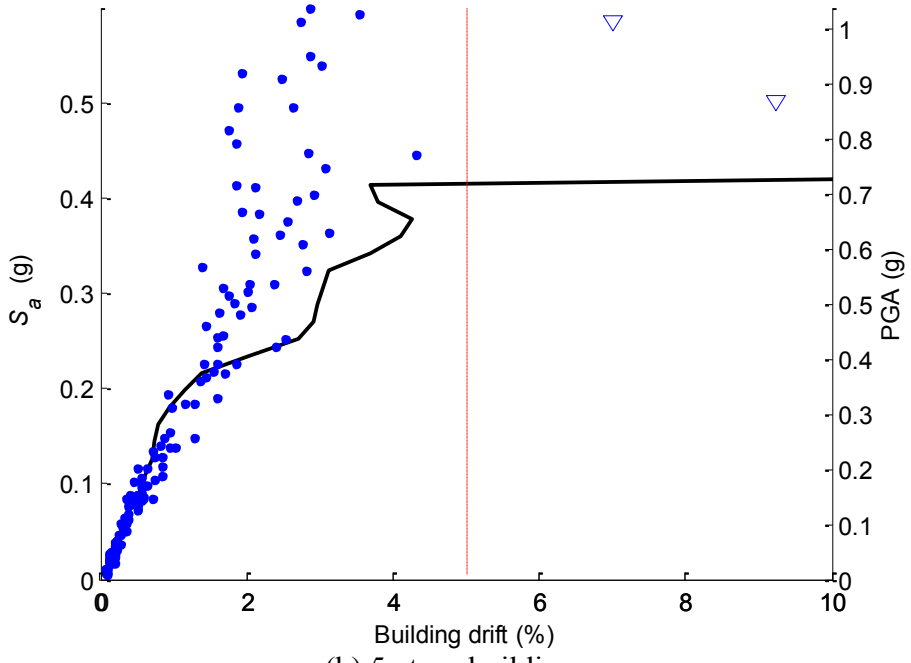

(b) 5-story building

Fig. A.8. IDA and nonlinear dynamic analysis results based on the overall maximum responses in a real scale

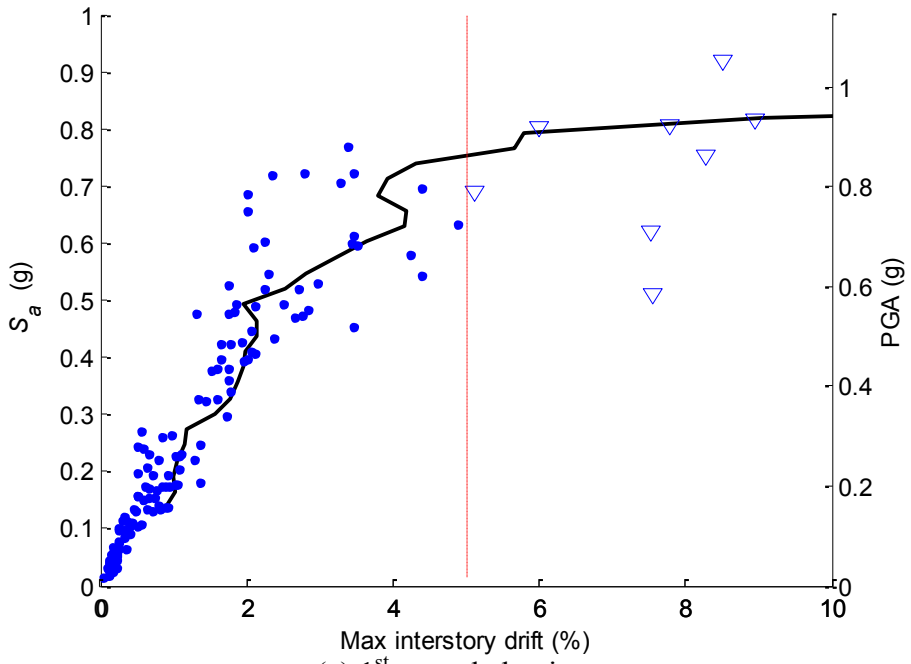

(a) 1st-story behavior

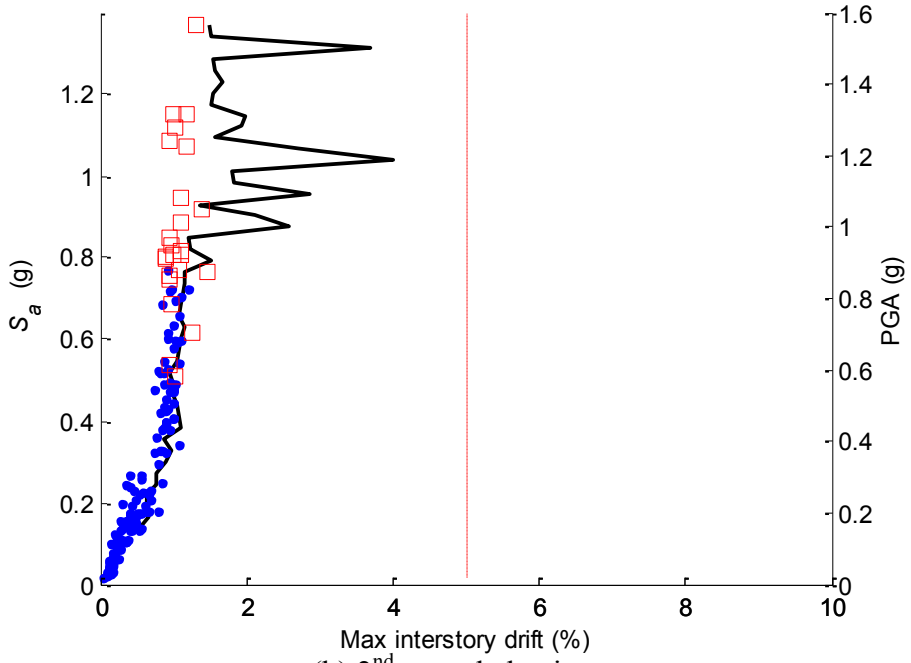

(b) 2nd-story behavior

Fig. A.9. IDA and nonlinear dynamic analysis results based on the story-specific responses in a real scale (2-story building)

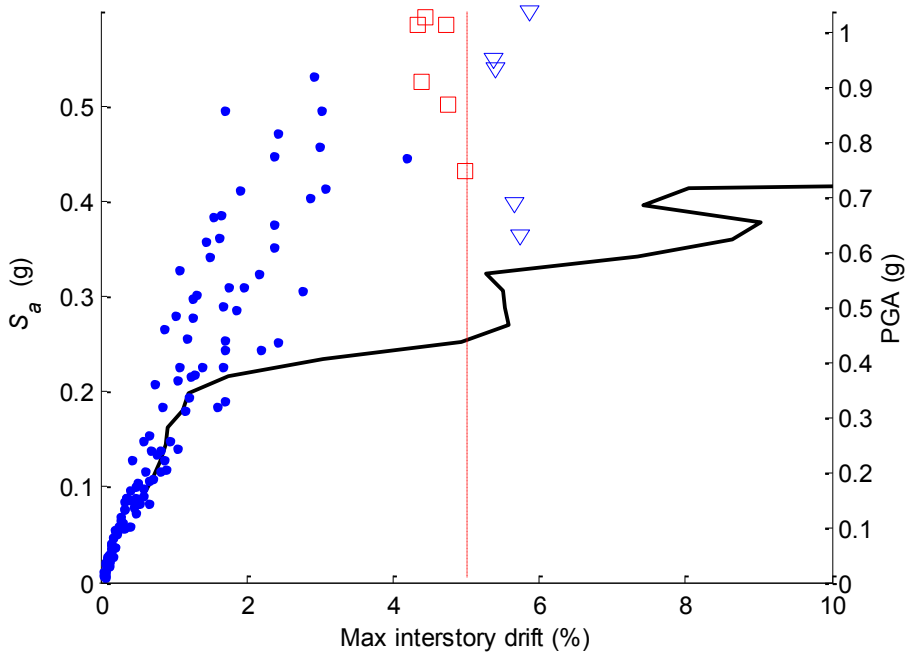

(a) 1st-story behavior

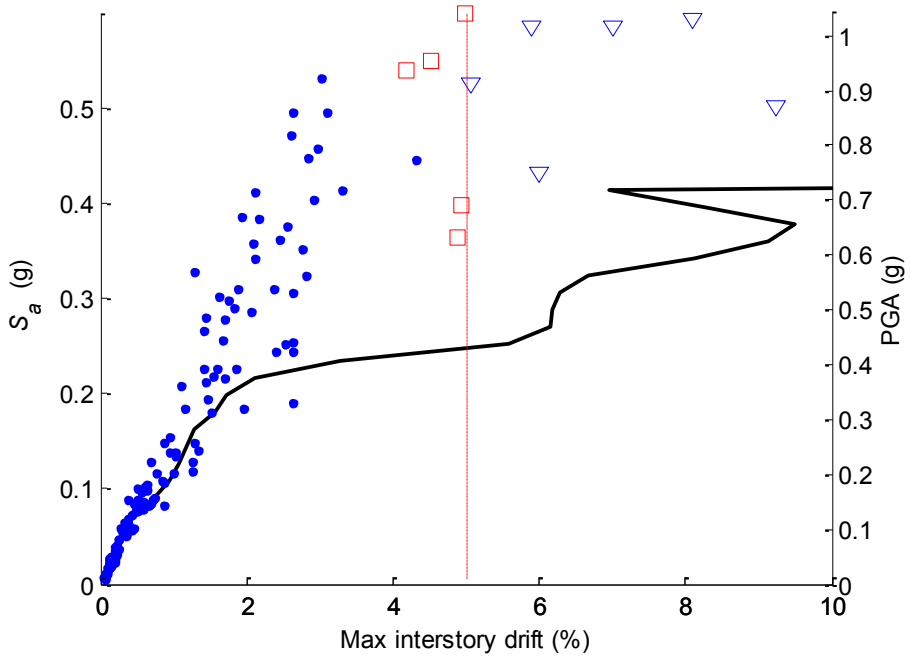

(b) 2nd-story behavior

Fig. A.10. IDA and nonlinear dynamic analysis results based on the story-specific responses in a real scale (5-story building)

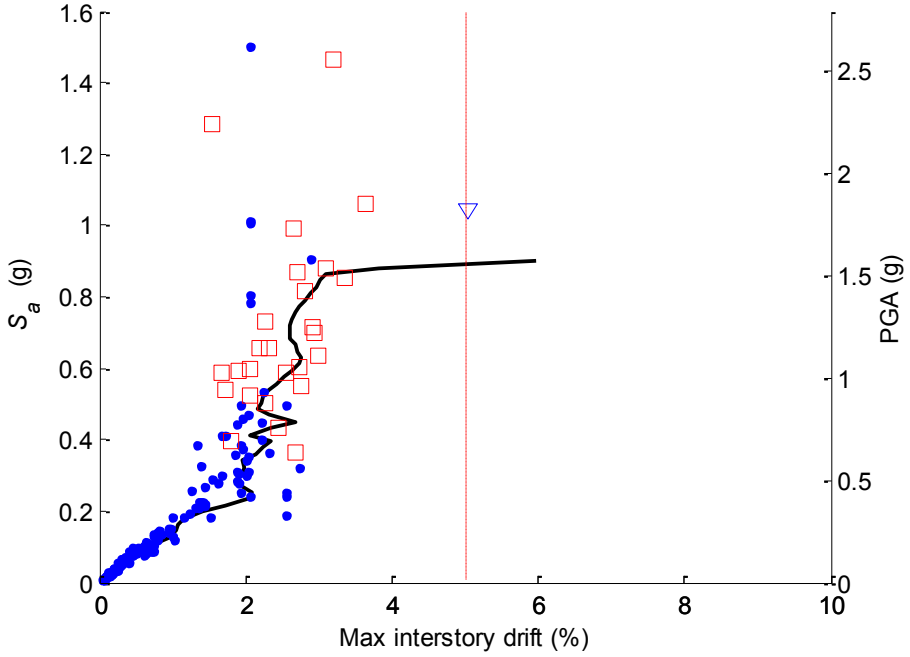

(c) 3rd-story behavior

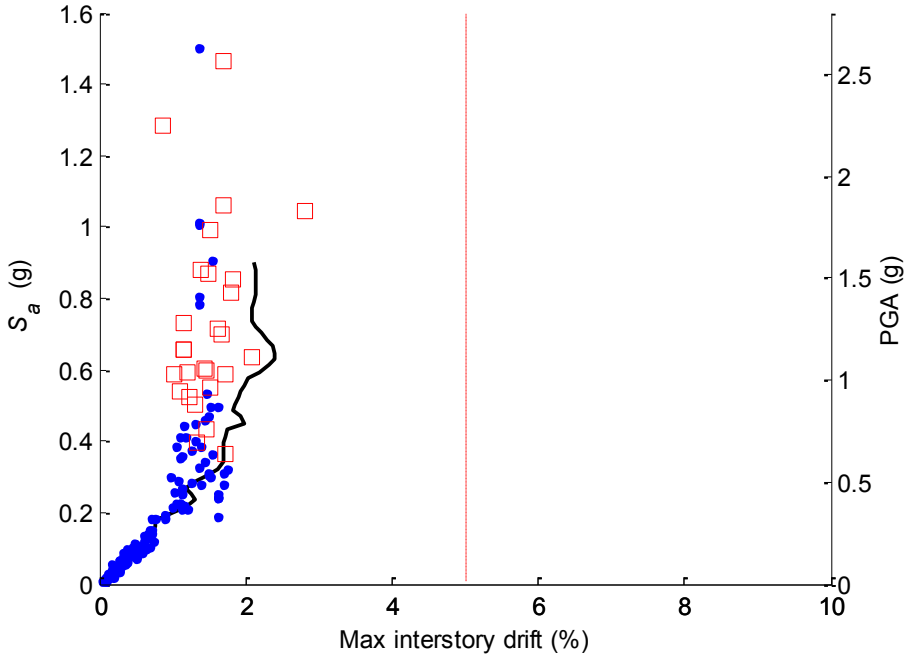

(d) 4th-story behavior

Fig. A.10. Continued

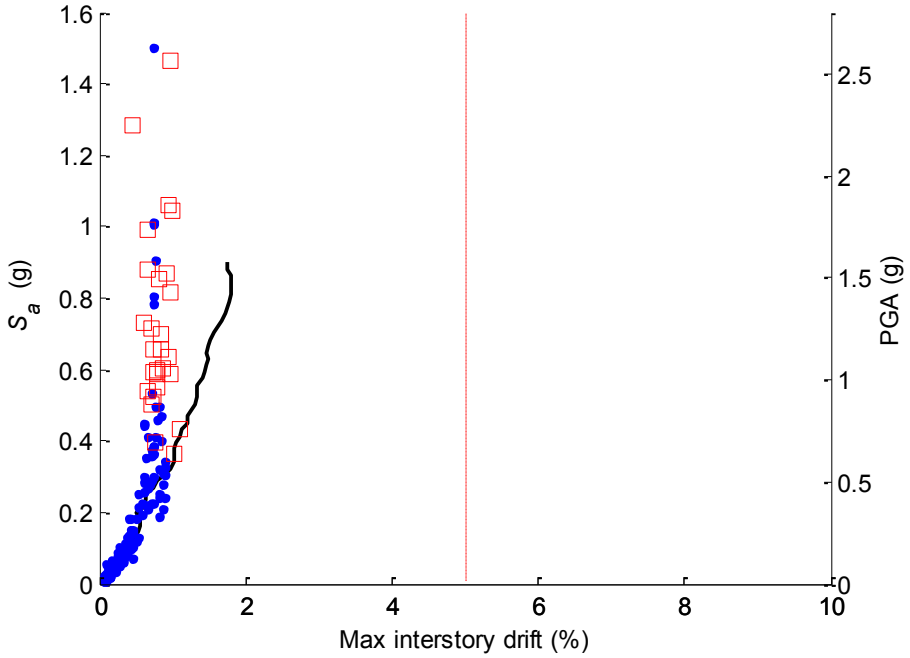

(e) 5th-story behavior

Fig. A.10. Continued

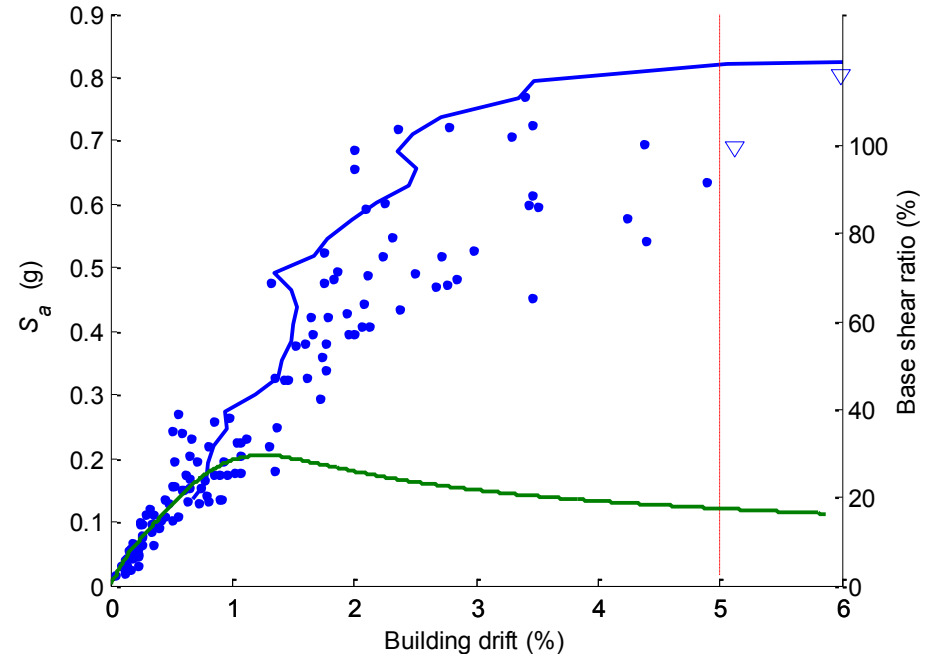

(a) 2-story building

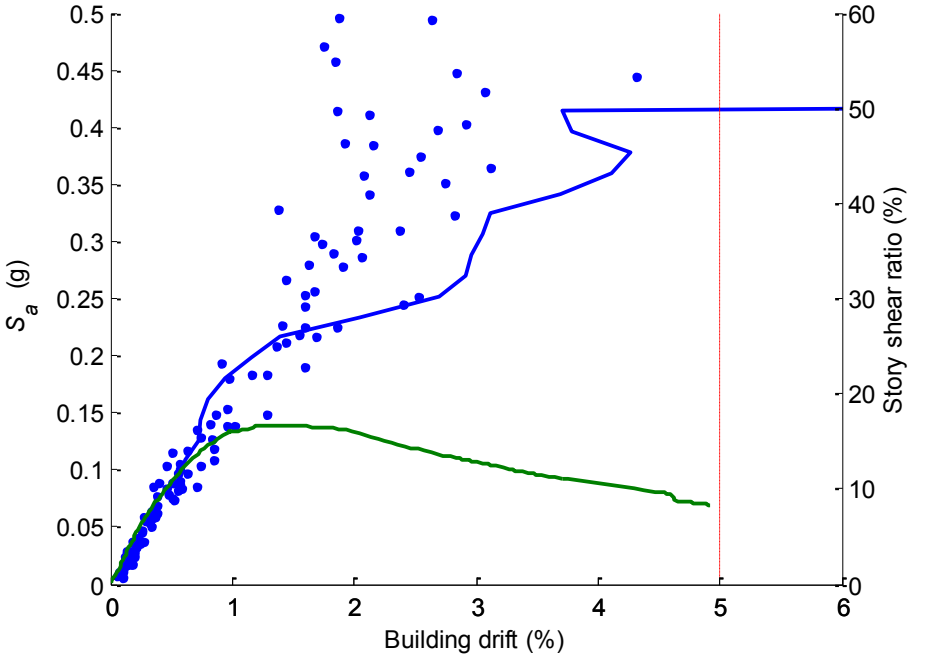

(b) 5-story building

Fig. A.11. IDA and push-over curves based on the overall maximum responses

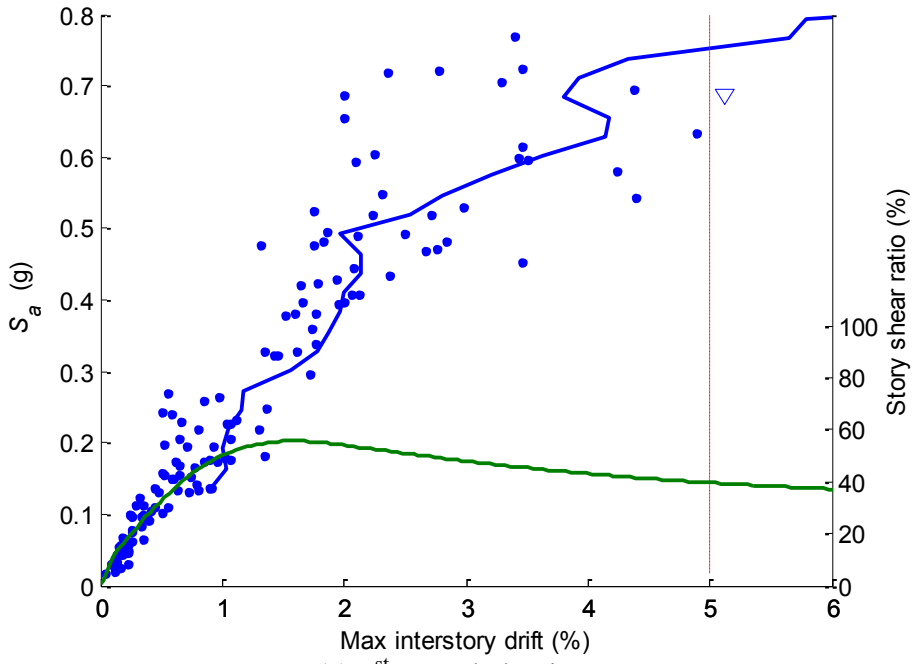

(a) 1st-story behavior

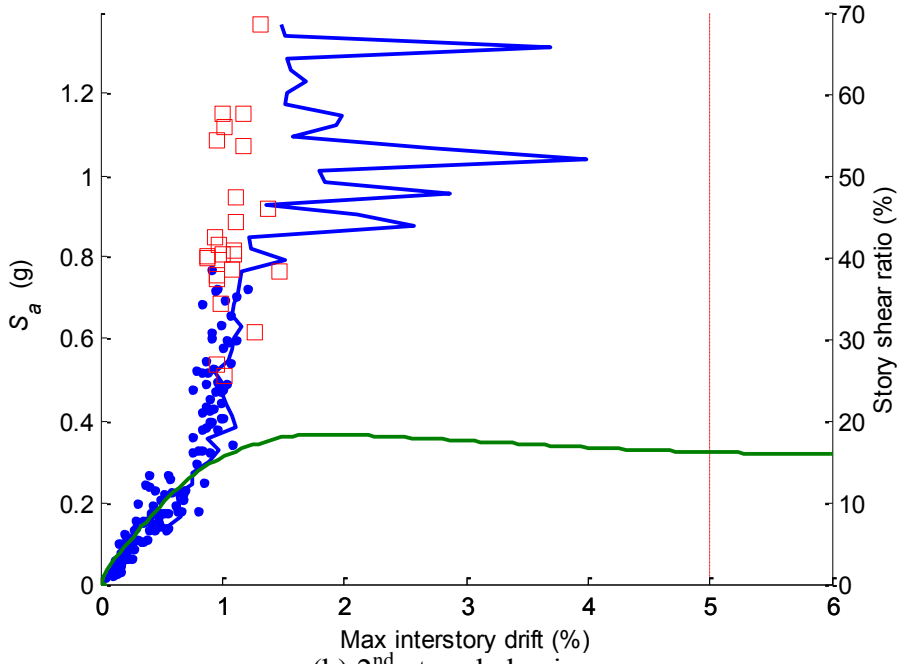

(b) 2nd-story behavior

Fig. A.12. IDA and push-over curves based on the overall maximum responses for the 2-story building

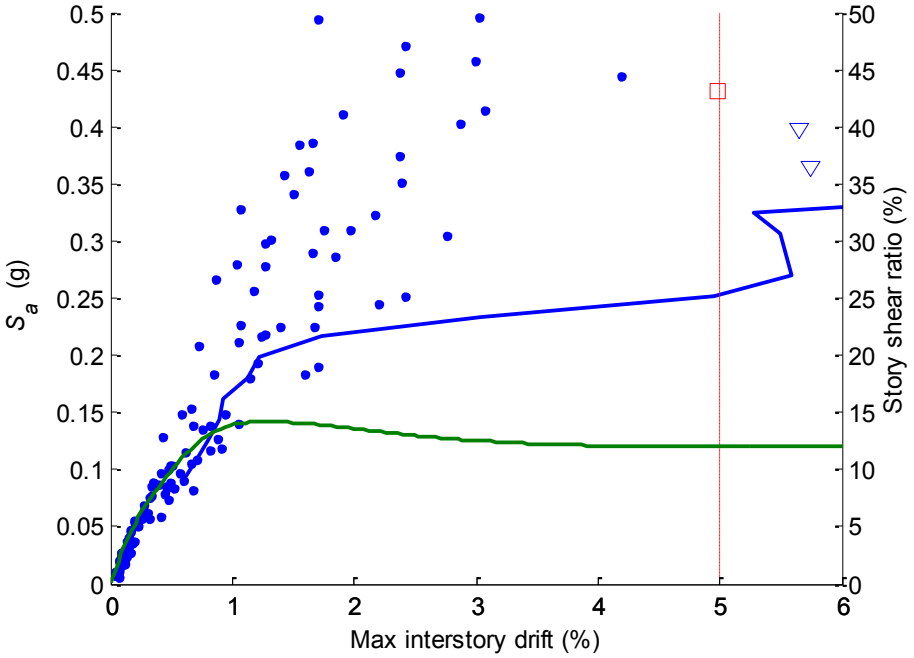

(a) 1st-story behavior

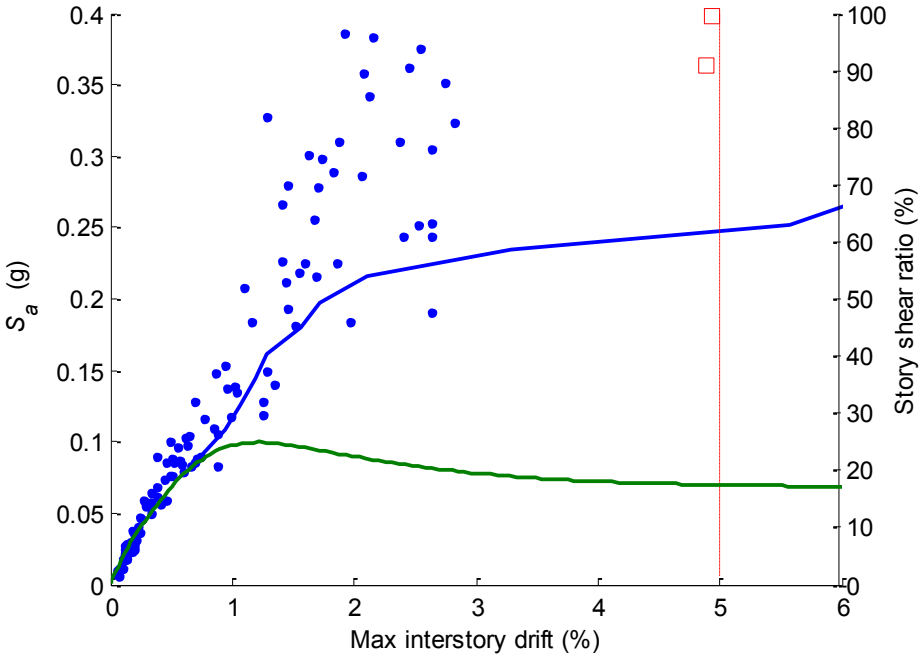

(b) 2nd-story behavior

Fig. A.13. IDA and push-over curves based on the overall maximum responses for the 5-story building

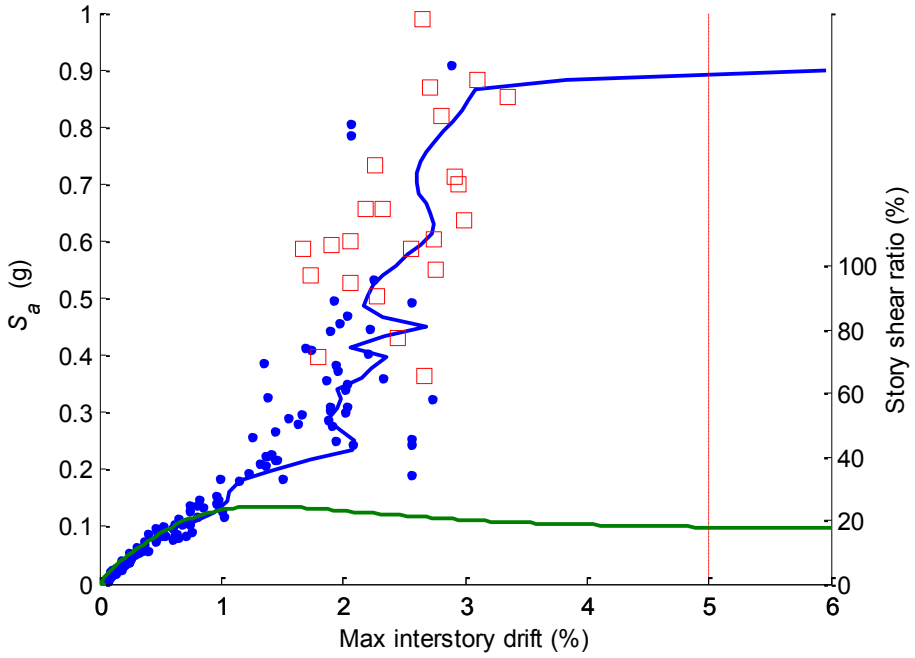

(c) 3rd-story behavior

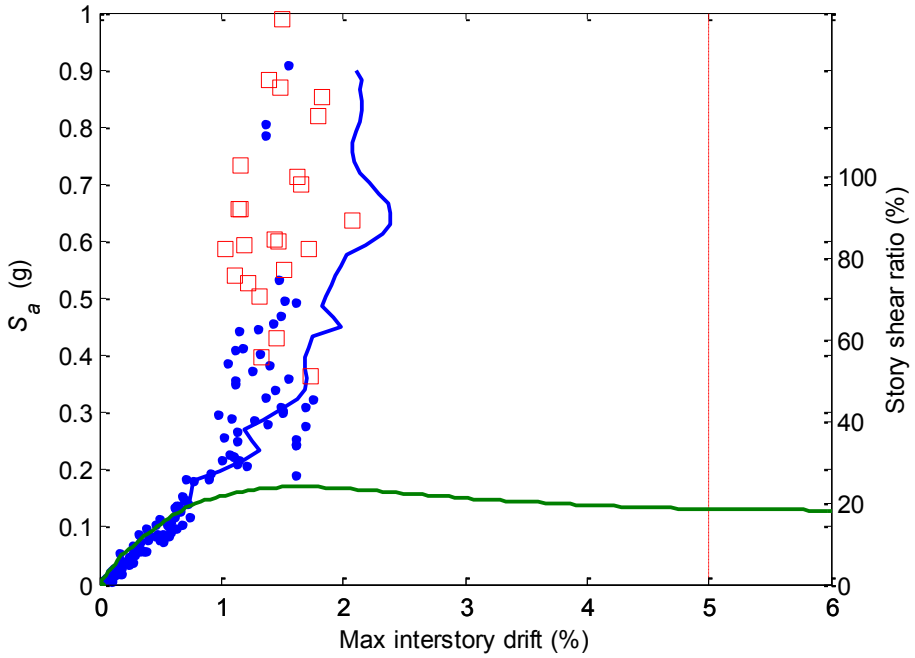

(d) 4th-story behavior

Fig. A.13. Continued

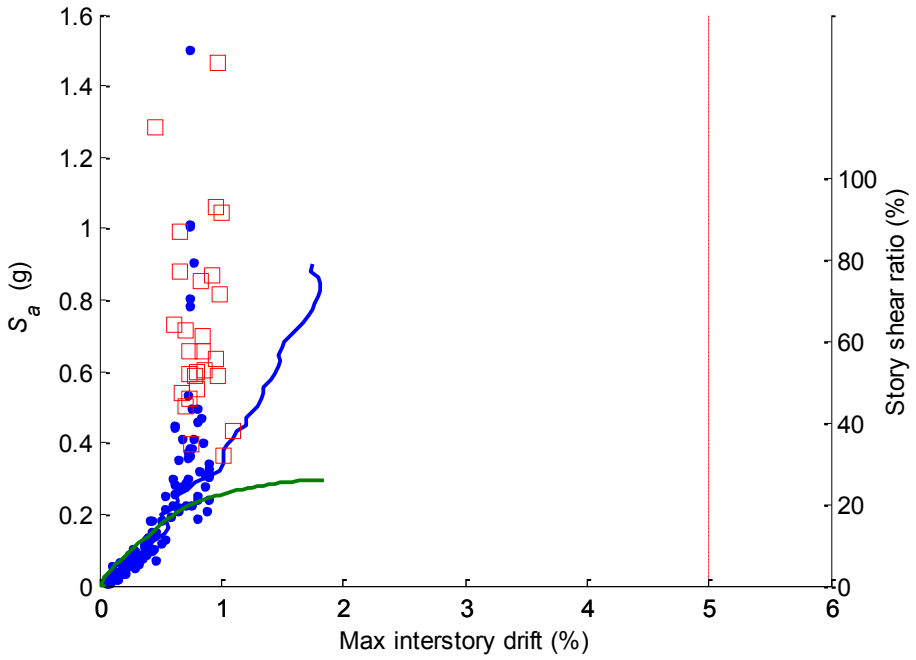

(e) 5th-story behavior

Fig. A.13. Continued

VITA

Jong Wha Bai was born in Seoul, Korea. He studied at Yonsei Univeristy in Seoul, where he received his Bachelor of Science degree in civil engineering in 2000. After graduation, he enrolled in the master's program in civil engineering at Texas A&M University, where he has worked as a research assistant. He worked with Dr. Hueste, and his research was focused on seismic retrofitting and evaulation for reinforced concrete (RC) structures as a part of the Mid-America Earthquake (MAE) Center project. He graduated in May 2004 with a M.S. degree and continued his doctoral studies in civil engineering at Texas A&M University. During his doctoral studies, he worked as a research assistant with Dr. Hueste and Dr. Gardoni. His research was focused on earthquake engineering and structural reliability including seismic performance evaluation, seismic fragility analysis, and loss estimation. He graduated in December 2011 with a Ph.D. degree in civil engineering from Texas A&M University. He can be contacted through the following addresses:

Address: California Baptist University
School of Engineering
8432 Magnolia Ave.
Riverside, CA 92504
E-mail: jbai@calbaptist.edu